ISTANBUL TECHNICAL UNIVERSITY ★ GRADUATE SCHOOL OF SCIENCE ENGINEERING AND TECHNOLOGY

DESIGN AND IMPLEMENTATION OF SENSORLESS VECTOR CONTROLLED DRIVE FOR PMSMs

M.Sc. THESIS

Burak GÖRDÜK

Department of Electrical Engineering

Electrical Engineering Programme

JUNE 2019

ISTANBUL TECHNICAL UNIVERSITY ★ GRADUATE SCHOOL OF SCIENCE ENGINEERING AND TECHNOLOGY

DESIGN AND IMPLEMENTATION OF SENSORLESS VECTOR CONTROLLED DRIVE FOR PMSMs

M.Sc. THESIS

Burak GÖRDÜK
(504161012)

Department of Electrical Engineering

Electrical Engineering Programme

Thesis Advisor: Asst. Prof. Murat YILMAZ

JUNE 2019

ISTANBUL TEKNİK ÜNİVERSİTESİ ★ FEN BİLİMLERİ ENSTİTÜSÜ

SÜREKLİ MIKNATISLI SENKRON MOTORLAR İÇİN SENSÖRSÜZ VEKTÖR KONTROLLÜ SÜRÜCÜ TASARIMI VE GERÇEKLENMESİ

YÜKSEK LİSANS TEZİ

Burak GÖRDÜK
(504161012)

Elektrik Mühendisliği Anabilim Dalı

Elektrik Mühendisliği Programı

Tez Danışmanı: Dr. Öğr. Üyesi Murat YILMAZ

HAZİRAN 2019

Burak GÖRDÜK, a M.Sc. student of İTU Graduate School of Science Engineering and Technology 504161012, successfully defended the thesis entitled "DESIGN AND IMPLEMENTATION OF SENSORLESS VECTOR CONTROLLED DRIVE FOR PMSMs", which he prepared after fulfilling the requirements specified in the associated legislations, before the jury whose signatures are below.

Thesis Advisor :	**Asst. Prof. Murat YILMAZ** İstanbul Technical University	.....
Jury Members :	**Asst. Prof. Deniz YILDIRIM** Istanbul Technical University	.....
	Prof. Dr. K. Nur BEKİROĞLU Yıldız Technical University	.....

Date of Submission : 2 May 2019
Date of Defense : 10 June 2019

FOREWORD

First of all, I would like to thank to my advisor at ITU, Asst. Prof. Murat Yılmaz, who carefully guided me throughout this thesis. I would also like to thank to Kerem Erenay and Pavotek for their willingness to help and support me on completing my master's degree. Lastly, I appreciate all the support from my family and friends.

May 2019

Burak GÖRDÜK
(Electrical Engineer)

TABLE OF CONTENTS

Page

ABBREVIATIONS

PMSM : Permanent Magnet Synchronous Motor
EMF : Electromotive Force
RPM : Revolutions Per Minute
FOC : Field Oriented Control
MRAC : Model Reference Adaptive Control
DTC : Direct Torque Control
DSC : Direct Self Control
SVM : Space Vector Modulation
EKF : Extended Kalman Filter
SMO : Sliding Mode Observer
BLDC : Brushless DC
DSP : Digital Signal Processor
ADC : Analog to Digital Converter
DAC : Digital to Analog Converter
PCB : Printed Circuit Board
FSM : Finite State Machine

SYMBOLS

$u_a, u_b, u_c, u_\alpha, u_\beta, u_d, u_q$	: Phase voltages
$i_a, i_b, i_c, i_\alpha, i_\beta, i_d, i_q$	: Phase currents
$\psi_a, \psi_b, \psi_c, \psi_\alpha, \psi_\beta, \psi_d, \psi_q,$	: Flux linkages
L	: Inductance
R	: Resistance
$L_S, L_a, L_b, L_c, L_\alpha, L_\beta, L_d, L_q$	: Phase inductances
R_S, R_a, R_b, R_c	: Phase resistances
$M_{ab}, M_{ac}, M_{bc}, M_{\alpha\beta}$	: Mutual inductances
$e_a, e_b, e_c, e_\alpha, e_\beta$	: Induced back-EMFs
p	: Number of pole pairs
θ_e	: Rotor electrical position
ω_e	: Rotor electrical speed
T_e	: Electrical torque
J_m	: Mechanical inertia
B_m	: Viscous friction coefficient
T_L	: Load torque
U_{DCB}	: DC bus voltage
ρ	: Derivative operator
$U_0, U_{60}, U_{120}, U_{180}, U_{240}, U_{300}$	: Phase vectors
O_{000}, O_{111}	: Null vectors
S_A, S_B, S_B	: Phase states
T, T_0, T_{60}, T_{null}	: Duration for applied vector

LIST OF TABLES

Page

LIST OF FIGURES

Page

DESIGN AND IMPLEMENTATION OF SENSORLESS VECTOR CONTROLLED DRIVE FOR PMSMs

SUMMARY

Systems based on electric motors became an important part of our life today. Many applications such as electricity generation, ventilation and transportation, white and brown goods depend on electric motors. Approximately 50% of electrical power generated globally is consumed by electric motors. With the very fast growing electric vehicle industry, this ratio is expected to increase even more.

High technology applications like defense industry, aviation and aerospace require the use of higher performance components and techniques due to nature of these industries. Industrial, white and brown goods applications however, count on sustainable, easy to manufacture low cost products. In such industries, domestic and international regulations push manufacturers to use efficient and environment friendly technologies.

For electric drive systems, the requirement on using higher performing components is generally satisfied by replacing induction motors with permanent magnet motor, which has higher efficiency. Permanent Magnet Synchronous Motors (PMSM) use permanent magnets placed on the rotor in order to generate armature field. This, in turn eliminates the electrical losses caused by rotor windings and mechanical losses due to friction between brushes and slip rings. Since stator field should rotate synchronous to rotor field, drive systems require rotor position information. This information can be obtained using sophisticated sensors like Hall effect sensors, encoders and resolvers. In many applications though, increased size, complexity and costs due to position sensors are not desired. Thus, necessity of sensorless rotor position estimation schemes has emerged. Since its first introduction to literature, many different methods are presented about position estimation.

This thesis presents the design of a sensorless vector control system for PMSM. A three-phase inverter development board is obtained from market. Controller board and software for this inverter board is designed in this study. Two different position estimation methods are investigated in detail. One is based on estimating motor back-EMFs (Electromotive Force) in two axis stationary reference frame. State estimation is based on two Luenberger observers. Another method depends on estimating stator flux vectors by back-EMF integration. Verification of the position estimation schemes are done using simulations. It is observed that extended back-EMF observer is more accurate and dynamic. Embedded software is developed by transforming simulation models into discrete time functions. System verification is done using hardware experiments with a test setup. No-load to full-load performance of drive system along with dynamic changes in load configuration are observed. For a 3000 rpm (revolutions per minute) motor speed range from 200 to 3000 rpm is covered with full-load while up to 4000 rpm is covered with reduced load and field weakening. System is found dynamic and stable under these operating conditions. Position estimation was accurate as to ensure correct operation of the motor.

SÜREKLİ MIKNATISLI SENKRON MOTORLAR İÇİN SENSÖRSÜZ VEKTÖR KONTROLLÜ SÜRÜCÜ TASARIMI VE GERÇEKLENMESİ

ÖZET

Elektrik makinalarına dayalı sistemler günümüzde hayatımızın önemli bir parçası olmuş durumdadır. Elektrik üretiminden havalandırma ve iklimlendirmeye, ulaşımdan beyaz eşyalara ve hatta her gün kullandığımız kişisel eşya ile araçlara kadar sayısız uygulama elektrik motoru kullanımına dayanmaktadır. Günümüzde küresel olarak üretilen elektrik enerjisinin neredeyse yarısı elektrik motorları tarafından tüketilmektedir. Elektrikli araçların günden güne daha da yaygınlaşması ve son kullanıcılara erişiminin kolaylaşması nedeniyle bu oranın giderek artması beklenmektedir.

Savunma sanayi, havacılık, uzay ve otomotiv gibi yüksek teknoloji kullanımı fazla olan uygulamalarda sektörün doğası gereği yüksek performanslı yöntemlerin ve komponentlerin kullanımı gerekli olmaktadır. Endüstriyel uygulamalar ve beyaz eşya sektöründe ise bu gereklilik devletler ve uluslararası otoritelerin regülasyonları sonucu oluşmaktadır. Elektrikli sürüş uygulamalarında yüksek performans gereksinimi daha verimli elektrik motorları ve sürücü sistemleri kullanılması ile sağlanmaktadır. Bu da genellikle eski nesil asenkron motorların daha yüksek verime sahip mıknatıslı motorlar ile değiştirilmesi sonucu elde edilmektedir.

Sürekli mıknatıslı senkron motorlar endüvi alanı üretmek için rotora yerleştirilmiş mıknatısları kullanırlar. Bu sayede rotor sargısı, fırça ve bilezik kullanımının önüne geçilmiş olur. Bunun sonucu olarak rotor sargısı üzerinde oluşacak elektriksel kayıplar ve fırça ile bilezik arasındaki sürtünme sonucu oluşacak mekanik kayıpların önüne geçilerek toplam verimin yükseltilmesi sağlanır. Stator manyetik alanının rotor manyetik alanı ile senkron bir şekilde dönmesi gereklidir. Bu nedenle kullanılacak olan sürücü sistemleri rotor manyetik alanına dik bir manyetik alan vektörü oluşturacak faz gerilimlerini statora uygulamalıdır. Sürekli mıknatıslı senkron motorların sürüşünde kullanılan sürücü sistemleri rotor açı bilgisine ihtiyaç duymaktadır. Rotor açısı konum algılayacak şekilde tasarlanmış sensörlerin kullanımı ile elde edilebilir. Bu sensörlerden başlıcaları manyetik alan algılayıcılar, enkoderler ve açı algılayıcılardır. Sensör kullanımı sürüş için büyük öneme sahip olan rotor açısı bilgisini sağlamak ile beraber sisteme inkar edilemez bir yük bindirmektedir. Motor hacminin, üretim karmaşıklığının ve maliyetinin artması ile sensör kullanımı sonucu artan bakım gereksinimi tasarımcıları ve araştırmacıları sensörsüz konum algılama teknikleri üzerinde çalışmalar yapmaya itmiştir. Özellikle beyaz eşya uygulamalarında olmak üzere, birçok alanda sensörsüz vektör kontrol yöntemi yaygın olarak kullanılmaktadır. Servo uygulamaları gibi hassas konum bilgisi ve konum kontrolü gerektiren uygulamalarında ise sensörsüz konum algılama yöntemleri yetersiz kaldığı için kullanılmamaktadır.

Bu çalışmada sürekli mıknatıslı senkron motorlar için sensörsüz alan yönlendirmeli kontrole yönelik bir sürücü sistemi geliştirilmiştir. Sürücü sistemi üç fazlı evirici katı, kontrol katı ve kontrol için geliştirilmiş gömülü sistem yazılımından

oluşmaktadır. Çalışmanın kapsamı bu sürücü sisteminin kontrol katı ve gömülü sistem yazılımı kısımlarının tasarlanmasını içermektedir. Üç fazlı evirici katı piyasada hazır halde bulunabilen bir geliştirme kartı olarak temin edilmiştir. Bu geliştirme kartı 48V ve 15A'e kadar plaka değerine sahip üç fazlı motorları sürebilecek donanıma sahiptir. Şönt direnç ve işlemsel kuvvetlendiriciler ile oluşturulmuş akım ölçme yapıları, aşırı akım koruması için karşılaştırıcı devresi, bara gerilim ölçme devresi ve kontrol katı için gerekli düşük gerilimi yaratacak anahtarlamalı güç kaynağı bu kart üzerinde hazır olarak bulunmaktadır.

Kontrol katı ise üç fazlı evirici kartına kolayca takılabilir biçimde bir modül kartı olarak tasarlanmıştır. Tasarım süreci uygun özelliklere sahip bir mikrodenetleyicinin ve çevresel elemanların seçimi, şematik çizimi ve baskı devre tasarımı aşamalarından oluşmuştur. Şematik çizimi ve baskı devre tasarımı için Altium programı kullanılmıştır. Kart boyutu ve komponent yerleşimleri temin edilmiş olan üç fazlı evirici kartına uygun olacak şekilde belirlenmiş ve baskı devre tasarımı iki katlı olacak şekilde yapılmıştır. Kontrol kartı ile üç fazlı evirici kartı arasındaki giriş çıkış ve besleme bağlantılarının uygun şekilde yapılması sağlanmıştır. Kontrol kartı daha sonrasında üretilmiş ve dizgisi yapılmıştır.

Sensörsüz olarak rotor elektriksel açısının tahmini için iki farklı yöntem incelenmiştir. İlk olarak genişletilmiş endüklenen gerilim gözlemleyicisi detaylı olarak analiz edilmiştir. Luenberger gözlemleyicisi yapısında olan bu tahmin yöntemi sistem modelinin denetleyici içerisinde kurulmasına dayalıdır. Sistemin durum değişkenlerinin tahmini için ölçülen ve bilinen durum değişkenleri sistem modeli kullanılarak işlenir. Sistem modeli oluşturulurken bilinçli olarak bir durum değişkeni modelden çıkartılır ve bunun yerine bir kompanzatör yerleştirilir. Sistem modeli kullanılarak tahmin edilen durum değişkeni ile ölçülen durum değişkeni arasındaki hatanın sıfırlanmasında bu kompanzatör kullanılırsa, sürekli hal durumunda kompanzatörün çıkışı bilinçli olarak sistem modelinden çıkartılmış durum değişkenine eşit olmaktadır. Bu gözlemleyici yapısı sürekli mıknatıslı senkron motorda endüklenen gerilim tahmini için kullanılacak şekilde düzenlenmiştir. Bunun için motorun iki fazlı sabit düzlemdeki elektriksel modeli kullanılmıştır. Motor modelinden genişletilmiş endüklenen gerilim kısmı çıkartılarak oluşturulan sistem modeli α ve β eksen akımlarını tahmin edecek şekilde oluşturulmuştur. Tahmin edilen akım ile ölçülen akım arasındaki hata ise iki adet PI kontrolör ile kompanze edilerek sistem modeline eklenmektedir. Sürekli hal durumunda bu PI kontrolörlerin çıkışı modelden çıkartılmış olan genişletilmiş endüklenen gerilime eşit olmaktadır. Endüklenen gerilim rotor elektriksel açısının sinüs ve kosinüs bileşenlerini içermektedir. Elde edilen bu sinüs ve kosinüs bileşenleri ise bir açık takip gözlemleyicisi kullanılarak rotor elektriksel açısına ve filtrelenmiş rotor eletriksel hızına dönüştürülmektedir.

Rotor açısının tahmini için stator akı tahmin yöntemi ayrıca incelenmiştir. Bu yöntem motorun iki fazlı sabit düzlemdeki elektriksel modelini kullanmaktadır. Akı ifadesi faz akımları, endüktans matrisi ve rotor açısının sinüs ve kosinüs terimlerini içermektedir. Endüktans matrisi değer olarak oldukça küçük olduğu için akı ifadesine olan etkisi yok sayılabilir. Bu nedenle, akı ifadesinin rotor açısının sinüs ve kosinüs terimlerini doğrudan verdiği varsayımı yapılabilmektedir. Stator akısı endüklenen gerilimin integralinin alınması sayesinde tahmin edilebilir. Fakat bu işlem doğrudan integral operatörü kullanılarak yapılamamaktadır. İntegrali alınan terimlerin zamanda değişken olmayan (DA) bileşenler içermesi ve başlangıç değerinin belirsizliği doğrudan integral operatörünün kullanımı sonucu karşılaşılan problemlerdendir.

Bunun yerine, aralarında türev operatörü bulunan iki adet alçak geçiren süzgeç kullanılmıştır. Süzgeçlerin zaman sabitleri yeterince büyük seçildiğinde, integral işlemini gerçekleştirmek ile beraber DA bileşenlerin temizlenmesini sağlamaktadır.

Açı ve hız tahmin algoritmalarının başarımının testi için MATLAB Simulink aracı kullanılmıştır. Bunun için bir alan yönlendirmeli kontrol sistemi modellenmiştir. Sistem modelinde motordan ölçülen üç faz akımları elektriksel açı tahmini ile Clarke ve Park dönüşümleri kullanılarak d-q eksen akımlarına dönüştürülmüştür. Referans d-q eksen akımları ile hesaplanan d-q eksen akımları arasındaki hatanın giderilmesi için d-q ekseninde referans gerilimleri çıkış olarak veren iki adet PI kontrolör kullanılmıştır. Referans gerilimi daha sonrasında ters Clarke ve ters Park dönüşümleri kullanılarak üç fazlı sistemin referans gerilimlerine dönüşütürülmüş ve statora uygulanmıştır. Hız kontrolü için sabit ivmelenmeye sahip bir referans rampa fonksiyonu kullanılmıştır. Hızlanma ve yavaşlama ayrı şekilde belirlenen ivmelenme değerlerinde rampanın kontrolü sağlanmıştır. Referans rampa ile tahmin edilen rotor hızı arasındaki hata çıkış limitasyonuna sahip bir PI kontrolörden geçirilerek referans q eksen akımı oluşturulmuştur.

Genişletilmiş endüklenen gerilim gözlemleyicisi motorun α-β koordinat sisteminde düzenlenmiş bir modeli üzerine kurulmuş bir blok olarak modellenmiştir. Ölçülen akımlar, uygulanan gerilimler ve rotor açısal hızının giriş olarak kullanıldığı bu blok tahmin edilen rotor elektriksel açısının sinüs ve kosinüs bileşenlerini içeren iki sinyali çıkış olarak vermektedir. Bu sinüs ve kosinüs sinyalleri ise bir açı takip gözlemleyicisinde, trigonometrik eşitliklerden faydalanarak açı hatasına dönüştürülmektedir. Açı hatasının sırasıyla PI kontrolör ve integratör bloğundan geçirilmesi sayesinde rotor açısal hızı ve konumunun elde edilmesi mümkün olmaktadır. Sürüş sisteminin başarımı yüksüz ve yüklü durumlarda incelenmiştir. Bununla birlikte ani yük değişimleri altında sistemin dinamik başarımı da gözlenmiştir. Açı tahmini ile rotorun gerçek açısı karşılaştırılarak sistemin dinamik ve yüksek hassasiyete sahip olduğu gözlenmiştir.

Stator akı tahmin algoritması motorun α-β koordinat sistemindeki matematiksel modelinden faydalanılarak kurulmuştur. Uygulanan faz gerilimleri, ölçülen faz akımları ve faz dirençleri kullanılarak her adımda endüklenen gerilim hesaplanmıştır. Bu endüklenen gerilimler ise alçak geçiren süzgeçler ve türev operatöründen oluşturulmuş olan integral bloğuna gönderilmektedir. İntegral bloğunun çıkışında ise rotor elektriksel açısının kosinüs ve sinüs terimlerini vermektedir. Açı takip gözlemleyicisi kullanılarak bu terimlerden açı ve hız bilgisinin elde edilmesi sağlanmıştır. Simülasyon sonuçlarında başlangıç anında oluşan DA bileşenlerin tahmin başarımını düşürdüğü gözlemlenmiştir. Alçak geçiren süzgeçler DA bileşenleri temizledikten sonra hız ve açı tahminleri hassas ve dinamik hale gelmektedir. Süzgeçlerin zaman sabitlerinin azaltılması sonucu başlangıç anındaki hız tahmin performansının arttığı görülmüştür. Fakat, kalıcı hal durumunda açı tahmininde kalıcı hal hatası oluşmaktadır. Akı tahmin algoritmasının sonuçları genişletilmiş endüklenen gerilim gözlemleyicisi ile kıyaslandığında yeterince hassas, dinamik ve gürbüz olmadığı belirlenmiştir. Bu nedenle deneysel testler için genişletilmiş endüklenen gerilim gözlemleyicisi seçilmiştir.

Gömülü sistem yazılımı IAR Embedded Workbench geliştirme ortamında tasarlanmıştır. Motor sürücü yazılımı birden çok sonlu durum makinası kullanılarak oluşturulmuştur. Üç fazlı eviricide kullanılacak anahtarlama frekansı ve akım kontrol döngüsünün sıklığı 16 kHz olarak seçilmiştir. Rotor zaman sabitinin akım zaman

sabitinden daha büyük olması nedeniyle hız kontrol döngüsünün sıklığı 200 Hz olarak seçilmiştir. Her anahtarlama döngüsünde bir yazılım kesmesi yaratılarak üç faz akım ölçümleri yapılmaktadır. Ölçülen üç faz akımlar daha sonrasında iki fazlı senkron döner düzleme dönüştürülüp bu düzlemde gerçeklenmiş olan hız kontrolörüne gönderilmektedir. Bu sayede q eksen akımının doğrudan kontrolü sağlanmaktadır. Genişletilmiş endüklenen gerilim gözlemleyicisi ve açı takip gözlemleyicisi ayrık zaman sistem fonksiyonları şeklinde geliştirilmiştir. Açık çevrim yol verme işlemi için açık çevrim hız rampası ve bu rampadan türetilmiş açık çevrim pozisyon bilgisi kullanılarak motorun 200 rpm'e kadar hızlanması sağlanmıştır.

Sürücü sisteminin doğrulanması için deneysel çalışmalar gerçekleştirilmiştir. 24 V, 62 W, 3000 rpm plaka değerlerine sahip olan bir motorun sürücü sistemi ile sürüşü gerçekleştirilmiştir. Motoru nominal yük seviyesinde yükleyebilecek bir test düzeneği oluşturulmuştur. Motora akuple bir generatörün çıkışına yerleştirilmiş üç fazlı köprü doğrultucu ve ayarlanabilir dirençten oluşan bu yükleme düzeneği ile yüksüz ve tam yükte çalışma durumlarında sistemin başarımı incelenmiştir. Sistem yüksüz durumdaki motoru 200 rpm ile nominal hız aralığında kontrol etmekle beraber alan zayıflatma yaparak 4000 devir/dk hızına çıkartabilmiştir. Ani yük değişiklikleri uygulanarak sistemin dinamik başarımı gözlenmiştir. Geçici ve kalıcı hal durumlarında sistemin kararlı ve dinamik olduğu görülmüştür.

1. INTRODUCTION

1.1 Background of Study

Electric motor driven systems became the backbone of the way of life we know today. Countless applications such as electricity generation, ventilating and air conditioning, industrial production lines, transportation, white and brown goods and even everyday use widgets of people now count on electric machines. It is estimated that half of the power generated globally is consumed by electric motors [1]. This percentage most certainly will increase more especially due to electric vehicles gaining more and more reputation along with the increasing accessibility for public. In many high-tech applications such as defense industry, aerospace, aviation and electric vehicles, nature of the application and sector requires using of the best performing technologies and components. This is primarily caused by these industries having a tight competition on performance and challenges faced. For some other industries such as white and brown goods and industrial applications, energy efficiency is not always the focus. For such industries, domestic and global regulations provide requirements on using of efficient and environment friendly technologies [2].

These requirements translate into electric drive systems as utilization of more efficient and reliable motors with efficient and smart drivers. This high-level specification on drive systems design is then followed as replacing old fashioned induction and DC motors with efficient permanent magnet motors.

Permanent Magnet Synchronous Motors (PMSM) count on permanent magnets placed on rotor for field flux generation. This eliminates using of field windings, slip rings and brushes. Thus, eliminating electrical and mechanical losses caused by resistance of field windings and friction between slip rings and brushes. These motors should have a rotating stator field synchronous to rotor field. Thus, using of a driver is necessary with such motors. Objective of the driver is to apply three-phase voltages to stator, which generates a field vector that is perpendicular to rotor field

vector in order to generate maximum torque and drive the motor in an efficient way. Nature of these drive systems require accurate rotor position information. This information can be obtained by utilizing sophisticated position sensors like Hall-effect sensors, encoders and resolvers. Although these sensors provide position information that is crucial for vector control, an undeniable burden comes with utilization of position sensors. Increased size, complexity and cost of motor production combined with the increased maintenance frequency due to position sensors, push designers and researches on developing methods of rotor position estimation without position sensors. In many products, especially home appliances, sensorless vector control is much appreciated and used. Any application that requires precision position information such as servo systems though cannot utilize such sensorless schemes.

Since its first introduction to literature, many different methods are developed for sensorless position estimation. One of which, depends on estimation of induced back-EMF voltage due to rotor field flux. These schemes use sophisticated observers for back-EMF and rotor position estimation and they are used intensively by many application design engineers and semiconductor companies [3-5].

1.2 Objectives and Organization of Thesis

This thesis covers the studies conducted for designing a sensorless vector control system for PMSM. Objectives of the thesis include sensorless position estimation of the rotor, independently controlling field and torque flux, operating the motor within nominal speed and nominal load range along with the field weakened reduced load range and ensure stable operation under load disturbances.

Two different position estimation methods are investigated. First, a Luenberger type observer is implemented for back-EMF estimation in two-phase stationary reference frame. Design of this observer model from motor mathematical model is explained in detail. Back-EMF signals then processed using an angle-tracking observer, which extracts rotor electrical position and speed. Then position estimation based on stator flux estimation method is analyzed in detail.

MATLAB Simulink tool is used for verification of position estimation schemes. Initial starting of the motor is done using open loop ramp. Operation of the machine

with no load, full load and transient changes in load is tested. The position and speed estimation is found accurate. System remained stable under load disturbances. Speed and position estimation performance of both methods are compared. It is seen that extended back-EMF observer is more accurate and dynamic. Stator flux estimation method caused estimation errors at initial start due to initial offset, which is then cleared by the low pass filters.

A three-phase inverter development board is obtained from market. In order to control the inverter board, a controller stage is designed for this study. Schematics design is done considering the necessary external peripherals for the microcontroller. Printed circuit board (PCB) design is done as a two-layer board that can be used as a plug-in module with the inverter board. Extended back-EMF observer model is transformed into discrete time equations and developed as embedded software functions. Open loop startup is achieved using alignment and a speed ramp. Position information is generated from this speed ramp until rotor estimated speed reaches 200 rpm. Beyond this point, motor is driven with close loop speed control.

Laboratory experiments are conducted in a test setup. Operation in nominal speed range with no load and full load as well as transient loading is tested. Operation beyond nominal speed is achieved by field weakening. Drive system responded fast and maintained stable operation under load disturbances.

Organization of the thesis is as follows;

Chapter 1 gives the general information regarding the background and motivation of the study along with a review on literature.

Chapter 2 explains theory of operation and modeling of PMSM.

Chapter 3 presents the theory of vector control and its application on PMSM.

Chapter 4 explains the design phase of the study. Hardware and software design steps are presented in this chapter.

Experimental results are given in Chapter 5. These results are obtained by conducting laboratory experiments with a test setup created for the study.

Chapter 6 gives the conclusion of the study and summarizes design steps and results with certain techniques to improve the study further.

1.3 Literature Review on Advanced Control Methods of AC Motors

For years, AC motors have been used in very wide applications in the industry. Its reliable operation, low maintenance requirements, low costs and simple operation resulted in AC machine having no competitor for most of the applications throughout the years. However, due the technological improvements in almost any field of the industry required smarter use of electric motors. This necessity caused variable frequency inverters to catch attention. Combining these inverters with advanced speed and torque controllers, reliable and high performance operation of AC motors was obtained thanks to very fast response of these controllers in dynamic and steady state operation.

With the growth of semiconductor material technology and electronic devices, variable speed drivers became an option with little expensiveness [6]. The maturity of AC motor's literature also provided a ground for research in advanced control methods. One disadvantage of the AC motors over DC motors is the high-order nonlinear dynamic characteristic and lack of an accurate and simple approximation for modeling the machine analytically, as investigated by Robert G. Schieman [7]. Many approaches have been proposed. These include computer simulations [8], analysis with complex variables [9], and transfer functions [10].

Approaches consisting of different reference frame analysis are also proposed [11]. One of the most well-known and appreciated method is Field Oriented Control (FOC) proposed by F. Blaschke in early 1970s. The FOC provided the ability of controlling torque and field current independently [12]. This ability was considered as one of the advantageous features of DC motors due to their torque and flux being decoupled. Control of the motor is implemented in rotating reference frame and thus, this control method uses vector transformations between stationary and rotating reference frame [13]. FOC has proven its virtue over scalar control in terms of dynamic behavior. G.O Garcia et al. compared FOC and scalar control with same hardware experiments, showing that FOC has a wider and flatter bandwidth while scalar control gives poor speed response performance with oscillations during transients [14].

Controlling the machine in rotating reference frame required accurate rotor flux information. This information was used in order to decouple torque component of the

stator current from the flux component. Blaschke's patented method of obtaining the control vector angle depended on directly sensing rotor flux and speed [15]. Thus, it was called as direct FOC. Hasse however, developed the indirect FOC method by utilizing calculation of the rotor flux. His method eliminated the requirement of the rotor flux sensors nevertheless rotor speed, voltage and current sensors were still required along with the accurate motor parameters. These known values are then used in order to compute rotor flux [16]. It is obvious that this is a feed-forward system unlike the feedback structure of direct FOC. Although it is simpler to implement, motor parameters have to be defined as accurate as possible to compute rotor flux properly [17].

Being highly dependent on the motor parameters is a major issue of the indirect FOC method. Change of the stator resistance due to temperature and stator inductance due to saturation during operation can reduce the performance of drive system. Use of incorrect parameters might then result in transient oscillations and steady state error of the computed state variables [18]. Many studies were done with the goal of overcoming this issue and developing new techniques [19]. L.J Garces proposed one of the first in early 1980's. He defined a way of adaptation of the change in rotor time constant. This parameter was important to compute slip frequency in induction motors [20]. T. Matsuo and T.A Lipo have utilized injection of a defined negative current perturbation, which is then sensed as negative voltage and decomposed. This allowed online resistance measurements to be made on the machine [21]. The proposed scheme however, caused generation of inverse electromagnetic force and second order harmonics that lead to detract from a smooth torque output. Koyama et al. presented a new technique in which they utilized stator voltage and current sensors to obtain actual stator resistance. This way, the need of a stator resistance calculation or integration is eliminated and accurate identification of rotor time constant is achieved [22]. The downside is the cost burden due to additional voltage sensors. Extraction of the fundamental voltage signal was also difficult due to high frequency PWM signals. Methods using Model Reference Adaptive Control (MRAC) for parameter identification were also presented [23, 24]. These schemes use a controller structure, which continuously update machine model in order to compensate with the changes in parameters. This is achieved by implementing the machine model inside the controller and continuously calculating the model

reference error with the help of actual measurements from the system. Block scheme for MRAC is given in Figure 1.1

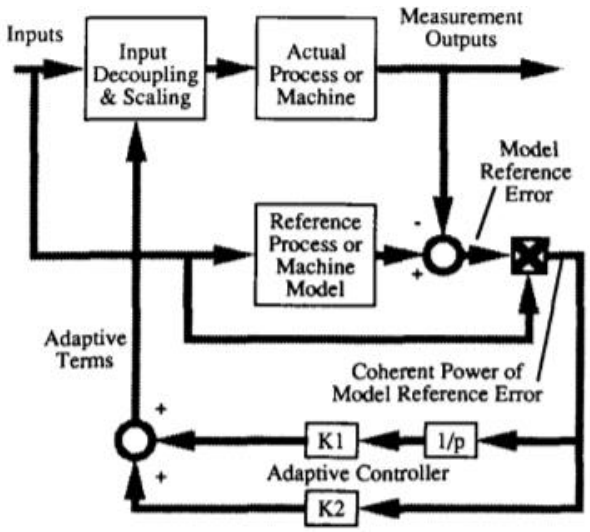

Figure 1.1 : MRAC block scheme [23].

C. Liu used a slip compensation method for a current source inverter used for FOC. Benefit of using a slip compensator is the reduced torque pulsations in the low speed operation [25]. Nonetheless, the modified algorithm requires a more complicated control scheme.

Along with the developments made on FOC, a new control method was being developed in the late 1980's called Direct Torque Control (DTC) or Direct Self Control (DSC)[26]. It was introduced as an alternative control method to FOC for induction machines [27, 28]. I. Takahashi stated his new control method as being a "quick-response and high efficiency" control. DTC differs from FOC by requiring of neither a current control loop nor vector transformations and space vector modulation (SVM) but explicit torque/flux regulators. Moreover, DTC does not necessitate rotor position sensing. This sole feature itself greatly simplifies the control complexity. Even though it is considered as simple, DTC can achieve sufficient torque performance [29]. With that said, it should be noted that DTC brings several drawbacks as well. These drawbacks can be listed as, devolving performance during low speed operation caused by torque and current ripple along with the variable switching frequency and degradation in control ability. Since its introduction, many researches were conducted in order to propose solutions to these disadvantageous features of DTC. Habetler et al. implemented the space vector modulation in DTC. This technique provided a fixed frequency operation while maintaining the torque

control characteristics [30]. Several different schemes were proposed regarding of modulation used in DTC. One of which, modulates duty ratio to create voltage vectors. The results show that torque ripple is greatly decreased [31]. Computing the duty ratio was also an optimization problem, which became the subject of several studies [32, 33].

Since the introduction of FOC, an advanced motor control method that does not necessitate rotor position or speed sensors was the wish of many scientists and engineers. This was mainly due to shaft sensors bringing complexity in hardware manner and difficulty in space constraint applications. Sensorless vector control made its way to literature in late 1980's especially emerging from T. Ohtani's studies [34]. In his proposed method, a rotor flux estimator with a lag circuit imposing the induced voltage of motor and command of the rotor flux, thus enabling calculation of rotor flux even at standstill. He also states his method as being less dependent to motor parameters than conventional vector control strategies. Systems utilizing MRAC were also developed for speed estimation from measured voltage and current values [35]. Estimated speed is then used as feedback of the vector control system. MRAC based systems contain pure integrators that are affected from resistance change due to thermal variations. F.Z Peng proposed a new method of estimating rotor speed without using pure integrations and knowledge of stator resistance value [Peng]. His method was depending on instantaneous reactive power of the rotor flux and proved itself by being robust against parameter variations and achieving wider bandwidth. J. Holtz and J. Quan used a pure integrator for stator flux estimation [36]. With the help of a nonlinear inverter model, their model self-adjusted voltage distortions while drift components were compensated by offset identification. This method shown high dynamic performance even at very low speeds but unable to estimate speed at near standstill points.

An additional emphasis should be laid on position estimation schemes used in sensorless vector control. Various types of observers, state filters and controllers are proposed as position estimators. Luenberger type observers can be used in such schemes, providing observation of system state vector while identifying the system parameters [37]. In this case, extended Luenberger observer is utilized for a nonlinear dynamical system and it observes rotor flux while identifying rotor time constant simultaneously. Elmas and La Parra have used an extended Luenberger

observer for speed and position estimation in a switched reluctance motor drive [38]. They have implemented the controller inside a Texas Instruments' digital signal processor and successfully controlled the drive. Kim and Sul proposed of using a reduced order observer to estimate induced back-EMF of a PMSM in rotating reference frame [39]. Due to lack of back-EMF resolution in low speed regions, this study covered the speed range of 150 to 2500 RPM.

Estimation of rotor position from flux linkages that are obtained by the use of integrators are also presented [40]. The problem with these schemes is that integration drift and offset may eventually degrade the estimator performance. Using of an Extended Kalman Filter (EKF) is proposed to eliminate the errors caused by these drifts and offsets [41]. Qiu, Wu and Kojori demonstrated a robust controller for PMSM based on EKF in 2004 [42]. Structure of the EKF is given in Figure 1.2.

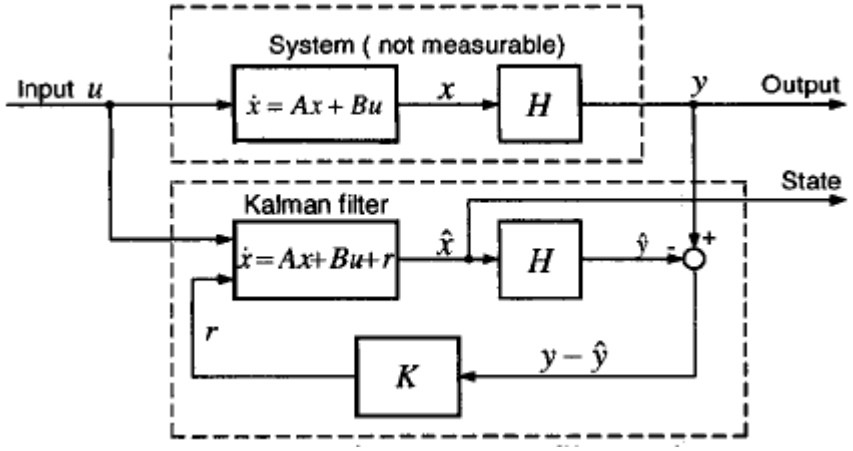

Figure 1.2 : Structure of EKF [42].

Though EKF performs well under nominal conditions, this method has issues at startup due to divergence of the EKF estimator. Moreover, computational complexity of EKF is also a burden to processing power in the digital controller side.

Use of Sliding Mode Observers (SMO) is proposed for electric drives due to their nature of reducing order, disturbance rejection and parameter insensitivity [43]. Robustness of the controller is supported by the use of adaptive methods in a Brushless DC Motor (BLDC) driver, which filled the gaps of unfavorable aspects of EKF [44]. SMO is further investigated in drive systems of PMSM for back-EMF estimation [45]. Adaptive SMO for rotor speed estimation is given as a block scheme in Figure 1.2.

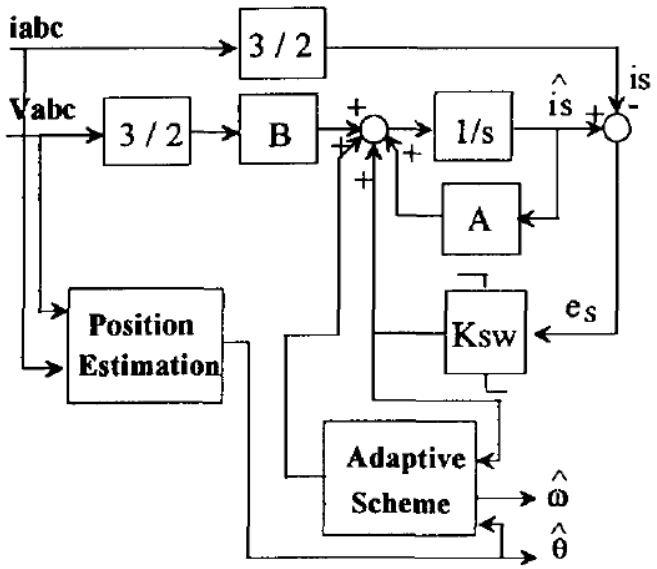

Figure 1.3 : Adaptive SMO for rotor speed estimation [45].

To further reduce computational burden on the controller, an easily implementable sliding mode controller is presented based on Lyapunov stability criteria [46].

Although the fundamental model based methods achieved a good performance over the nominal operating conditions, zero to low speed operation of these methods still suffer from lack of resolution, causing open loop startup schemes to be used. Saliency based methods are proposed to overcome this issue. These schemes utilize injection of a high frequency signals into machine. Schroedl proposed his method of rotor position detection of a standstill PMSM [47]. Idea of the proposed method is to apply a test voltage phasor and simultaneously observe the measured current phasor. Change of the current phasor according to applied voltage phasor will be affected by rotor position. This is caused by the saliency of the rotor and saturation due to permanent magnets placed on the rotor. Injected signals can be generated by various methods. Schroedl used discrete voltage pulses for reluctance motor [48]. Signal injection method can be used not only in standstill but also in normal operation to estimate rotor position online. This however, brings some limitations over the signal that is injected. These signals should be identified from the measured and decomposed current components. Thus, they have to be defined independently from the voltage vector applied to the stator. This brings an upper and lower limit to frequency of the signals to be injected. At maximum rotational speed, these signals should not have a frequency that is less than the frequency of the driving voltage vector. Upper limit of injected signal frequency is defined by PWM frequency [49].

Signal injection methods are divided into two categories. P.L. Jansen, R.D. Lorenz, F. Briz and many researchers used constant amplitude, rotating signal that is injected to stationary reference frame [50-52]. Second method is to apply amplitude-modulated signals into synchronous reference frame [53, 54]. Briz showed that injecting zero-sequence carrier signals into stationary reference frame could be problematic due to filters necessary to filter out third harmonics of the fundamental excitation from the measured signal. The phase distortion caused by the filters should be compensated [55]. Xu and Zhu proposed of utilizing zero-sequence pulsating signal injection into synchronous reference frame [56]. This method proved being more robust since the signal is amplitude modulated by saliency and thus phase shifts are eliminated. This method combines the high bandwidth and robust zero-sequence method with the more accurate and more dynamic method of pulsating injection.

2. THEORY AND MATHEMATICAL MODEL OF PERMANENT MAGNET SYNCHRONOUS MOTORS

2.1 Structure of Permanent Magnet Synchronous Motors

Structure of PMSM is quite similar to induction motors. It has a stator that is made of laminated stacks due to alternating current behavior in order to limit eddy currents. Stator consists of three-phase windings. Stator structure of a PMSM is identical to an induction machine stator as given in Figure 2.1.

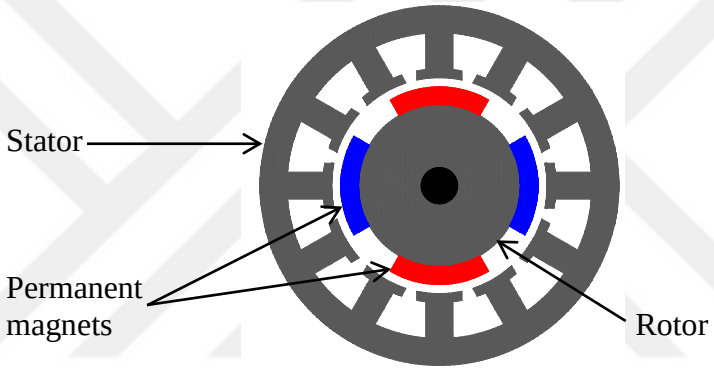

Figure 2.1 : Structure of a PMSM.

Rotor of the PMSM has permanent magnets mounted on it in order to generate field flux instead of the rotor windings used on a synchronous motor. Replacement of the filed windings with permanent magnets means absence of the excitation losses. Thus, a PMSM will have higher efficiency than a synchronous motor. Permanent magnets provide higher magnetic flux density inside the air-gap thus increasing the dynamic performance along with the torque output.

There is a variety of different PMSM structure types as given in a simplified diagram in Figure 2.2. These types can be divided into two regarding the direction of the field flux. These are radial flux and axial flux motors.

2.1.1 Radial flux motors

Radial flux means that the direction of field flux of the machine is perpendicular to the shaft. Most of the motors will have radial flux structure. Higher power outputs are achievable by the increasing the stack size of the motors.

According to the placement of rotor and stator, PMSM can be divided into two distinct types. These are called as inner rotor type and outer rotor type.

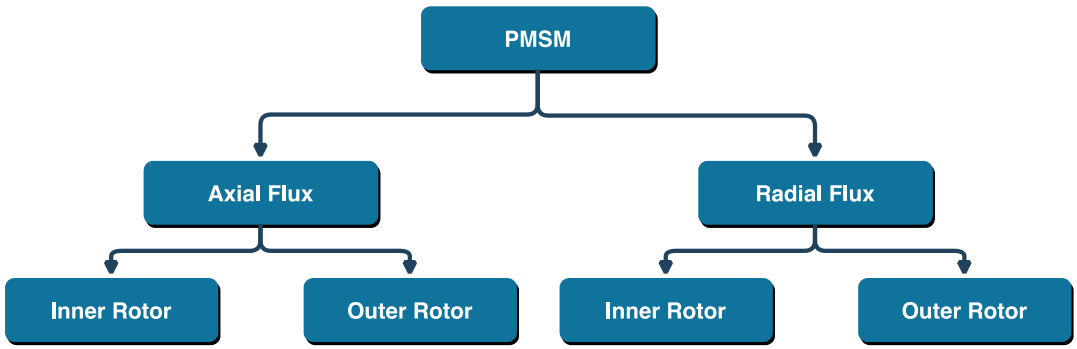

Figure 2.2 : Different types of PMSM regarding motor structure.

2.1.1.1 Inner rotor type

An inner rotor PMSM has its rotor placed inside the stator and held by bearings in both sides. Permanent magnets are magnetized radially and poled alternately. Due to magnet pole area being smaller than pole are on the rotor surface, open circuit flux density is less than the flux density of the magnet itself. In this structure, magnets are protected against centrifugal forces and thus the machine can operate at very high speeds without the risk of magnets coming off.

Due to small diameter of the rotor, their inertia is small. This leads to better dynamic performance in terms of acceleration and transient response. Since the stator windings are placed outer frame, thermal performance of the machine increases with simple cooling mechanisms.

Placement of the permanent magnets into rotor affects machine's characteristics. Thus, different rotor designs exist as given in Figure 2.3. Most used types are surface, spoke and buried permanent magnet rotors.

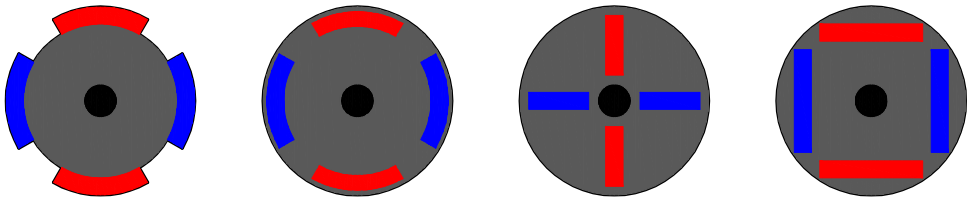

Figure 2.3 : Different rotor types of PMSM as surface mount, inset, spoke type and barrier type respectively.

Inner rotor PMSM are generally used in applications where high output power, fast transient response is necessary and higher speeds are demanded. These can be listed as industrial servo systems, pumps, traction systems and electric vehicles.

2.1.1.2 Outer rotor type

Outer rotor motors have the stator inside the machine, while having the rotor fixed to outer surface of the machine. Rotor usually utilizes an external high conductivity non-ferromagnetic cylinder that protects the magnets against demagnetization and centrifugal forces as well as providing an asynchronous starting torque. This cylinder also acts as a damper and thus improves smoothness of the output. Structure of an outer rotor PMSM is given in Figure 2.4.

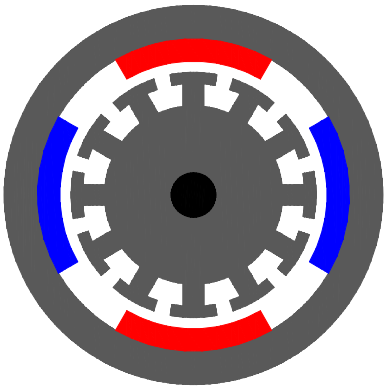

Figure 2.4 : Structure of an outer rotor PMSM.

Due to big rotor diameter, this type of motors has higher inertia than inner rotor types. This feature allows very precise control and smooth operation in terms of speed.

Outer rotor type PMSM is used generally in applications that require precise speed control with small ripple such as hard disk and compact disk drives and drones. These types of motors are also used in applications in which direct drive of the load is preferred with reduced volume of the drive systems. These applications include gimbal motors and light electric vehicle motors such as electric bicycles, scooters and load carrier vehicles.

2.1.2 Axial flux motors

Axial flux machines have the direction of permanent magnet flux in parallel with axis of the shaft. Axial motors have higher torque density and smaller volume

compared to radial flux motors. They can provide high torque output and low speeds essentially eliminating the use of redactors in applications that desire low speed but high torque operation. These applications include traction motors and electric vehicles. Axial flux motors also divide into two regarding the placement of the rotor. Figure 2.5 shows an axial PMSM structure with the stator placed between two rotors.

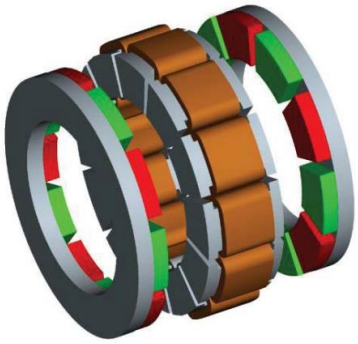

Figure 2.5 : Structure of an Axial PMSM [57].

2.2 Mathematical Model of Permanent Magnet Synchronous Motors

Electrical circuit model of PMSM is given in Figure 2.6. R_S and L_S are resistance and inductance of each phase.

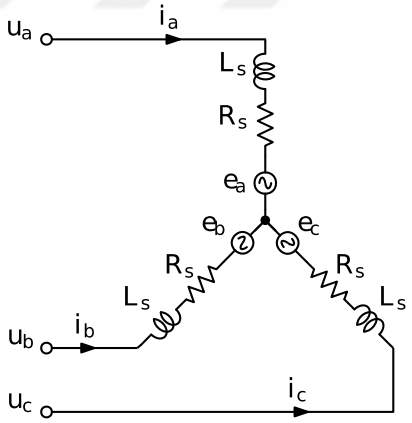

Figure 2.6 : Electrical model of PMSM.

The three-phase permanent magnet synchronous motor can be mathematically modeled with the phase voltages expressed as in equation 2.1

$$\begin{bmatrix} u_a \\ u_b \\ u_c \end{bmatrix} = R_S \begin{bmatrix} i_a \\ i_b \\ i_c \end{bmatrix} + \rho \begin{bmatrix} \psi_a \\ \psi_b \\ \psi_c \end{bmatrix} \tag{2.1}$$

Where;

u_a, u_b and u_c are the three-phase voltages,

i_a, i_b and i_c are the three-phase currents,

Ψ_a, Ψ_b and Ψ_c are the flux linkages.

ρ is the derivative operator.

Three-phase flux linkages are expressed in equation 2.2.

$$\begin{bmatrix} \psi_a \\ \psi_b \\ \psi_c \end{bmatrix} = [L] \begin{bmatrix} i_a \\ i_b \\ i_c \end{bmatrix} + \psi_{PM} \begin{bmatrix} \cos(\theta_e) \\ \cos(\theta_e - 2\pi/3) \\ \cos(\theta_e + 2\pi/3) \end{bmatrix} \tag{2.2}$$

The inductance matrix *[L]* is expressed as given in equation 2.3.

$$[L] = \begin{bmatrix} L_a & M_{ab} & M_{ac} \\ M_{ab} & L_b & M_{bc} \\ M_{ac} & M_{bc} & L_c \end{bmatrix} \tag{2.3}$$

Where;

M_{ab}, M_{ac} and M_{bc} are the mutual inductances,

L_a, L_b and L_c are the self-inductance of the phases,

Ψ_{PM} is the flux linkage of the permanent magnets,

θ_e is the rotor electrical position.

Phase voltages can be expressed as given in equation 2.4 after substituting flux linkages given in equation 2.2.

$$\begin{bmatrix} u_a \\ u_b \\ u_c \end{bmatrix} = R_S \begin{bmatrix} i_a \\ i_b \\ i_c \end{bmatrix} + \rho[L] \begin{bmatrix} i_a \\ i_b \\ i_c \end{bmatrix} + [L] \cdot \rho \begin{bmatrix} i_a \\ i_b \\ i_c \end{bmatrix} + \begin{bmatrix} e_a \\ e_b \\ e_c \end{bmatrix} \tag{2.4}$$

Where;

e_a, e_b and e_c are induced back-EMF voltages of phase a, b and c which are expressed as given in equation 2.5.

$$\begin{bmatrix} e_a \\ e_b \\ e_c \end{bmatrix} = \omega_e \cdot \psi_{PM} \cdot \rho \begin{bmatrix} \cos(\theta_e) \\ \cos(\theta_e - 2\pi/3) \\ \cos(\theta_e + 2\pi/3) \end{bmatrix} \tag{2.5}$$

Maximum torque is generated when stator field vector is perpendicular to flux linkage of permanent magnets. Considering only the fundamental signals, generated torque on the machine air gap is expressed in equation 2.6.

$$T_e = \frac{i_a \cdot e_a}{\omega_e} + \frac{i_b \cdot e_b}{\omega_e} + \frac{i_c \cdot e_c}{\omega_e} \tag{2.6}$$

Where;

ω_e is the electrical speed of rotor,

T_e is the electrical torque generated in air gap.

In this expression, phase back-EMF waveforms are generated according to winding distributions on the stator and the generated flux according to magnetization technique used on permanent magnets. Stator windings of a PMSM are usually distributed in such a way to generate sinusoidal back-EMF voltage. For the torque equation, phase currents and back-EMFs should match. Otherwise, torque ripple can be generated on the output that is not desired. In order to maintain a smooth torque output, phase currents has to be generated sinusoidal.

Electrical torque in the air gap can be coupled with mechanical characteristics of the machine in order to compute operating point of the machine as given in equation 2.7.

$$J_m \cdot \frac{d}{dt}\omega_e = T_e - T_L - B_m \cdot \omega_e \tag{2.7}$$

Where;

J_m is mechanical inertia,

B_m is viscous friction coefficient

T_L is mechanical load applied on the shaft

2.2.1 Vector transformations

Expressing the machine in three-phase system can be complex as shown in mathematical model of the machine in equations 2.2, 2.3 and 2.4. The expressions will become even more complex if controllers and estimators are introduced into three-phase model. Thus, it is necessary to utilize certain transformations to decrease the complexity and computation burden.

Since a star-connected three-phase stator will have phase variables depending on each other, this system can be reduced and modeled as a two-phase system. The transformation given in equation 2.8 is Clarke transformation, which is obtained when I_α is superposed with I_a of the original transformation matrix [58]. It transforms the three-phase variables into two-phase variables. The transformation is done in stationary reference frame. That means in steady state operation, α and β variables will change according to rotor position. In fact, α and β variables have sinusoidal waveform with 90° phase shift that represents three-phase variables a, b and c.

$$\begin{bmatrix} f_\alpha \\ f_\beta \end{bmatrix} = \frac{2}{3} \begin{bmatrix} 1 & \cos\left(\frac{2\pi}{3}\right) & \cos\left(\frac{4\pi}{3}\right) \\ 0 & \sin\left(\frac{2\pi}{3}\right) & \sin\left(\frac{2\pi}{3}\right) \end{bmatrix} \cdot \begin{bmatrix} f_a \\ f_b \\ f_c \end{bmatrix} \tag{2.8}$$

The inverse Clarke transformation given in equation 2.9 provides transformation of two-phase variables with stationary reference frame into three-phase variables [58].

$$\begin{bmatrix} f_a \\ f_b \\ f_c \end{bmatrix} = \frac{2}{3} \begin{bmatrix} 1 & 0 \\ \cos\left(\frac{2\pi}{3}\right) & \sin\left(\frac{2\pi}{3}\right) \\ \cos\left(\frac{4\pi}{3}\right) & \sin\left(\frac{2\pi}{3}\right) \end{bmatrix} \cdot \begin{bmatrix} f_\alpha \\ f_\beta \end{bmatrix} \tag{2.9}$$

Representation of three-phase currents in two-phase stationary reference frame is shown on the space vector diagram given in Figure 2.7. In this representation, the current vector that has the two components i_α and i_β is rotating with speed ω_e with reference to α-β axis.

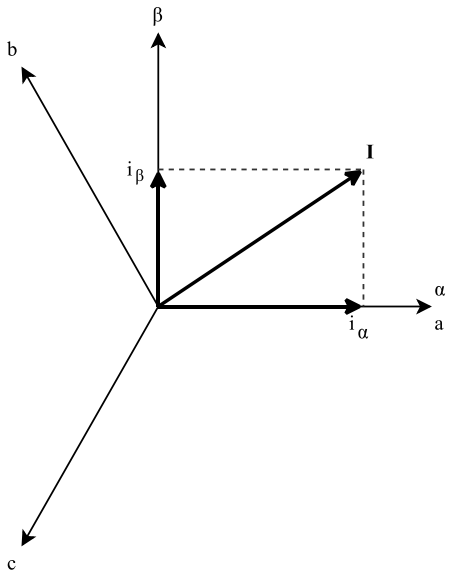

Figure 2.7 : Stator current vector in abc and αβ coordinate system.

Another special transformation comes in handy when modeling the machine that transforms 2 phase stationary reference frame variables into 2 phase synchronous reference frame variables. This is called synchronous reference frame due to its fictitious dq axis being locked with machine's rotor. In steady state operation, this axis rotates with speed ω_e and in phase with electrical position. The transformation is called Park transformation and given in equation 2.10 [59].

$$\begin{bmatrix} f_d \\ f_q \end{bmatrix} = \begin{bmatrix} \cos(\theta) & \sin(\theta) \\ -\sin(\theta) & \cos(\theta) \end{bmatrix} \cdot \begin{bmatrix} f_\alpha \\ f_\beta \end{bmatrix} \tag{2.10}$$

Inverse Park transformation given in equation 2.11 is used to transform d-q axis variables back into α-β axis variables [59]. This transformation is useful when control of the machine is done in d-q axis. Reference variables on the output of the controller should be transferred into α-β axis reference variables, which are then transferred into applied three-phase voltages via space vector modulated three-phase inverter.

$$\begin{bmatrix} f_\alpha \\ f_\beta \end{bmatrix} = \begin{bmatrix} \cos(\theta_r) & -\sin(\theta_r) \\ \sin(\theta_r) & \cos(\theta_r) \end{bmatrix} \cdot \begin{bmatrix} f_d \\ f_q \end{bmatrix} \tag{2.11}$$

Space vector diagram given in Figure 2.8 shows the relationship between two-phase stationary reference frame and two-phase synchronous reference frame according to electrical position.

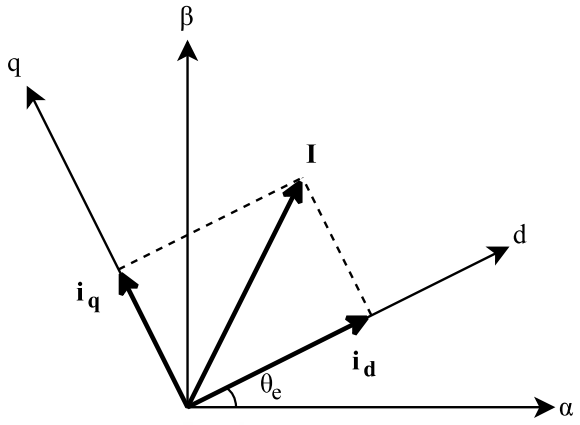

Figure 2.8 : Stator current vector in abc and αβ coordinate system.

2.2.2 PMSM in stationary reference frame

Phase variables of u_α and u_β can be expressed as scalar variables in α-β axis as given in equation 2.12.

$$\begin{bmatrix} u_\alpha \\ u_\beta \end{bmatrix} = \begin{bmatrix} R_S & 0 \\ 0 & R_S \end{bmatrix} \cdot \begin{bmatrix} i_\alpha \\ i_\beta \end{bmatrix} + \begin{bmatrix} 1 & 0 \\ 0 & 1 \end{bmatrix} \cdot \rho \begin{bmatrix} \psi_\alpha \\ \psi_\beta \end{bmatrix} \tag{2.12}$$

A surface permanent magnet machine will have direct and quadrature inductances L_d and L_q almost equal. Interior magnet type machines will have saliency on the rotor, thus direct and quadrature inductances will have large difference. To introduce machine saliency into flux linkage expression, following approaches given in equation 2.13 and 2.14 are used for expressing saliency and mean inductance.

$$L_\Delta = \frac{L_d - L_q}{2} \tag{2.13}$$

$$L_0 = \frac{L_d + L_q}{2} \tag{2.14}$$

Saliency introduced flux linkage expression is given in equation 2.15.

$$\begin{bmatrix}\psi_\alpha\\ \psi_\beta\end{bmatrix}=\begin{bmatrix}L_0+L_\Delta\cos(2\theta_e) & L_\Delta\sin(2\theta_e)\\ L_\Delta\sin(2\theta_e) & L_0-L_\Delta\cos(2\theta_e)\end{bmatrix}\cdot\begin{bmatrix}i_\alpha\\ i_\beta\end{bmatrix}+\psi_{PM}\cdot\begin{bmatrix}\cos(\theta_e)\\ \sin(\theta_e)\end{bmatrix} \tag{2.15}$$

Phase voltage equation is then rearranged as given in equation 2.16 with substitution of flux linkages given in equation 2.15.

$$\begin{bmatrix}u_\alpha\\ u_\beta\end{bmatrix}=\begin{bmatrix}R_S & 0\\ 0 & R_S\end{bmatrix}\cdot\begin{bmatrix}i_\alpha\\ i_\beta\end{bmatrix}+[L]\cdot\rho\begin{bmatrix}i_\alpha\\ i_\beta\end{bmatrix}$$
$$+\omega_e\left(2L_\Delta\cdot\begin{bmatrix}-\sin(2\theta_e) & \cos(2\theta_e)\\ \cos(2\theta_e) & \sin(2\theta_e)\end{bmatrix}+\psi_{PM}\cdot\begin{bmatrix}\cos(\theta_e)\\ \sin(\theta_e)\end{bmatrix}\right) \tag{2.16}$$

In this expression, machine inductance matrix is expressed as given in equation 2.17.

$$[L]=\begin{bmatrix}L_0+L_\Delta\cos(2\theta_e) & L_\Delta\sin(2\theta_e)\\ L_\Delta\sin(2\theta_e) & L_0-L_\Delta\cos(2\theta_e)\end{bmatrix} \tag{2.17}$$

In α-β axis, electrical torque generated in the air gap is expressed as given in equation 2.18.

$$T_e=\frac{3}{2}\cdot 2p\cdot\left(\psi_\alpha\cdot i_\beta+\psi_\beta\cdot i_\alpha\right) \tag{2.18}$$

Where;

p is the number of pole pairs.

Since the model is created with saliency introduced, it is wise to express the torque generated due to saliency and include it as a part of total torque. Due to saliency in the rotor, permanent magnets will intend to align the rotor in such a way to achieve minimum reluctance in flux path. This torque is referred as reluctance torque, it is the main torque component of a switched or synchronous reluctance motor and permanent magnet assisted synchronous reluctance motors. Reluctance torque is expressed in α-β axis as given in equation 2.19.

$$T_{rel}=\frac{3}{2}\cdot 2p\cdot\left(-L_\Delta\cdot i_\alpha\cdot i_\beta\cos(2\theta_e)-\frac{1}{2}\left(i_\alpha{}^2+i_\beta{}^2\right)\sin(2\theta_e)\right) \tag{2.19}$$

Synchronous torque, generated due to flux of permanent magnets and generated flux of phase currents is given in equation 2.20.

$$T_{syn} = \frac{3}{2} \cdot 2p \cdot \psi_{PM} \cdot \left(i_\beta \cos(\theta_e) + i_\alpha \sin(\theta_e) \right) \tag{2.20}$$

Total electrical torque of the machine is composed of these two components and is expressed as given in equation 2.21.

$$T_e = T_{rel} + T_{syn} \tag{2.21}$$

2.2.3 PMSM in rotating reference frame

Stator voltage equation of the motor is obtained using Clarke and Park transformations on the fundamental model with the assumption of angle input of the Park transformation is rotor electrical angle. This way, obtained d-q axis variables are defined in a synchronous rotating reference frame. Stator voltages expressed with currents and flux linkages as given in equation 2.22.

$$\begin{bmatrix} u_d \\ u_q \end{bmatrix} = \begin{bmatrix} R_S & 0 \\ 0 & R_S \end{bmatrix} \cdot \begin{bmatrix} i_d \\ i_q \end{bmatrix} + \begin{bmatrix} 1 & -\omega_e \\ \omega_e & 1 \end{bmatrix} \cdot \rho \begin{bmatrix} \psi_d \\ \psi_q \end{bmatrix} \tag{2.22}$$

Flux linkage variables in d-q axis are expressed as given in equation 2.23. Machine saliency is introduced in this expression by the use of direct and quadrature inductances L_d and L_q.

$$\begin{bmatrix} \psi_d \\ \psi_q \end{bmatrix} = \begin{bmatrix} L_d & 0 \\ 0 & L_q \end{bmatrix} \cdot \begin{bmatrix} i_d \\ i_q \end{bmatrix} + \psi_{PM} \cdot \begin{bmatrix} 1 \\ 0 \end{bmatrix} \tag{2.23}$$

This flux linkage expression given in equation 2.23 is then substituted into the stator voltage equation as given in equation 2.24.

$$\begin{bmatrix} u_d \\ u_q \end{bmatrix} = \begin{bmatrix} R_S & -\omega_e L_q \\ \omega_e L_d & R_S \end{bmatrix} \cdot \begin{bmatrix} i_d \\ i_q \end{bmatrix} + \begin{bmatrix} L_d & 0 \\ 0 & L_q \end{bmatrix} \cdot \rho \begin{bmatrix} i_d \\ i_q \end{bmatrix} + \omega_e \cdot \psi_{PM} \cdot \begin{bmatrix} 0 \\ 1 \end{bmatrix} \tag{2.24}$$

Electromagnetic torque can be obtained by a simple expression of flux linkages and currents as given in equation 2.25.

$$T_e = \frac{3}{2} \cdot 2p \cdot \left(\psi_d \cdot i_q - \psi_q \cdot i_d \right) \tag{2.25}$$

Equation 2.26 is obtained when flux linkages of direct and quadrature axis are substituted with equation 2.23.

$$T_e = \frac{3}{2} \cdot 2p \cdot \left(\left(L_d - L_q \right) \cdot i_d \cdot i_q + \psi_{PM} \cdot i_q \right) \tag{2.26}$$

Again, assuming a salient pole machine, electromagnetic torque consists of two components as given in equation 2.27.

$$T_e = T_{rel} + T_{syn} \tag{2.27}$$

Where, synchronous torque can be expressed only by the quadrature axis current as given in equation 2.28.

$$T_{syn} = \frac{3}{2} \cdot 2p \cdot \left(\psi_{PM} \cdot i_q \right) \tag{2.28}$$

While the reluctance torque is expressed by machine saliency as given in equation 2.29.

$$T_{rel} = \frac{3}{2} \cdot 2p \cdot \left(\left(L_d - L_q \right) \cdot i_d \cdot i_q \right) \tag{2.29}$$

In a permanent magnet synchronous motor, most of the torque will be generated due to quadrature axis current. Thus, it is fair to assume quadrature axis current i_q will represent and control the torque output of the machine itself. However, it should be noted that in a highly salient machine as per MTPA approach, direct axis current i_d has to be utilized to generate maximum torque. For most of the applications that use low saliency machines, i_d is kept zero in operations below nominal speed and torque is generated and measured solely by i_q.

3. CONTROL OF PERMANENT MAGNET SYNCHRONOUS MOTORS

State of the art PMSM drive systems utilize three different control methods. They can be categorized into two as scalar and vector control. Scalar control method utilized for PMSM is referred as V/f control. Most used types of vector control methods are divided into two as FOC and DTC.

V/f control method does not use a feedback system. Instead, 120° phase shifted three-phase AC voltage is applied to the stator as an open loop system. Speed adjustment is achieved by keeping a constant ratio between amplitude and frequency of the voltages applied. This control method consists of three regions for operation. Compensation region covers the standstill to low speed operation of the machine, where voltage amplitude and frequency is small. In this region, voltage drop across phase windings and switch elements on the inverter is not negligible. Thus, higher voltage amplitude has to be applied in order to compensate for voltage drops. Once the machine is started up, linear control region is entered. This is where the constant ratio between amplitude and frequency is applied up to nominal speed. Beyond nominal speed, further increasing of voltage amplitude is not applicable due to risk of damaging insulations of the windings. Thus, field weakening operation is achieved by increasing only the frequency of applied voltages.

Scalar control is a simple control method to implement. It does not require complex and trigonometric calculations, thus a higher performing controller is not necessary. Scalar control of PMSM is generally used in applications that do not require good dynamic control of the machine such as fans. Stability issues also arise in high frequency operation. Speed stabilizing loops are necessary in such schemes for better performance [60].

FOC transforms machine from three-phase stationary reference frame into two-phase rotating reference frame. Thus, enabling independent control of torque and field flux components of the motor current. Two current controllers are used for d-q axis current control. Speed controller creates torque current reference. Generation of stator voltage vector is done using SVM. FOC requires rotor position and speed

information. Reference frame transformations and high sampling rate current measurements require more processing power than V/f control schemes. FOC ensures a smooth speed controlled system with fast dynamic response. Current and speed controllers utilize linear PI controllers. This makes tuning of the driver simple. Motor parameters and system parameters regarding to the application is taken into consideration while driver is tuned.

DTC is based on controlling torque and flux of the motor independently. Instead of linear controllers, DTC utilizes non-linear hysteresis controllers for torque and flux control. Modulation is not required in this scheme. Instead, a switching table is used in order to utilize optimum vector. Figure 3.1 shows the block diagram of DTC.

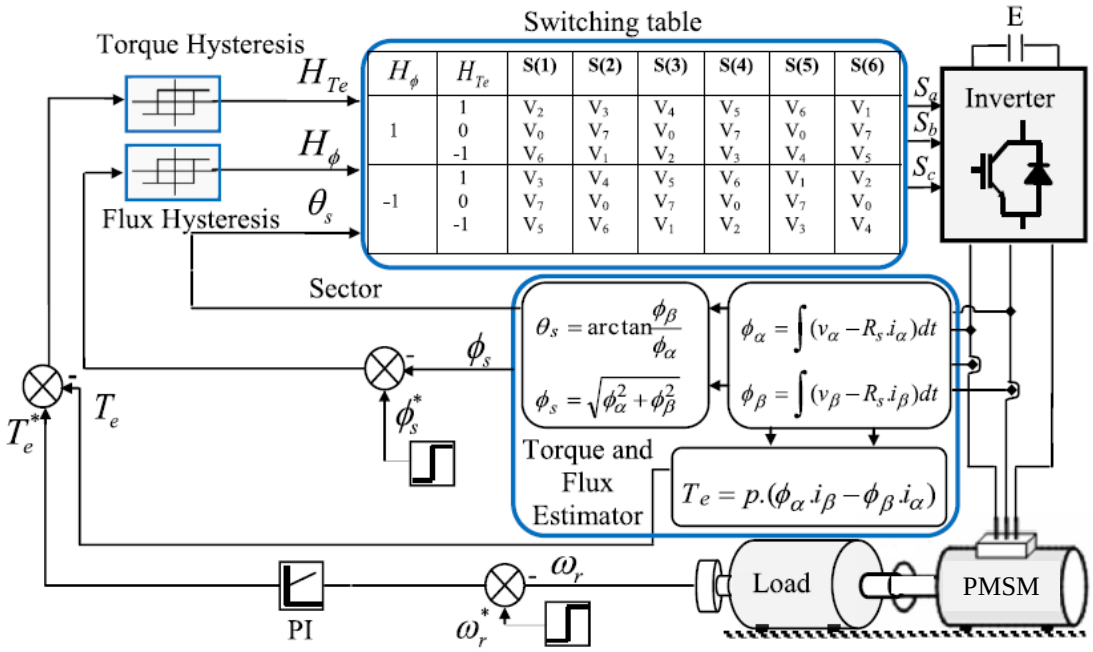

Figure 3.1 : Block diagram of DTC [61].

DTC does not utilize current controllers. Instead, current is controller indirectly via flux and torque controllers. Parameter dependency of DTC is smaller than FOC. The biggest advantage of the DTC is very fast dynamic response feature. Steady state and transient performance of torque control is good and preferable for applications require fast dynamic control of the machine.

Several drawbacks come with DTC. These can be listed as deteriorated speed control performance in low speed operation, variable switching frequency due to nature of hysteresis control and arising torque and current ripple due to variable switching frequency [62]. Table 3.1 is obtained if the three control methods are compared.

Table 3.1 : Comparison of PMSM control methods.

	Dynamic Response	Speed Control	Complexity	Tuning
V/f	Bad	Bad	Small	Easy
DTC	Very Good	Good	Medium	Difficult
FOC	Good	Very Good	Medium	Medium

3.1 Theory of Field Oriented Control

FOC exploits the simple mathematical model of PMSM in d-q axis and utilizes speed and current controllers in d-q coordinate system. A generalized block scheme of FOC is given in Figure 3.2.

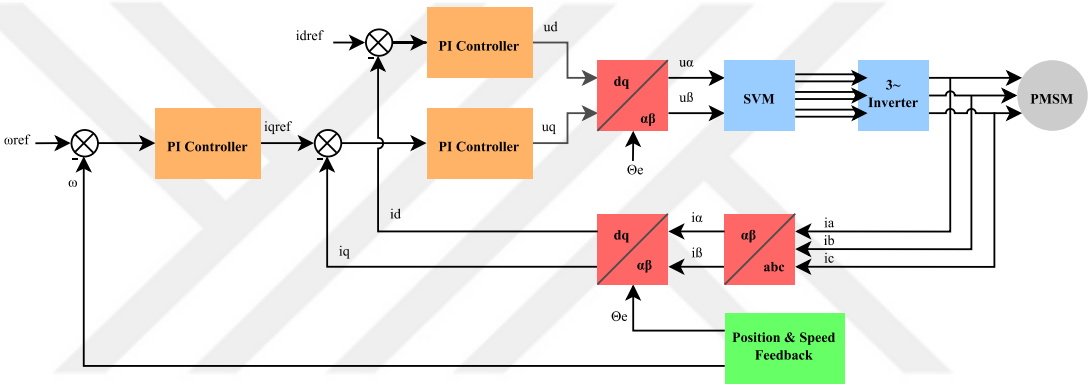

Figure 3.2 : Generalized block diagram of FOC.

It can be seen that there are two inner loops for current and one outer loop for speed control in a FOC system. Control frequency for the speed loop is generally determined based on the mechanical inertia of the system. In each control cycle, measured speed value is subtracted from speed reference value to obtain speed error. This error is than compensated by a PI controller that outputs reference quadrature axis current for current controllers. This PI controller has positive and negative output limits related with the driver hardware and motor demagnetization current to ensure proper operation.

Current control loops are related with time constant of the stator phases and usually a lot frequent than speed control loops. Actual FOC is done in these loops with reference frame transformations and space vector modulation. For this, each control cycle starts with sampling of the three-phase currents. Three-phase stationary

reference frame currents (i_a, i_b and i_c) are then transformed into two-phase stationary reference frame currents (i_α and i_b) with Clarke transformation shown in equation 3.1.

$$\begin{bmatrix} i_\alpha \\ i_\beta \end{bmatrix} = \frac{2}{3} \begin{bmatrix} 1 & \cos\left(\frac{2\pi}{3}\right) & \cos\left(\frac{4\pi}{3}\right) \\ 0 & \sin\left(\frac{2\pi}{3}\right) & \sin\left(\frac{2\pi}{3}\right) \end{bmatrix} \cdot \begin{bmatrix} i_a \\ i_b \\ i_c \end{bmatrix} \tag{3.1}$$

Two-phase synchronous reference frame currents (i_d and i_q) are then calculated using Park transformation shown in equation 3.2. It should be noted that Park transformation requires the knowledge of angle θ between d axis and α axis. This is equal to rotor electrical position θ_r assuming zero degree electrical position is obtained when rotor is aligned with phase a. Rotor position can be obtained using position sensors or utilizing position estimators. These methods are explained in section 3.3. For now, it is assumed that rotor electrical position is known and can be directly used in Park transformation.

$$\begin{bmatrix} i_d \\ i_q \end{bmatrix} = \begin{bmatrix} \cos(\theta_r) & \sin(\theta_r) \\ -\sin(\theta_r) & \cos(\theta_r) \end{bmatrix} \cdot \begin{bmatrix} i_\alpha \\ i_\beta \end{bmatrix} \tag{3.2}$$

With Park transformation is done, stator currents split into two components. Direct axis current i_d represents field flux component of the stator currents. Direction of this flux is determined with the sign of i_d current. Positive i_d current means field flux generated due to stator currents are in same direction with flux of permanent magnets and vice versa. Considering a non-salient machine operated below nominal speed. Electromagnetic torque will be generated by i_q and machine speed will increase if i_q is increased as shown in equation 2.7 and 2.26. Stator voltage equation in the quadrature axis is rearranged with i_q is switched to left hand side in equation 3.3. In this arrangement, maximum u_q will be limited due to DC bus voltage of the driver. If the limit is reached then machine will rotate at nominal speed at nominal load. In order to accelerate the machine further under this condition, numerator term has to be increased. This is achievable by weakening the field flux generated by permanent magnets by the utilization of negative i_d current.

$$i_q = \frac{u_q - \omega_e (L_d i_d + \psi_{PM})}{R_S} \tag{3.3}$$

Since u_q is constant, i_q will be increased related with the amount of i_d injected to stator. This operation point beyond nominal speed is referred as Flux Weakening or Field Weakening operation. This is utilized in many applications such as washing machines (spin dry) and electric vehicles. In normal operation below nominal speed, i_d current reference is kept zero. Applications with highly salient machines will however, utilize i_d current in below nominal speed operations in order to achieve maximum torque output as per MTPA approach.

Current controllers in synchronous frame outputs voltage references v_d and v_q. These reference values are then transformed into α-β coordinate system using an inverse Park transformation shown in equation 3.4.

$$\begin{bmatrix} u_\alpha \\ u_\beta \end{bmatrix} = \begin{bmatrix} \cos(\theta_r) & -\sin(\theta_r) \\ \sin(\theta_r) & \cos(\theta_r) \end{bmatrix} \cdot \begin{bmatrix} u_d \\ u_q \end{bmatrix} \tag{3.4}$$

3.2 Space Vector Modulation

SVM is a special modulation technique that is used in order to get three-phase sinusoidal output from a three-phase inverter. SVM is a direct way of converting α-β reference voltages to duty cycle values for the six switches in a three-phase inverter given in Figure 3.3.

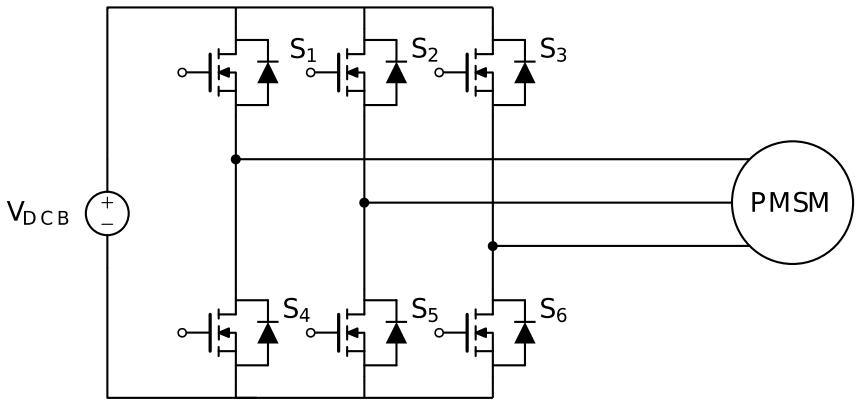

Figure 3.3 : Three-phase voltage source inverter.

Considering the three-phase inverter power stage, each leg can have two different states. Top switch of a leg is on while bottom switch is off or vice versa. Both of the switches in a leg is never turned on simultaneously since this will cause simply short-circuit the DC bus called as an arm shoot-through case. Both of the switches turned off will have no effect of driving the motor, thus each phase leg can have only two states.

It is considered that a phase leg is in active state (or its state is logical 1) when top switch of that leg is turned on. If the phase leg state is 0 then bottom switch is turned on. There are total of 8 different combination of states in a three-phase inverter. These combinations are shown in a three-phase vector diagram given in Figure 3.4. The three-phase diagram is divided into 6 parts that are referred as sectors.

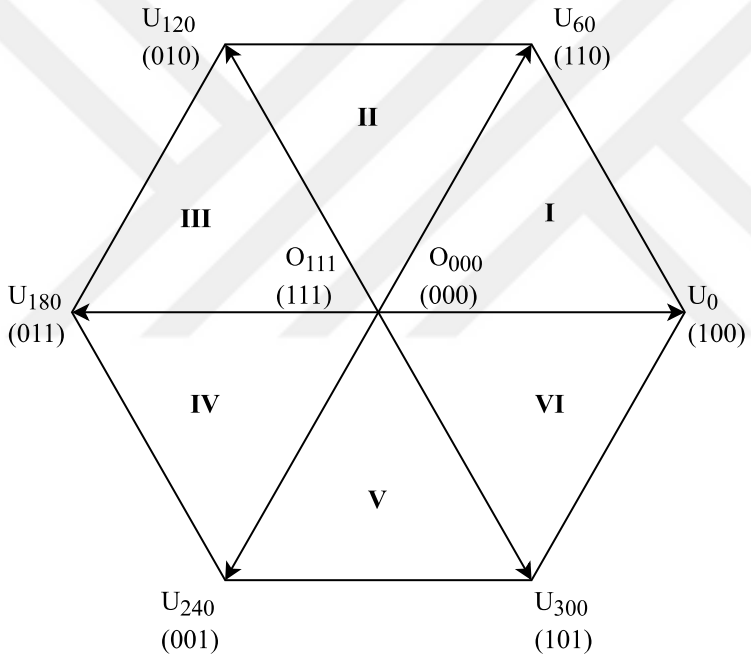

Figure 3.4 : Stator current vector in abc and αβ coordinate system.

Each state combination corresponds to a different vector. Two null vectors are located in the center since in these combinations, all three-phase legs are in same state causing the phase to phase voltage differences to become zero. Which, in turn generates no current. Thus, they are effectively zero vectors. The combinations are given in Table 3.2 with corresponding vector numeration. S_a, S_b and S_c shows the state conditions of each phase.

Table 3.2 : Possible switch combinations and corresponding vectors.

S_a	S_b	S_c	Vector
0	0	0	O_{000}
1	0	0	U_0
1	1	0	U_{60}
0	1	0	U_{120}
0	1	1	U_{180}
0	0	1	U_{240}
1	0	1	U_{300}
1	1	1	O_{111}

Considering a symmetrical machine, phase voltages can be expressed according to phase states in a matrix form as given in equation 3.5.

$$\begin{bmatrix} u_a \\ u_b \\ u_c \end{bmatrix} = \frac{U_{DCB}}{3} \begin{bmatrix} 2 & -1 & -1 \\ -1 & 2 & -1 \\ -1 & -1 & 2 \end{bmatrix} \cdot \begin{bmatrix} S_a \\ S_b \\ S_c \end{bmatrix} \tag{3.5}$$

This matrix equation can be transformed into α-β coordinate system as given in equation 3.6. using Clarke transformation.

$$\begin{bmatrix} u_\alpha \\ u_\beta \end{bmatrix} = \frac{2}{3} \begin{bmatrix} 1 & \frac{-1}{2} & \frac{-1}{2} \\ 0 & \frac{\sqrt{3}}{2} & \frac{-\sqrt{3}}{2} \end{bmatrix} \cdot \begin{bmatrix} u_a \\ u_b \\ u_c \end{bmatrix} \tag{3.6}$$

Space vector modulation technique is based on generation of any vector within maximum amplitude circle by modulating these eight main vectors. For example, the given phase vector $U_{\alpha\text{-}\beta}$ shown in Figure 3.5 can be generated by modulation of vectors U_0 and U_{60}.

This modulation is done in a similar manner with time division multiplexing. U_0 and U_{60} vectors are applied with corresponding duty cycles within a switching period. Rest of the switching period is filled with null vectors. Equations 3.7 and 3.8 shows the generation of phase vector by using space vector modulation.

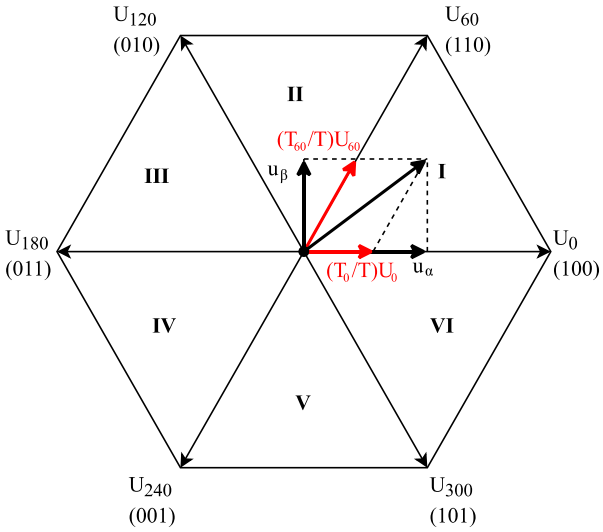

Figure 3.5 : Representation of a voltage vector with two main vectors in I. sector.

Phase voltages normalized to DC bus voltage in α-β coordinate system along with phase states and applied vectors are listed in Table 3.3.

Table 3.3 : Phase voltages in α-β corresponding to applied vector.

S_a	S_b	S_c	Vector	u_α	u_β
0	0	0	O_{000}	0	0
1	0	0	U_0	$\frac{2}{3}$	0
1	1	0	U_{60}	$\frac{1}{3}$	$\frac{1}{\sqrt{3}}$
0	1	0	U_{120}	$\frac{-1}{3}$	$\frac{1}{\sqrt{3}}$
0	1	1	U_{180}	$\frac{-2}{3}$	0
0	0	1	U_{240}	$\frac{-1}{3}$	$\frac{-1}{\sqrt{3}}$
1	0	1	U_{300}	$\frac{1}{3}$	$\frac{-1}{\sqrt{3}}$
1	1	1	O_{111}	0	0

$$T = T_{60} + T_0 + T_{null} \tag{3.7}$$

$$U_S = \frac{(T_{60}U_{60} + T_0U_0)}{T} \tag{3.8}$$

Where;

T: Switching period

T_0: Duration of applied vector U_0

T_{60}: Duration of applied vector U_{60}

T_{null}: Duration of null vector

Phase vector components u_α and u_β can be expressed with vector durations by using geometric rules as shown in equations 3.9 and 3.10.

$$u_\beta = \frac{T_{60}}{T}|U_{60}|\sin(60°) \tag{3.9}$$

$$u_\alpha = \frac{T_0}{T}|U_0| + \frac{u_\beta}{\tan(60°)} \tag{3.10}$$

In this case, required vector durations are obtained by substitution of normalized vector magnitudes and trigonometric values as shown in equations 3.11 and 3.12.

$$\frac{T_{60}}{T} = u_\beta \tag{3.11}$$

$$\frac{T_0}{T} = \frac{(-u_\beta + u_\alpha\sqrt{3})}{2} \tag{3.12}$$

Table 3.4 gives a generalized expression of obtaining vector durations according to the sector, that phase vector lies within.

Table 3.4 : Vector durations for each sector.

T_{ij}	Sectors					
	I	II	III	IV	V	VI
T_i	u_β	$\frac{(u_\beta + u_\alpha\sqrt{3})}{2}$	$\frac{-(u_\beta + u_\alpha\sqrt{3})}{2}$	$\frac{(u_\beta - u_\alpha\sqrt{3})}{2}$	$\frac{-(u_\beta - u_\alpha\sqrt{3})}{2}$	$-u_\beta$
T_j	$\frac{-(u_\beta - u_\alpha\sqrt{3})}{2}$	$\frac{(u_\beta - u_\alpha\sqrt{3})}{2}$	u_β	$-u_\beta$	$\frac{-(u_\beta + u_\alpha\sqrt{3})}{2}$	$\frac{(u_\beta + u_\alpha\sqrt{3})}{2}$

For example, a phase vector in sector III will have vector durations T_{180} and T_{120} obtained from table as given in equations 3.13 and 3.14.

$$\frac{T_{180}}{T} = \frac{-(u_\beta + u_\alpha \sqrt{3})}{2} \tag{3.13}$$

$$\frac{T_{120}}{T} = u_\beta \tag{3.14}$$

3.3 Obtaining Position and Speed Information for FOC

As FOC requires accurate information on rotor electrical position, various methods exist for obtaining this information. These methods are divided into two distinct groups. This division is made on regarding whether any sophisticated position sensor is used on the drive system or existing hardware on the driver is used to estimate rotor position. Both methods have advantages and disadvantages when one compared with the other. Thus, this is a tradeoff between features of these methods that engineers are faced. They choose what fits their application the best.

3.3.1 Sensored field oriented control

In this method special types of sensor are utilized on the motor that are responsible of indicate rotor position in a particular way. The drive system contains the requisite hardware and software for processing the output of position sensor in order to obtain rotor electrical position and speed information. Block diagram of a sensored FOC drive system is given in Figure 3.6.

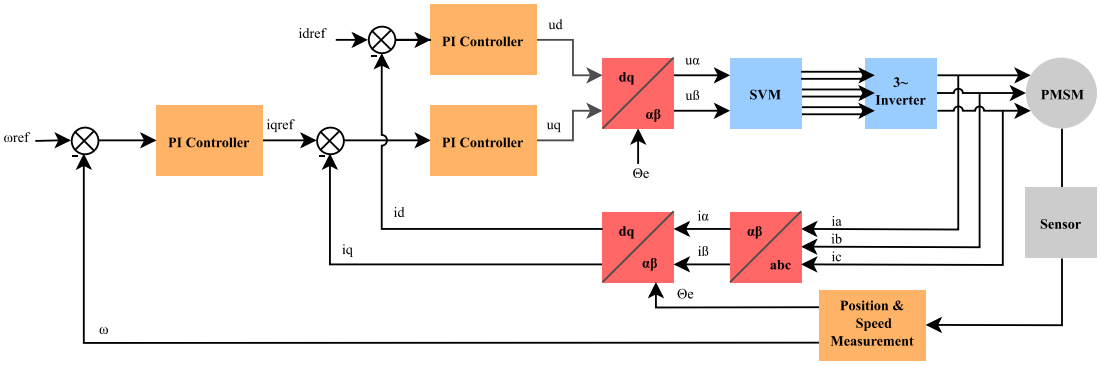

Figure 3.6 : Block diagram of a sensored FOC system.

Various types of position sensors exist and they are used in this method. Most used types are Hall-effect sensors, angle resolvers and encoders.

Hall-effect sensors detect magnetic fields in front of them. These sensors are placed in a convenient place on stator to detect magnetic poles of permanent magnets on the rotor as they pass near the sensor. Hall-effect sensors provide a small footprint but limited resolution on rotor position.

An encoder is a sensor that outputs information by digital pulses of ones and zeros. Encoder has a stationary and a rotating part. Rotating part is fixed to motor shaft while stationary part is fixed on motor's body. Coupling of these two parts provide encoder to detect position of the rotating part with reference to stationary part. These parts can be coupled optically or magnetically. Incremental encoders transmit relative position information by using two square wave signals that have 90° phase shift between them. An absolute encoder has the ability to transmit position information with multiple bits. Thus, this position is not relative to the previous step but relative to zero point of the encoder itself. Encoders provide accurate position information. They consume more space than Hall-effect sensors. Moreover, in order to obtain actual rotor position from an encoder, angle offset between encoder's zero point and rotor's zero point has to be subtracted. This process is called as calibrating and it has to be done at least once after a motor is coupled with an encoder.

Angle resolvers also contain two parts. A transmit coil that is fixed on the rotor is used to generate a rotating field. Two coils that are placed on the stator 90° degrees apart from each other sense this field. Processing of an angle resolver's output signals are not straightforward as Hall effect sensors and encoders. These analog signals have to be processed using observers to extract position information. Angle resolvers provide very high resolution -theoretically infinite as it outputs analog signals but limited to analog resolution of the processing device- but they consume a lot of space in machine body.

It is obvious that there is a tradeoff between resolution and consumed space when it comes to choosing a position sensor. It can be also observed that as the resolution is increased, complexity of processing the position information is also increased. The sensors also affect expected lifetime of the drive system.

In general, sensored motor control is mostly used in industrial applications where additional space consumption and the cost of the sensor are insignificant compared to reliable and accurate position information it provides. Any position control application will also utilize position sensors in sectors such as automotive, robotics, aviation and space.

3.3.2 Sensorless field oriented control

Sensorless FOC of a motor is achieved when there is no sophisticated position sensors utilized on the motor. Instead of a direct measurement of the rotor position, an estimation based on the values of state variables at a certain time is done. These state variables usually consist of applied voltages, measured currents and estimated state variables such as flux and back-EMF. Control block diagram of a sensorless FOC system is given in Figure 3.7.

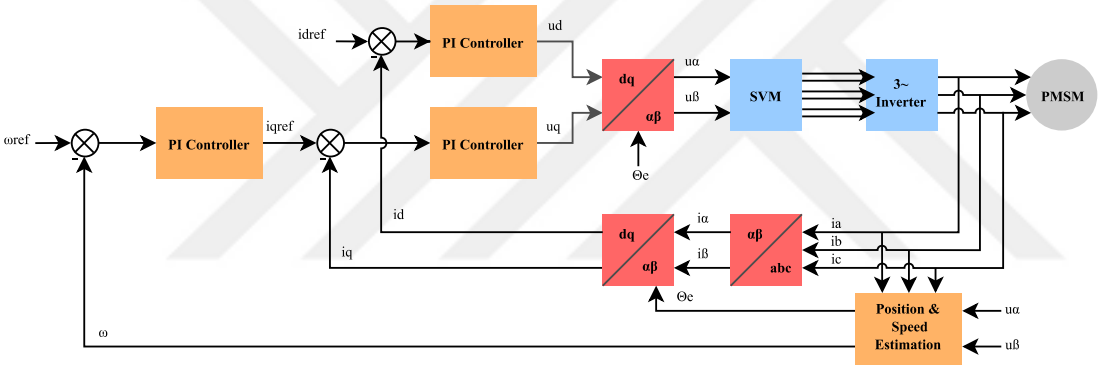

Figure 3.7 : Block diagram of a sensorless FOC system.

Since the first appearance of a sensorless motor control system in late 1980's, a lot of research has been done into exploring different ways of estimating rotor position. Today many different schemes are exist and just like sensor types, there are tradeoffs between the sensorless schemes. Most common types of sensorless control methods can be listed as flux or back-EMF estimation based on stator voltage integration, Luenberger type observers, Sliding Mode Observers and saliency based methods that utilize signal injection into the stator windings.

One of the simplest position estimation method is achieved by the estimation of the flux linkages by integrating the stator voltages [35, 36, 40]. In order to compensate the drift and offset caused by the integration, EKF is used in many applications [41, 42]. Using of a SMO instead of EKF is also resulted in successful control of the machine [43-46].

As the semiconductor technology grew and improved greatly, high performance microcontrollers are available with little cost to almost anyone. Thus, its appearance in many motor drive systems provides the ability of using more complex sensorless control algorithms that requires a lot of computation. Luenberger type observer is increasingly used in sensorless FOC applications [37-39]. In this method motor model without the back-EMF term is implemented inside the controller in order to estimate back-EMF and thus flux linkage. This estimation provides the electrical position of the rotor. Due to decreased amplitude of back-EMF in low speed regions, this method requires an open loop startup procedure.

Another position estimation method that requires high performance signal processing depends on estimation of the rotor position based on the saliency of the machine [47-56]. This is achieved by online measurement of the direct and quadrature axis inductances. In order to achieve such a measurement, stator windings are injected with a known frequency signal. This signal is then extracted using filters and observers from the measured state variables. Since this method provides rotor position detection even in standstill operation, it is possible to combine signal injection method with a back-EMF observer in order to cover all operating region of a machine.

Two different methods of estimating rotor position are investigated in this study. Extended back-EMF observer and stator flux estimator both use mathematical model of the machine in α-β coordinate system in order to estimate rotor position.

3.4 Extended Back-EMF Observer in Two-Phase Stationary Reference Frame

Extended back-EMF model of the PMSM in α-β coordinate system is obtained from the model in d-q coordinate system. Phase voltage equation given in equation 2.24 is re-written in a different form where the time derivative terms of currents are introduced into first matrix with derivative terms as given in equation 3.15.

$$\begin{bmatrix} u_d \\ u_q \end{bmatrix} = \begin{bmatrix} R_S + \rho L_d & -\omega_e L_q \\ \omega_e L_d & R_S + \rho L_q \end{bmatrix} \cdot \begin{bmatrix} i_d \\ i_q \end{bmatrix} + \omega_e \cdot \psi_{PM} \cdot \begin{bmatrix} 0 \\ 1 \end{bmatrix} \tag{3.15}$$

This model can be transformed into two-phase stationary reference frame using inverse Park transformation. Obtained model is given in equation 3.16.

$$\begin{bmatrix} u_\alpha \\ u_\beta \end{bmatrix} = \begin{bmatrix} R_S + \rho L_\alpha & -\omega_e M_{\alpha\beta} \\ \rho M_{\alpha\beta} & R_S + \rho L_\beta \end{bmatrix} \cdot \begin{bmatrix} i_\alpha \\ i_\beta \end{bmatrix} + \omega_e \cdot \psi_{PM} \cdot \begin{bmatrix} -\sin(\theta_e) \\ \cos(\theta_e) \end{bmatrix} \tag{3.16}$$

In this model, machine inductances are represented as L_α, L_β and $M_{\alpha\beta}$ which represent stator inductances in α and β axis along with the mutual inductance between α and β axis. Equations 3.17, 3.18 and 3.19 show how these inductance values are represented.

$$L_\alpha = L_0 + L_\Delta \cos(2\theta_e) \tag{3.17}$$

$$L_\beta = L_0 - L_\Delta \cos(2\theta_e) \tag{3.18}$$

$$L_{\alpha\beta} = L_\Delta \sin(2\theta_e) \tag{3.19}$$

The trigonometric terms with angle "$2\theta_e$" are introduced due to inductance matrix in equation 3.15 being asymmetrical. Inductance matrix is re-written according to equation 3.20.

$$\begin{bmatrix} u_d \\ u_q \end{bmatrix} = \begin{bmatrix} R_S + \rho L_d & -\omega_e L_q \\ \omega_e (L_d + L_q - L_q) & R_S + \rho (L_q + L_d - L_d) \end{bmatrix} \cdot \begin{bmatrix} i_d \\ i_q \end{bmatrix} + \omega_e \cdot \psi_{PM} \cdot \begin{bmatrix} 0 \\ 1 \end{bmatrix} \tag{3.20}$$

In this expression, "L_q-L_q" and "L_d-L_d" terms are introduced into inductance matrix in order to obtain a symmetrical matrix. Equation 3.20 is then re-arranged with a symmetrical inductance matrix as given in equation 3.21.

$$\begin{bmatrix} u_d \\ u_q \end{bmatrix} = \begin{bmatrix} R_S + \rho L_d & -\omega_e L_q \\ \omega_e L_q & R_S + \rho L_d \end{bmatrix} \cdot \begin{bmatrix} i_d \\ i_q \end{bmatrix} + \left((L_d - L_q) \cdot (\omega_e \cdot i_d - \rho i_q) + \omega_e \cdot \psi_{PM} \right) \cdot \begin{bmatrix} 0 \\ 1 \end{bmatrix} \tag{3.21}$$

Now, if the phase voltage equation given in equation 3.21 is transformed into two-phase stationary reference frame, a simpler mathematical model without any second harmonics term is obtained as given in equation 3.22.

$$\begin{bmatrix} u_\alpha \\ u_\beta \end{bmatrix} = \begin{bmatrix} R_S + \rho L_d & \omega_e \left(L_d - L_q \right) \\ -\omega_e \left(L_d - L_q \right) & R_S + \rho L_d \end{bmatrix} \cdot \begin{bmatrix} i_\alpha \\ i_\beta \end{bmatrix} + \left(\left(L_d - L_q \right) \cdot \left(\omega_e \cdot i_d - \rho i_q \right) + \omega_e \cdot \psi_{PM} \right) \cdot \begin{bmatrix} -\sin\left(\theta_e\right) \\ \cos\left(\theta_e\right) \end{bmatrix} \tag{3.22}$$

In this expression, rightmost term can be considered as the extended back-EMF part of the model as it contains crucial information of rotor electrical position. Extended back-EMF term in two-phase stationary reference frame is expresses as given in equation 3.23.

$$\begin{bmatrix} e_\alpha \\ e_\beta \end{bmatrix} = \left(\left(L_d - L_q \right) \cdot \left(\omega_e \cdot i_d - \rho i_q \right) + \omega_e \cdot \psi_{PM} \right) \cdot \begin{bmatrix} -\sin\left(\theta_e\right) \\ \cos\left(\theta_e\right) \end{bmatrix} \tag{3.23}$$

Where;

e_α is extended back-EMF part in α axis,

e_β is extended back-EMF part in β axis.

Equation 3.22 is then re-arranged with back-EMF term is replaced with back-EMF matrix and the model is transformed into Laplace domain as given in equation 3.24.

$$\begin{bmatrix} u_\alpha \\ u_\beta \end{bmatrix} = \begin{bmatrix} R_S + sL_d & \omega_e \left(L_d - L_q \right) \\ -\omega_e \left(L_d - L_q \right) & R_S + sL_d \end{bmatrix} \cdot \begin{bmatrix} i_\alpha \\ i_\beta \end{bmatrix} + \begin{bmatrix} e_\alpha \\ e_\beta \end{bmatrix} \tag{3.24}$$

This relatively easy model to implement estimators and observers will only estimate the extended back-EMF part of the model. Using of a Luenberger observer is very typical for such application that requires state estimation with a feedback observer. In order to obtain rotor position information, two current observers are used in α and β axis. These observers are based on motor model given in equation 3.24 except the extended back-EMF part is removed from this model. Both observers utilize a compensator that tries to correct error between the estimated and measured axis current. Expression of α and β axis currents of the observer with extended back-EMF part removed from motor model is given in equations 3.25 and 3.26.

$$i_\alpha = \frac{u_\alpha - \omega_e \left(L_d - L_q\right) i_\beta + L(\alpha)}{R_S + sL_d} \tag{3.25}$$

$$i_\beta = \frac{u_\beta + \omega_e \left(L_d - L_q\right) i_\alpha + L(\beta)}{R_S + sL_d} \tag{3.26}$$

Considering the observer is stable, current error in steady state will diverge to zero, making the compensators to output removed back-EMF part of the model. Compensator outputs *L(α)* and *L(β)* are expressed as given in equations 3.27 and 3.28.

$$L(\alpha) = -e_\alpha \tag{3.27}$$

$$L(\beta) = -e_\beta \tag{3.28}$$

Control block diagram of the extended back-EMF observer is given in Figure 3.8.

In this block diagram, estimated state variables are shown as $\hat{\imath}_\alpha$, $\hat{\imath}_\beta$, $\hat{e}_\alpha$ and $\hat{e}_\beta$. They represent the estimation of α-β axis currents and extended back-EMF terms. The compensator block is usually consists of a simple PI controller.

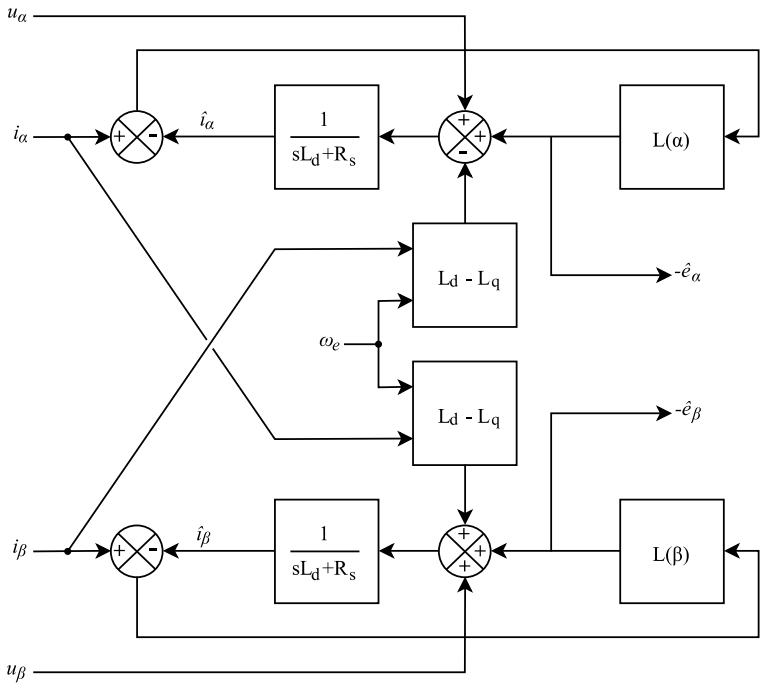

Figure 3.8 : Extended back-EMF observer block diagram in α-β reference frame.

3.5 Angle-Tracking Observer

Estimated back-EMF signal obtained from the observer has to be decomposed and rotor position has to be extracted from the back-EMF signals. This is achievable by using the simple arctangent formula given in equation 3.29.

$$\hat{\theta}_e = \tan^{-1}\left(\frac{\hat{e}_\alpha}{\hat{e}_\beta}\right) \tag{3.29}$$

Although this method is simple to implement, it has several drawbacks. This method only gives estimated rotor electrical position. This means additional computation has to be done in order to obtain estimated rotor speed. Using the derivative of estimated position most likely will output noisy speed estimation. Thus, additional computation for low pass filtering should be added into process. Furthermore, estimated position is unfiltered and thus may contain high frequency noise. Using an unfiltered position value for the vector transformations in FOC may result in stability issues along with unwanted torque ripple on the shaft. It is also not wise to utilize low pass filters on estimated rotor electrical position. This is mainly because unlike speed, position is a time-varying signal. Low pass filtering such signal will result in phase shift that is added to the estimated position signal. This phase shift will degrade the drive performance.

Instead of obtaining rotor electrical position with arctangent formula, many applications utilize an observer for this task. These observers are called as angle-tracking observers. A very simple angle-tracking observer can be implemented using the trigonometric subtraction formula of the sinus signal as given in equation 3.30.

$$\sin\left(\theta_e\right)\cos\left(\hat{\theta}_e\right) - \cos\left(\theta_e\right)\sin\left(\hat{\theta}_e\right) = \sin\left(\theta_e - \hat{\theta}_e\right) \tag{3.30}$$

This equation can be made if α and β components of estimated back-EMF signals are considered as sine and cosine values of θ_e. Right hand side of the equation is the sinus function of error between the position of back-EMF signal and estimated position obtained from angle-tracking observer's output. If this error is small, then this equation can be approximated to position error of the observer as given in equation 3.31.

$$\sin\left(\theta_e - \hat{\theta}_e\right) \approx \theta_e - \hat{\theta}_e \tag{3.31}$$

The control block diagram of an angle-tracking observer is given in Figure 3.9.

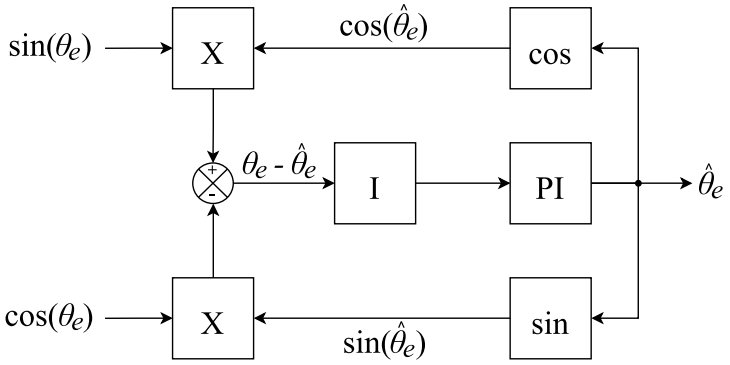

Figure 3.9 : Block diagram of angle-tracking observer.

Angle-tracking observer utilizes an integrator coupled with a PI controller for compensation. PI controller clears position error by outputting the estimated rotor electrical position while the integrator provides a filter to the input signal. For a more practical approach, integrator and PI controller block places are switched. This arrangement shown in Figure 3.10 provides rotor electrical speed as the output of PI controller and rotor electrical position as the output of the integrator. This arrangement is more convenient as it provides smooth information of speed and position simultaneously.

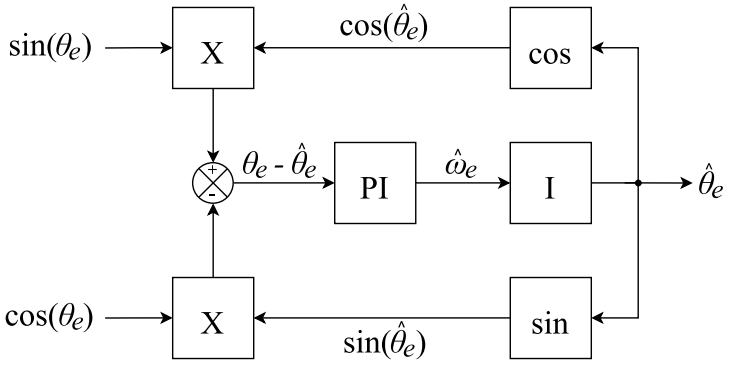

Figure 3.10 : Modified block diagram of angle-tracking observer.

3.6 Stator Flux Estimator

Besides the back-EMF observer, there is another common method of rotor position estimation based on motor fundamental model. This method is based on estimating

stator flux. Recalling the motor mathematical model in α-β coordinate system given in equation 3.32 and expression of flux linkages as given in equation 3.33.

$$\begin{bmatrix} u_\alpha \\ u_\beta \end{bmatrix} = \begin{bmatrix} R_S & 0 \\ 0 & R_S \end{bmatrix} \cdot \begin{bmatrix} i_\alpha \\ i_\beta \end{bmatrix} + \begin{bmatrix} 1 & 0 \\ 0 & 1 \end{bmatrix} \cdot \rho \begin{bmatrix} \psi_\alpha \\ \psi_\beta \end{bmatrix} \tag{3.32}$$

$$\begin{bmatrix} \psi_\alpha \\ \psi_\beta \end{bmatrix} = \begin{bmatrix} L_0 + L_\Delta \cos(2\theta_e) & L_\Delta \sin(2\theta_e) \\ L_\Delta \sin(2\theta_e) & L_0 - L_\Delta \cos(2\theta_e) \end{bmatrix} \cdot \begin{bmatrix} i_\alpha \\ i_\beta \end{bmatrix} + \psi_{PM} \cdot \begin{bmatrix} \cos(\theta_e) \\ \sin(\theta_e) \end{bmatrix} \tag{3.33}$$

Flux linkages actually consist rotor position information with the rightmost term of the expression as cosine and sine terms. Since the first matrix consists of inductances and value of inductances are neglectable, it can be said that flux linkages give the cosine and sine terms of rotor electrical position. These flux linkages can be estimated through back-EMF integration as shown in equation 3.31

$$\begin{bmatrix} \psi_\alpha \\ \psi_\beta \end{bmatrix} = \int \left(\begin{bmatrix} u_\alpha \\ u_\beta \end{bmatrix} - \begin{bmatrix} R_S & 0 \\ 0 & R_S \end{bmatrix} \cdot \begin{bmatrix} i_\alpha \\ i_\beta \end{bmatrix} \right) \approx \psi_{PM} \begin{bmatrix} \cos(\theta_e) \\ \sin(\theta_e) \end{bmatrix} \tag{3.31}$$

Pure integrators cannot be used in such method since this will be implemented digitally. There is a risk of saturation of the integrating variable. Also DC offset and drift problems may arise. Even a small offset will eventually lead to saturation. Instead of using an integrator, low pass filters are used. If the time constant of the filter is selected adequately high, it will act as an integrator and will eliminate DC components. Instead of one, two low pass filters can be used with a derivative operator in between in order to eliminate even higher DC offsets [63]. Block diagram of flux estimator is given in Figure 3.11.

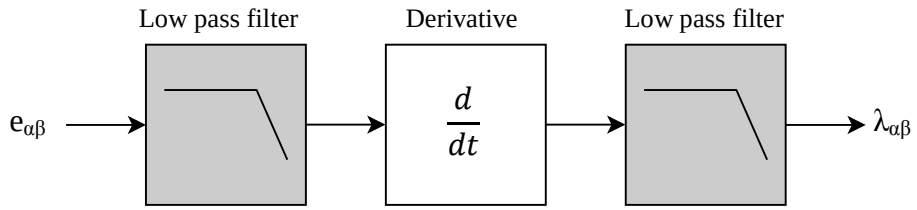

Figure 3.11 : Block diagram of flux estimator.

Position and speed can be extracted by using the angle-tracking observer after the flux linkages in α and β axis are estimated.

4. DESIGN OF A SENSORLESS FOC DRIVE SYSTEM FOR PMSM

4.1 Scope of Thesis

Main components of a PMSM FOC drive system is given in Fig 4.1. Controller component of the system can be made of a single chip or a specific board that contains the controller chip and interacts with the inverter. Control chip that the FOC and position detection algorithms are implemented can be an off the shelve microcontroller, digital signal processor (DSP) [64], application specific integrated circuit (ASIC) or an FPGA [65]. Structure inside the controller consists of a layer that interacts with the inverter. This layer typically has PWM outputs, analog to digital converter (ADC) inputs, fault inputs and miscellaneous digital inputs and outputs depending on the hardware design. This layer defined as solely hardware, which can be made of pins of a single chip or connectors of a controller board.

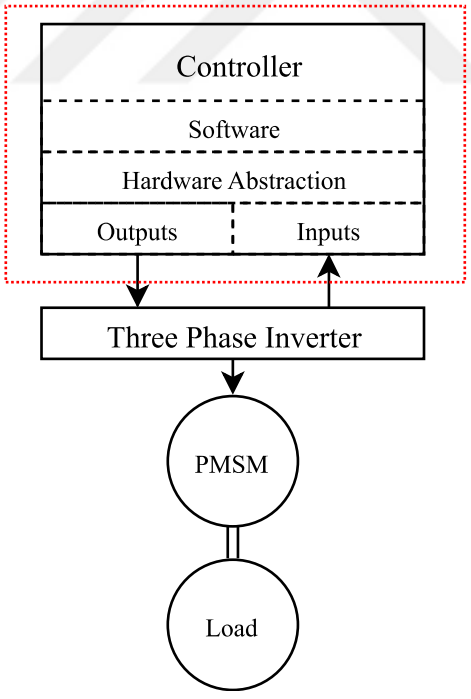

Figure 4.1 : Block diagram of a PMSM FOC system.

Hardware abstraction layer is however, the expression of the inputs and outputs inside the controller software. It is good practice to separate hardware related functions of a software from the functions that related solely on software. This is

where hardware abstraction comes handy. It interacts with the input/output peripherals of the controller. While doing so, hardware abstraction layer provides a solely software expression and control of these peripherals to the rest of the software. Three-phase inverter is usually a section of a specific power electronics board. This board consists of the power input and filtering, power supply generation, three-phase inverter, current and voltage measurement circuits, fault and protection circuits.

This thesis concentrates on the design of a controller board and requisite software development for FOC of a PMSM for existing three-phase inverter hardware. These components are shown in red dashed line in Fig 4.1. For the three-phase inverter hardware, STMicroelectronics X-NUCLEO-IHM08M1 development board given in Fig. 4.2 is selected.

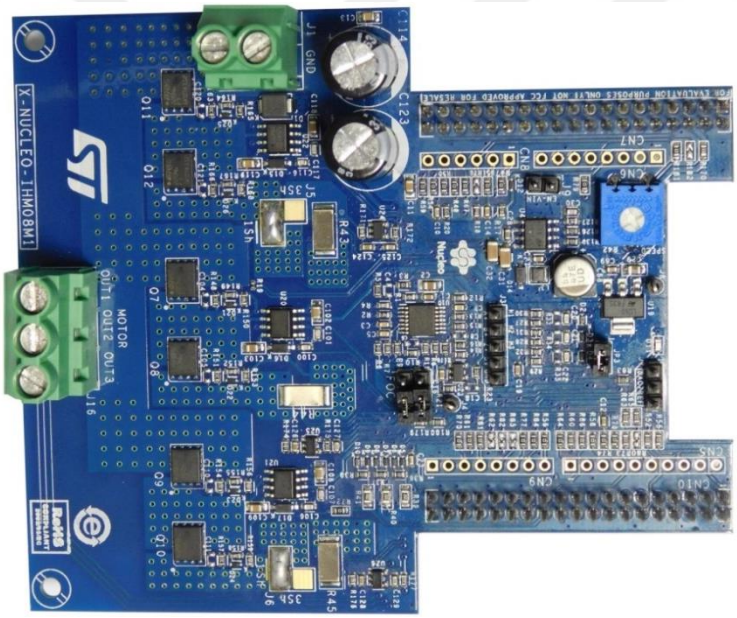

Figure 4.2 : X-NUCLEO-IHM08M1 Three-phase inverter board [66].

Key specifications of this development platform can be listed as below [66];

- 10V to 48V operating voltage range
- 15A output current
- Temperature sensor for over temperature protection
- Fixed current comparator for overcurrent protection
- 3 phase current feedback
- 3 phase voltage feedback

- DC bus voltage feedback
- Adjustable current comparator via PWM or digital to analog converter (DAC)
- 5V logic power supply generation

With the selection of three-phase inverter board, specifications for the controller board are also specified. MKV46F128VLL16 microcontroller from NXP is selected for the development and implementation of embedded software. This microcontroller provides ARM Cortex M4 core with operating clock frequencies up to 168MHz with 128kB RAM and 24kB ROM [67]. Advanced PWM peripherals with programmable dead time, high resolution and fault interlocking features are provided. Design of this study work consists of three parts, which are hardware design of the controller board, simulation of sensorless FOC and development of embedded software for the controller board.

4.2 Hardware Design

Schematics and PCB design of the controller board is made with Altium software. Schematic design of the controller board is made according to the signals that are used in X-NUCLEO-IHM08M1 development board. Two headers are used in order to connect the controller board to the inverter board. Four Light Emitting Diodes (LED) are placed for status indication. Isolated and non-isolated programming hardware for Serial Wire Debug (SWD) interface is also placed. Incremental encoder interface is added to schematics for evaluation of the position estimation algorithms. Additionally, Universal Serial Bus (USB) interface and other types of serial communication interfaces are placed for easier debugging of the controller. Schematics design of the controller is given in Figure 4.3.

PCB design of the board is done as a two-layer board. Placement of the components is made according to the layout of the inverter board in order to prevent any collisions. Headers are placed according to the headers on the inverter boar so that two boards connect easily. Total size of the controller board is 60 x 96.52 mm.

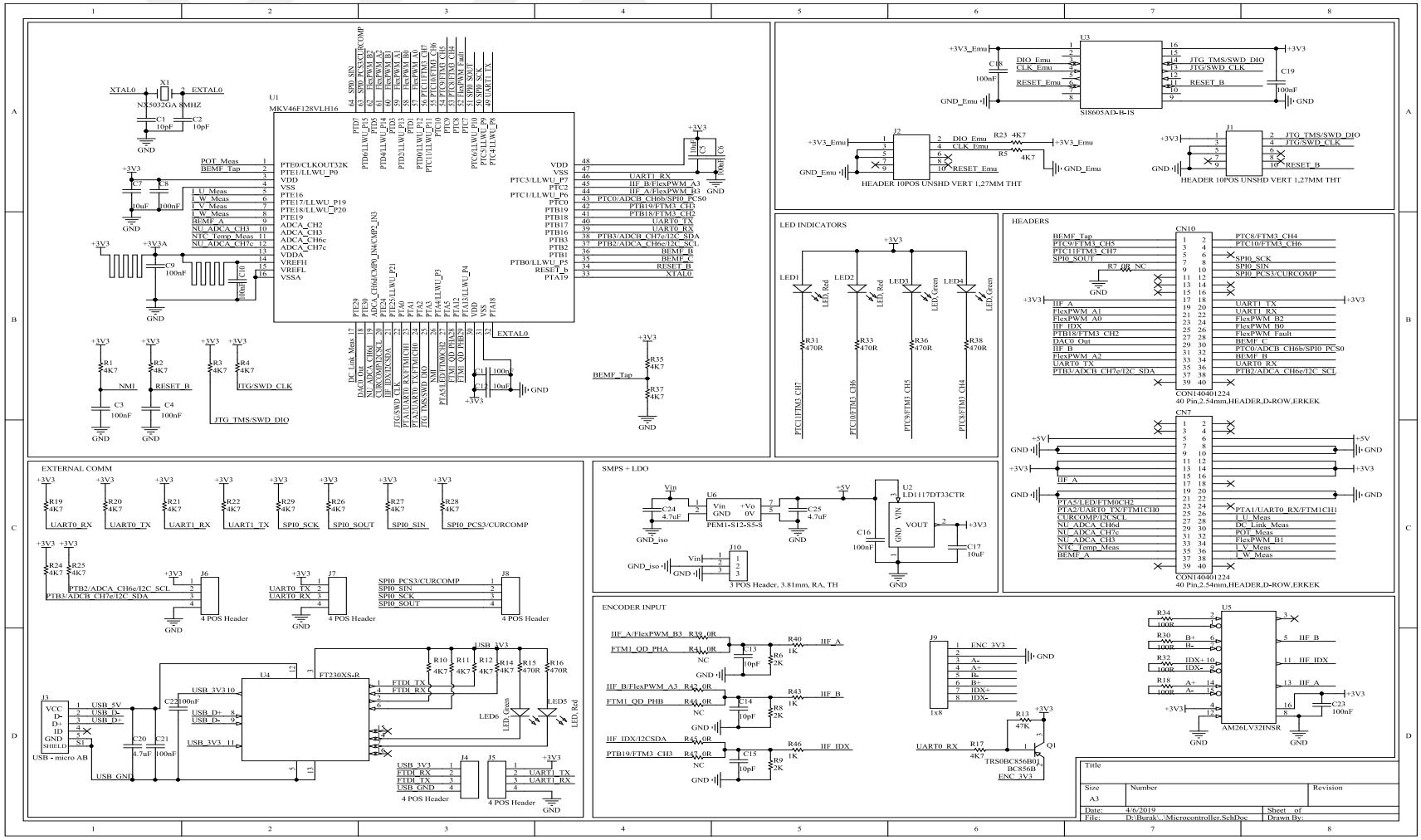

Figure 4.3 : Schematic design of the controller board.

Figure 4.4 shows the microcontroller section of the schematics. MKV46F128VLH16 microcontroller and its necessary external peripherals such as bypass capacitors, pull-up resistors and crystal oscillator are wired accordingly.

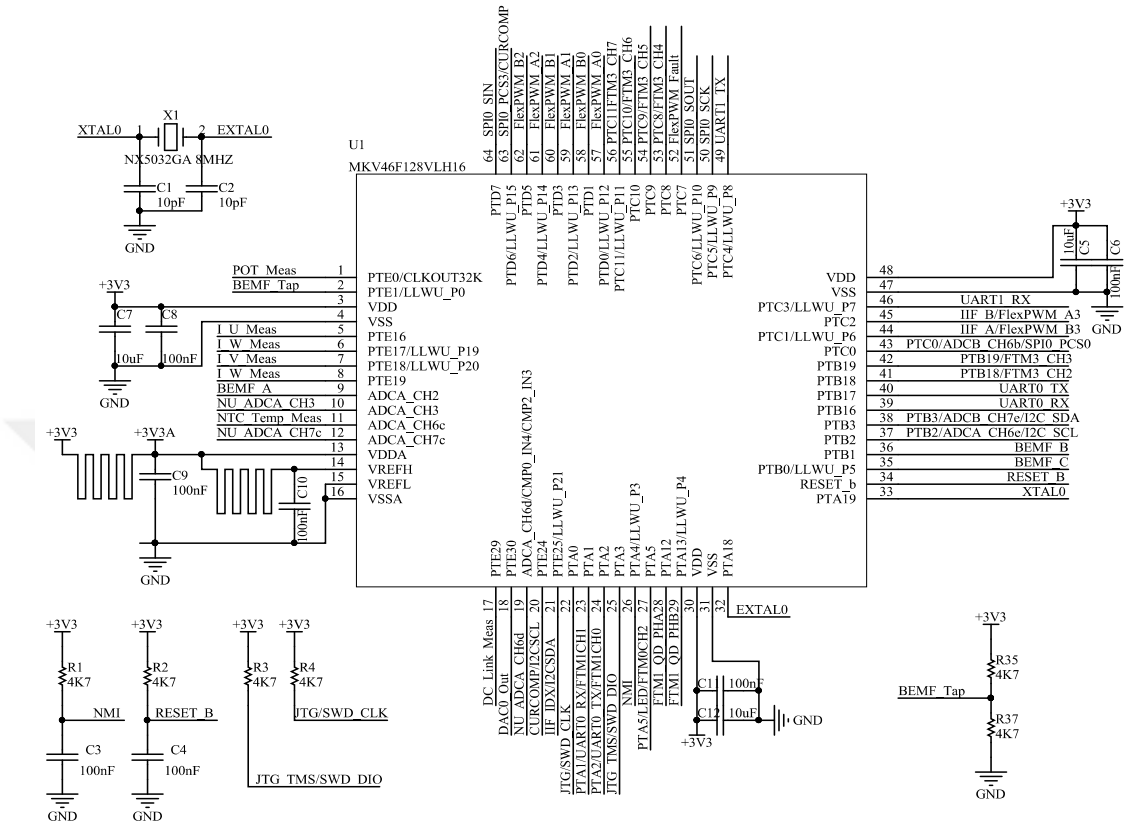

Figure 4.4 : Schematic design for microcontroller and its peripherals.

Design of isolated and non-isolated debugging hardware for SWD is shown in Figure 4.5.

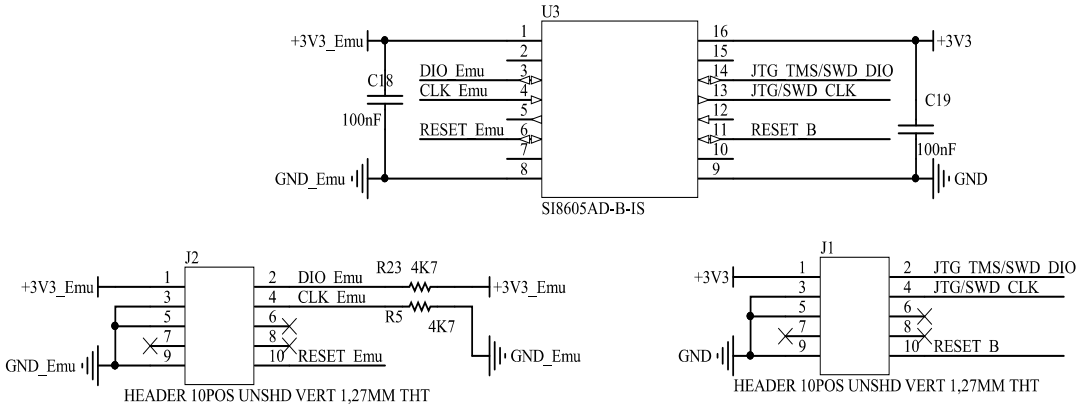

Figure 4.5 : Schematic design for isolated and non-isolated debugging.

Connection with the inverter board is done via two headers. Controller board is designed with matching connectors, that are wired according to the signals of inverter board. This section is shown in Figure 4.6.

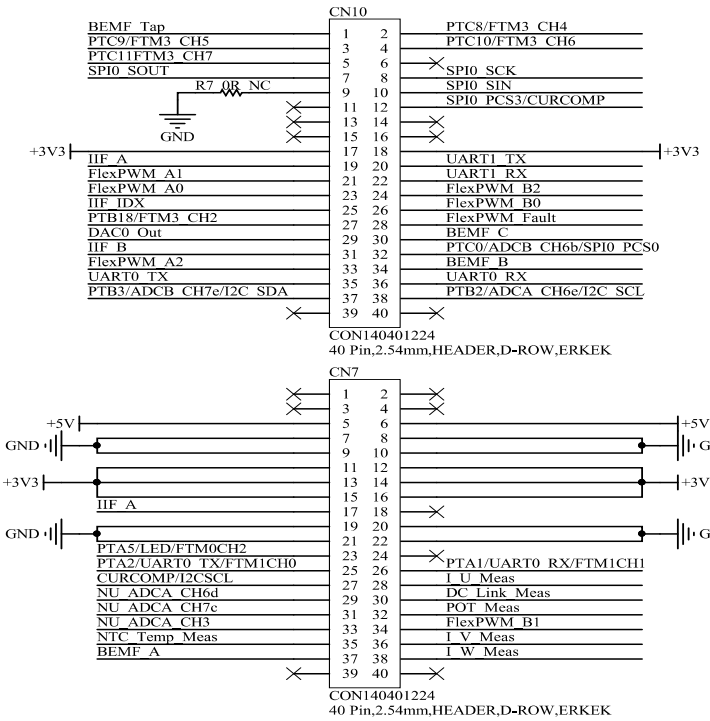

Figure 4.6 : Header connectors to match signals with inverter board.

The designed controller board is then manufactured and assembled as given in Figure 4.7.

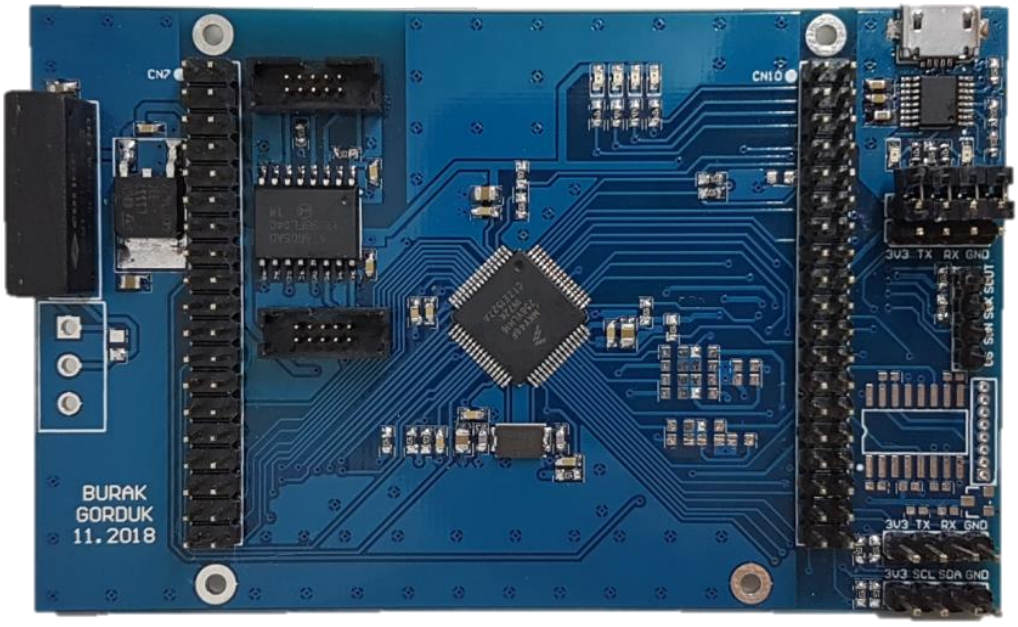

Figure 4.7 : Manufactured and assembled controller board.

Connection of the controller board with the inverter board is done easily as intended. Inverter board has a switching regulator that generates 5V output from the DC supply voltage and this 5V supply is sent to controller board. A linear regulator is used on controller board in order to generate 3.3V logic power supply that provides power for the microcontroller, operational amplifiers and comparators. Figure 4.8 shows the designed drive system.

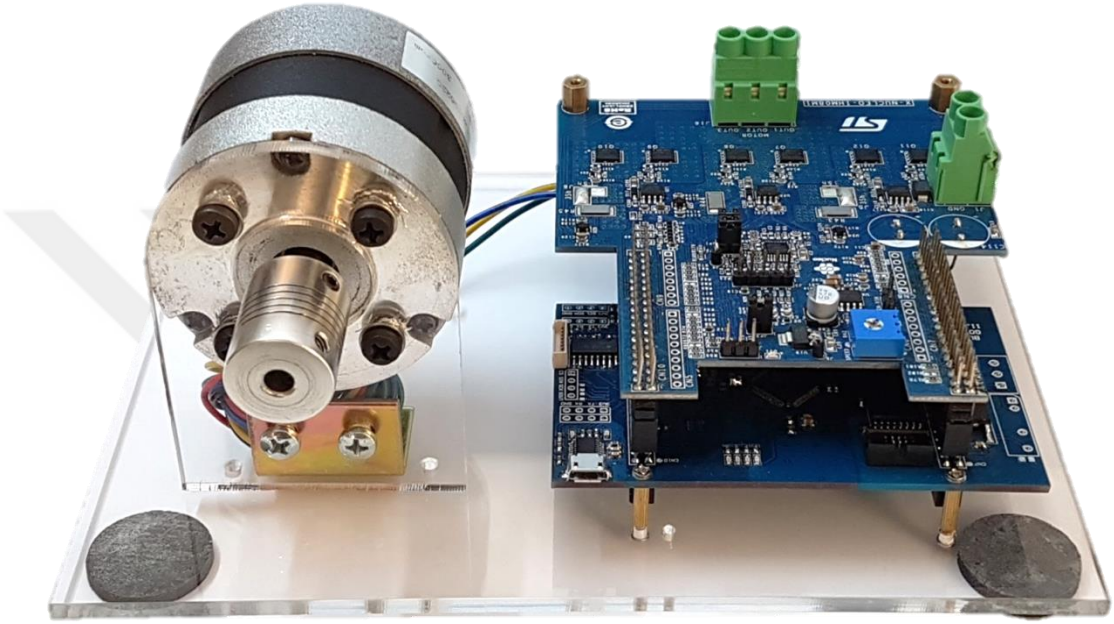

Figure 4.8 : Drive system with controller, inverter and motor.

DC input power is supplied to the system via a two contact screw terminal. Three-phase motor output is connected to a three-contact screw terminal.

4.3 Simulation of Sensorless FOC Using Extended Back-EMF Observer

In order to verify position estimation schemes, a simulation environment is created in MATLAB Simulink. The motor parameters given in Table 4.1 are used for the motor model. These motor parameters are obtained from an actual motor. This motor is used in experimental work phase of the study. Block diagram of the sensorless FOC system created in Simulink environment is given in Figure 4.9. System is modeled and simulated as a continuous system.

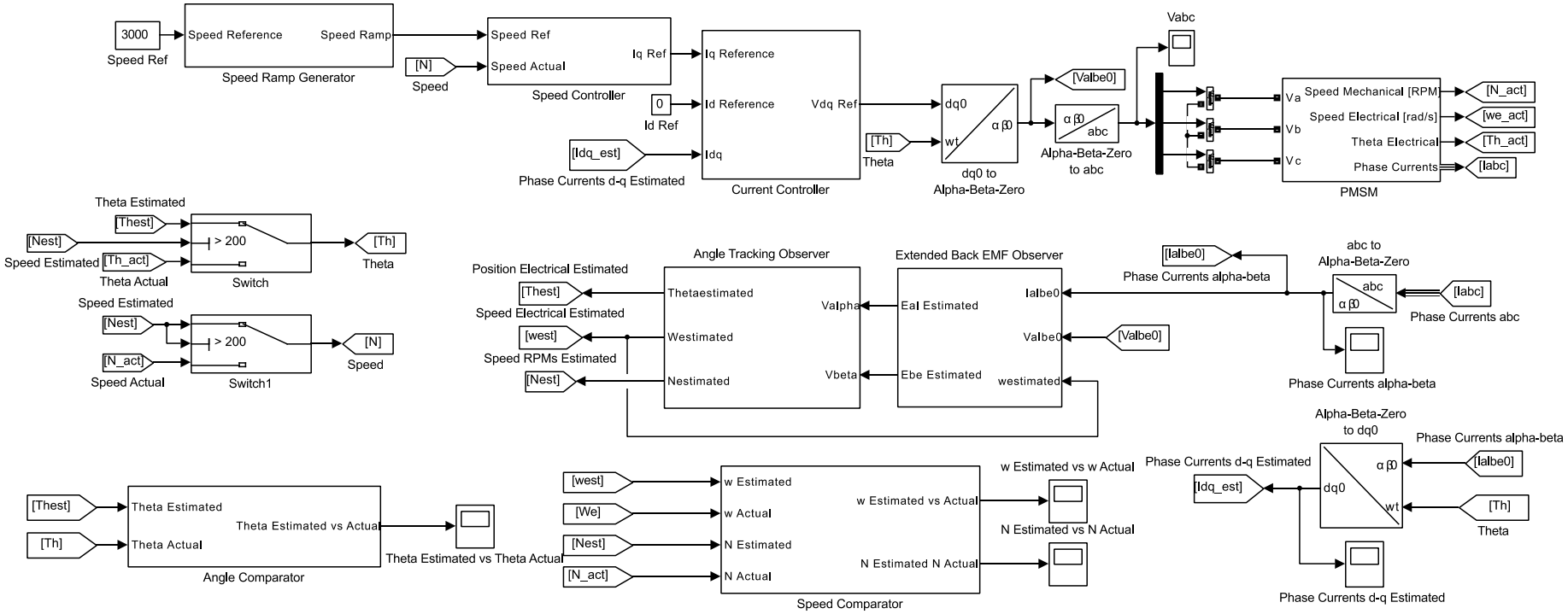

Figure 4.9 : Simulation block diagram of the sensorless FOC drive system.

Table 4.1 : Motor parameters used in simulation.

Parameter	Unit	Value
Phase Voltage	[V]	24
Power	[W]	62
Nominal Torque	[Nm]	0.2
Nominal Speed	[rpm]	3000
Pole Pairs	-	2
Back-EMF Constant	[V.sec/rad]	0.0023
R_S	[Ω]	0.437
L_d	[H]	0.000536
L_q	[H]	0.000548

Motor model block with the defined parameters in Table 4.1 is given in Figure 4.10.

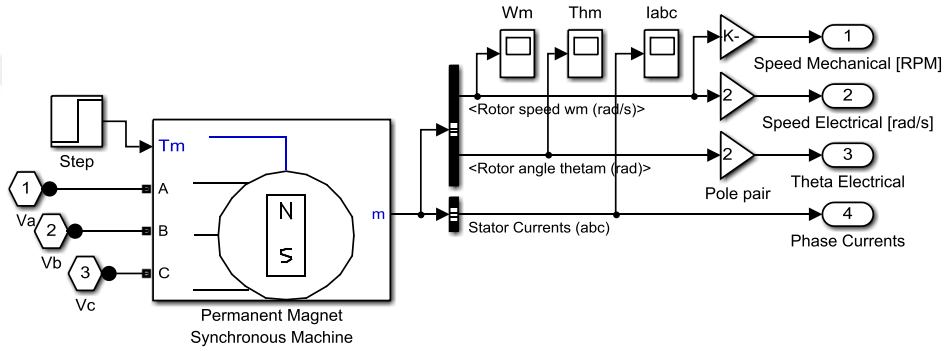

Figure 4.10 : Motor model in Simulink.

The simulation starts with no load and 3000 rpm speed reference. Nominal torque of 0.2 Nm is applied at 0.75 s simulation time. Speed reference is generated by speed ramp generator block shown in Figure 4.11.

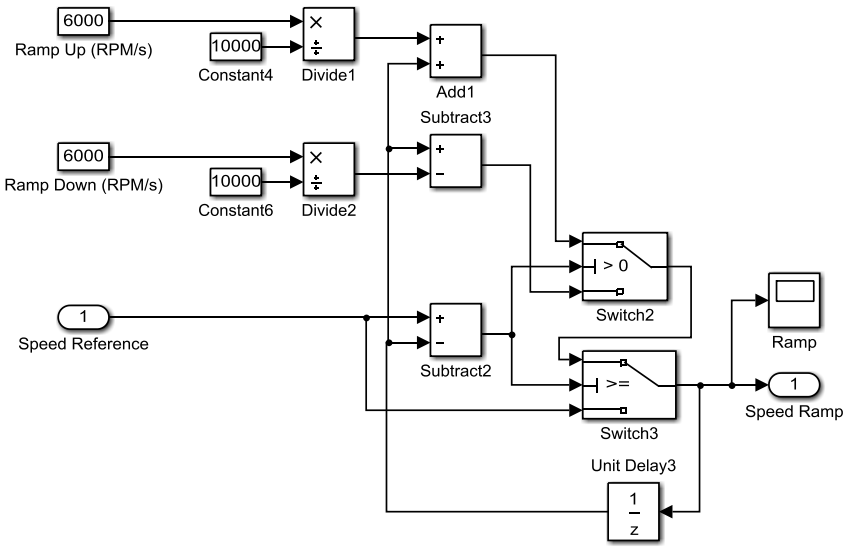

Figure 4.11 : Speed ramp generator model**.**

This provides an acceleration-controlled speed reference in order to minimize overshoots and guarantee stable operation. In this block, both the acceleration and deceleration can be individually controlled. Simulations are done with 6000 rpm/s selected as acceleration and deceleration ratio. Figure 4.12 shows 3000 rpm speed reference and output of speed ramp generator. Desired speed is achieved within 0.5 seconds.

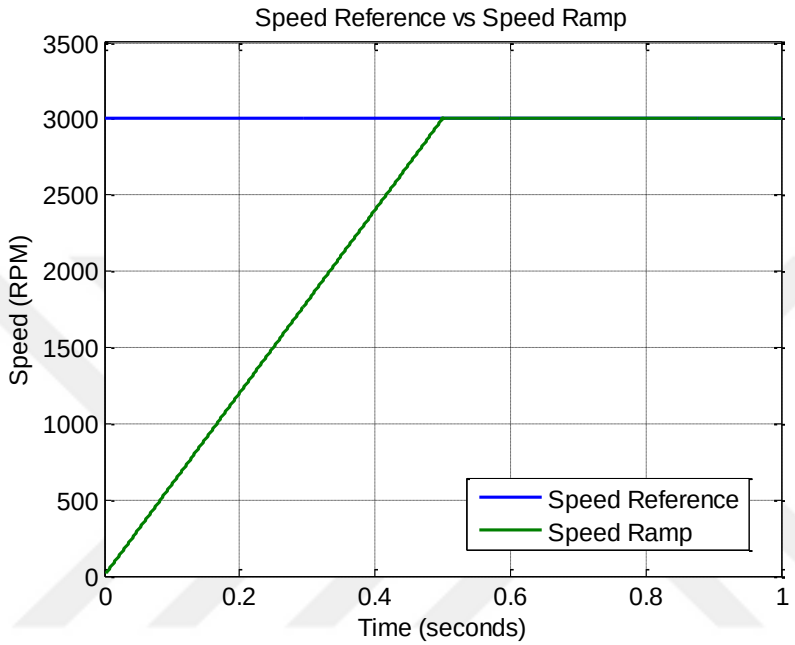

Figure 4.12 : Speed reference and ramp output.

Speed controller calculates the error between desired and estimated speed. This error is minimized using a PI controller that outputs the quadrature axis current reference with maximum output limited with maximum motor current. In operation below nominal speed, direct axis current reference is kept at zero. Speed controller block is given in Figure 4.13.

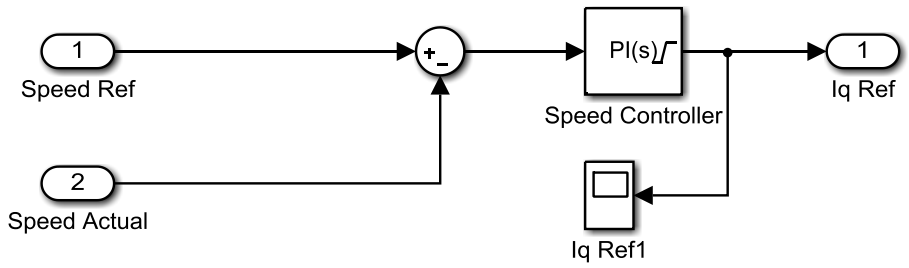

Figure 4.13 : Speed controller model.

Speed controller coefficients are tuned by observing step response of the system. Figure 4.14 shows the speed controller performance during operation.

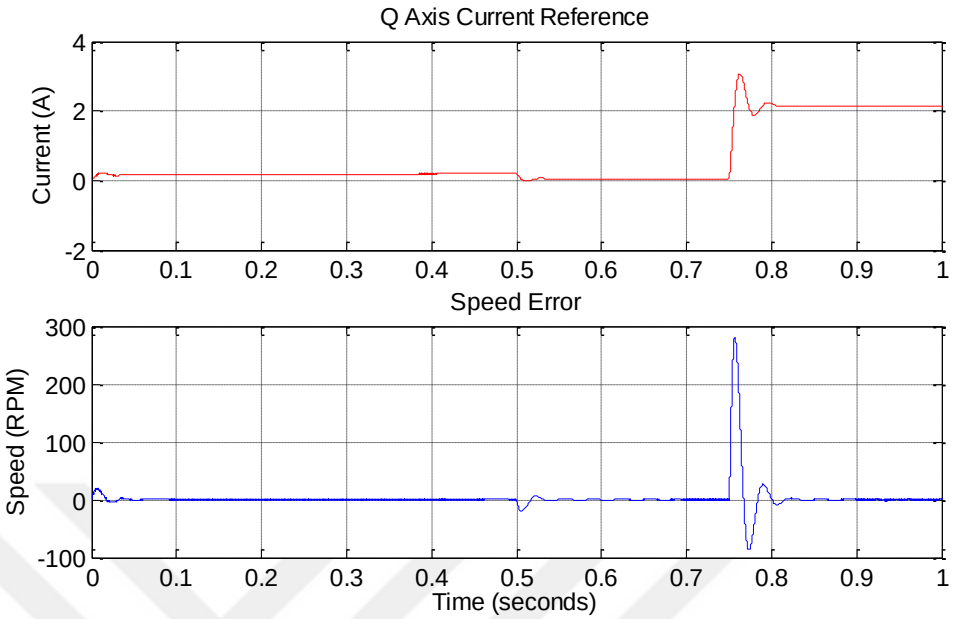

Figure 4.14 : Speed controller performance.

Two PI controllers for motor currents are used for compensation of error between current references and estimated currents i_d and i_q. Current controller block is shown in Figure 4.15.

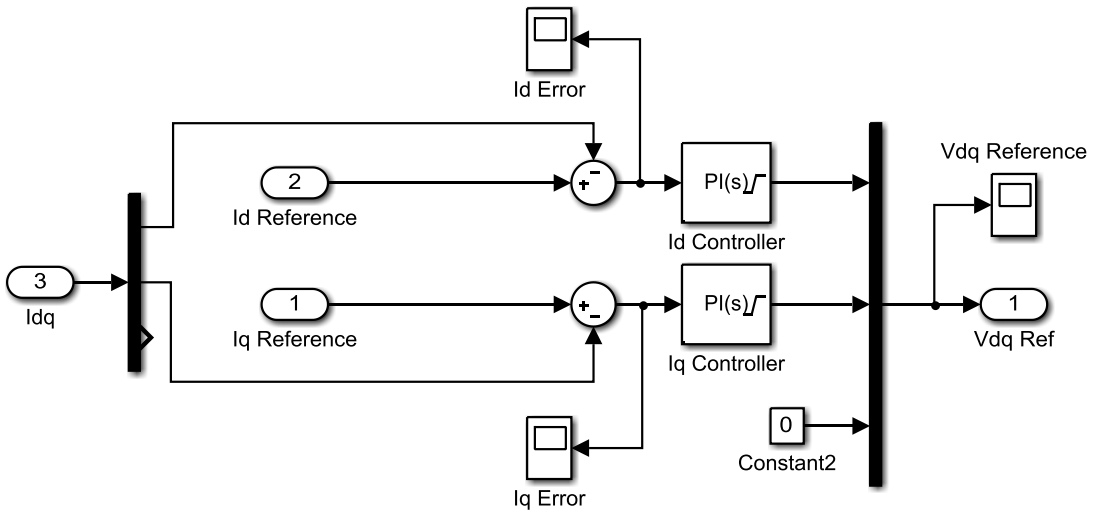

Figure 4.15 : Current controller model.

Both of the current controllers are tuned for the same coefficients. Figure 4.16 shows the performance of q axis current controller.

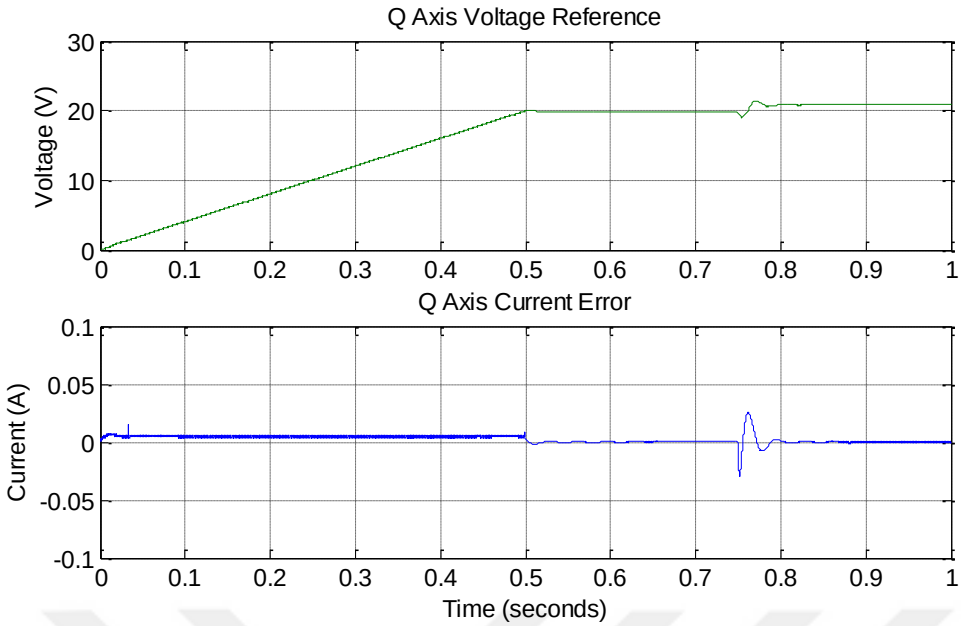

Figure 4.16 : Q axis current controller performance.

It can be seen that q axis current is controller with minimal error during transients. Performance of d axis current controller is given in Figure 4.17.

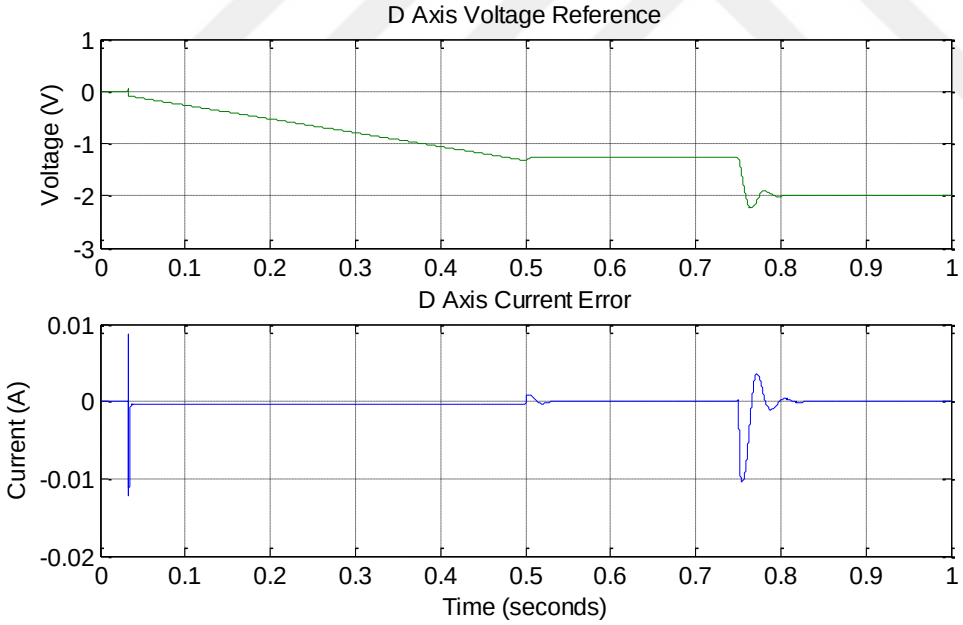

Figure 4.17 : D axis current controller performance.

Current controllers output d and q axis voltage references. These references are then transformed into two-phase stationary reference frame and finally to three-phase stationary reference frame. Voltage references then applied to the stator directly. Figure 4.18 shows the phase voltages along with zoomed-in view.

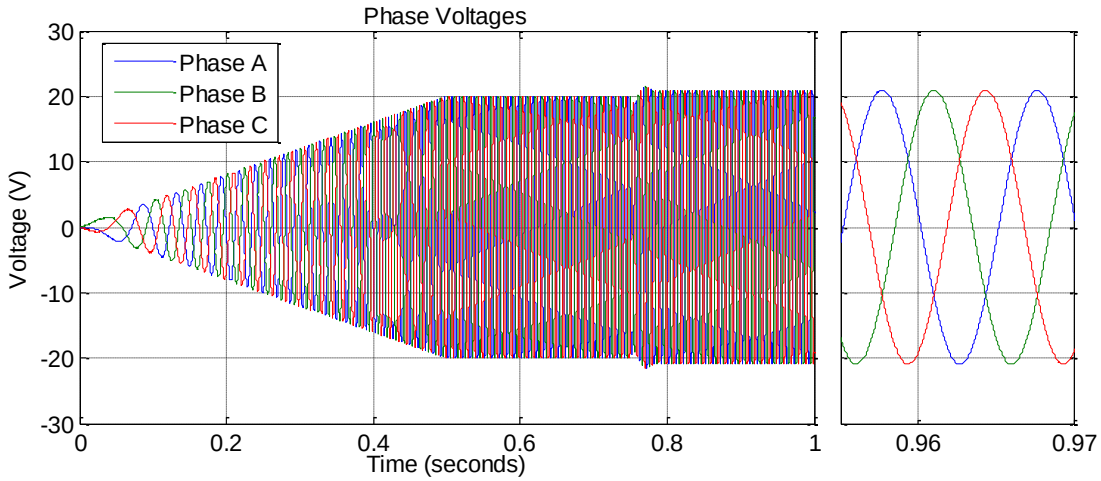

Figure 4.18 : Phase voltages with zoomed-in view.

Corresponding phase currents are given in Figure 4.19 synchronized with rotor electrical position.

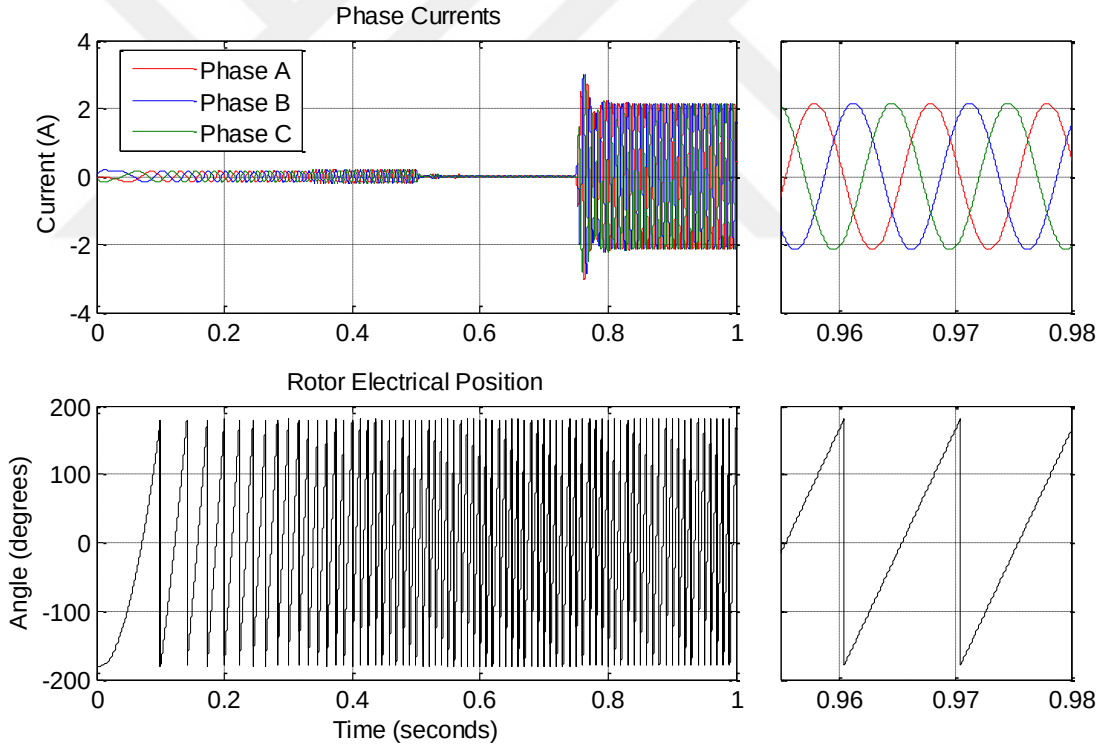

Figure 4.19 : Phase currents and electrical position with zoomed-in views.

Three regions can be observed from the phase currents. It can be seen that the acceleration current until 0.5 seconds. Then since desired speed is achieved and load is not present, current amplitude is very small. At the instant of full load transition, current amplitudes are increased in order to compensate for the speed drop.

Figure 4.20 shows the shaft speed under load disturbances. It is seen that the system response is fast and speed is recovered quickly with minimal overshoot.

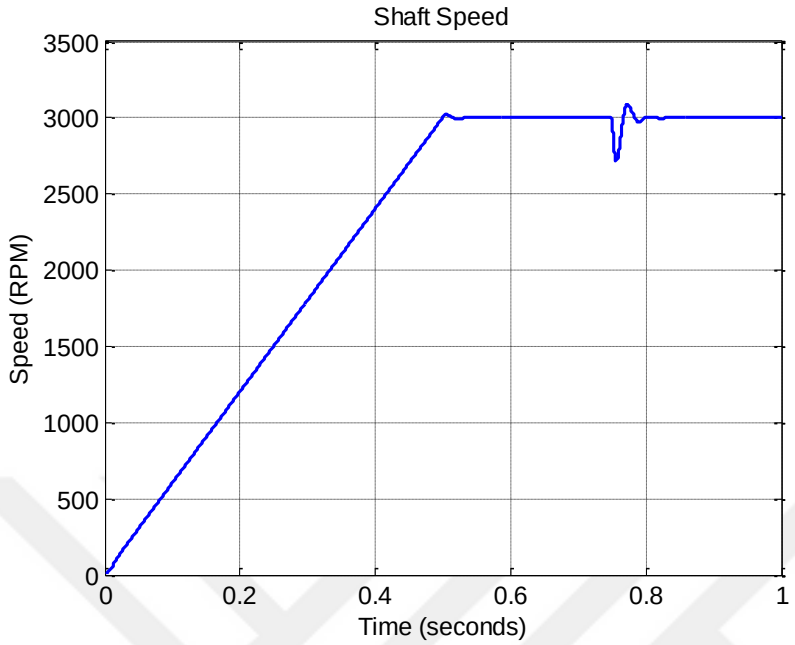

Figure 4.20 : Shaft speed with no-load startup to full load transition.

Three-phase currents are read from the motor model. Then, the currents are transformed into two-phase stationary reference frame α-β. Currents i_α, i_β and applied voltages at previous step u_α, u_β with the previous estimation of rotor electrical speed is entered as inputs into extended back-EMF observer model given in Figure 4.21.

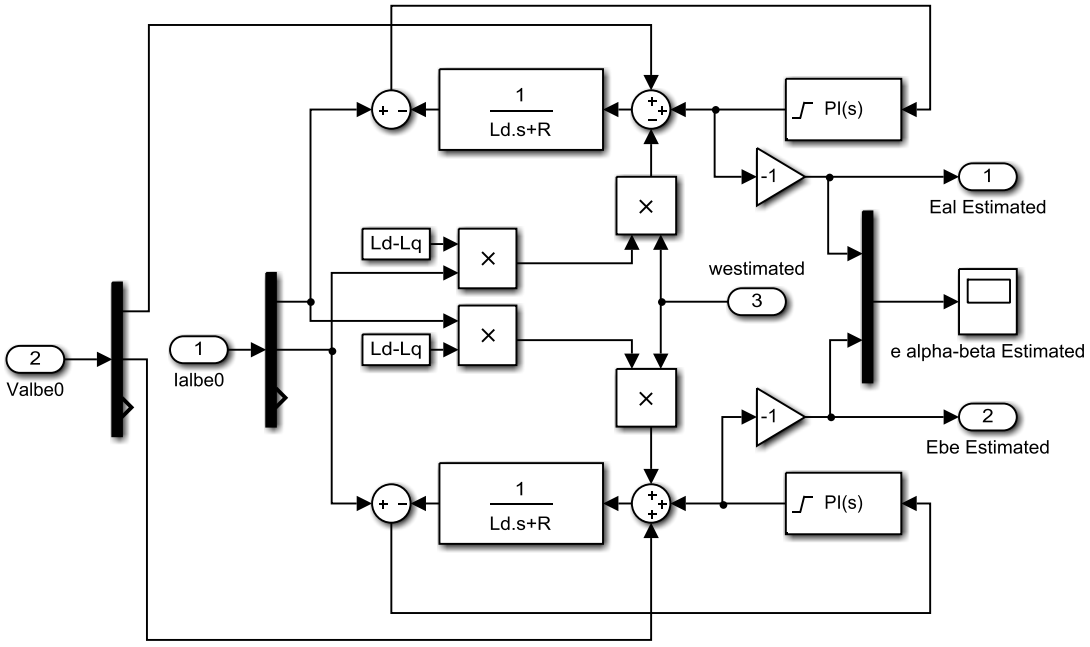

Figure 4.21 : Extended back-EMF observer model.

Output of the extended back-EMF observer are the back-EMF terms given in equation 3.23 Components of the back-EMF term α and β correspond to negative sine and positive cosine signals of rotor electrical position θ_e. The angle-tracking observer given in Figure 4.22 uses these sine and cosine signals to extract estimated rotor electrical position and speed.

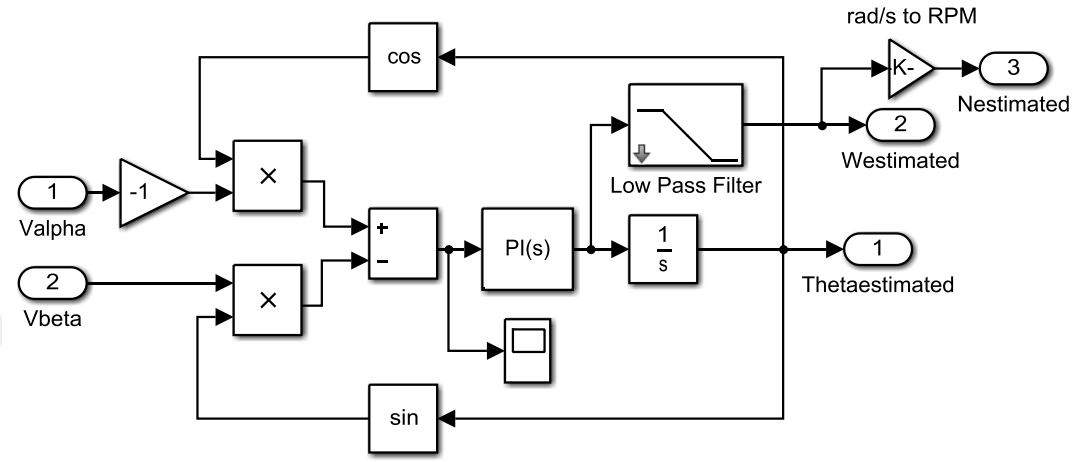

Figure 4.22 : Angle-tracking observer model.

Speed information is obtained before integrator block. Since this information contains high frequency noises, a lowpass filter with 0.5 ms time constant is used.

In another simulation environment, position estimation based on flux estimator is implemented. Extended back-EMF model is replaced with flux estimator model given in Figure 4.23. In this estimator model, two low pass filters are used with a derivative operator in between.

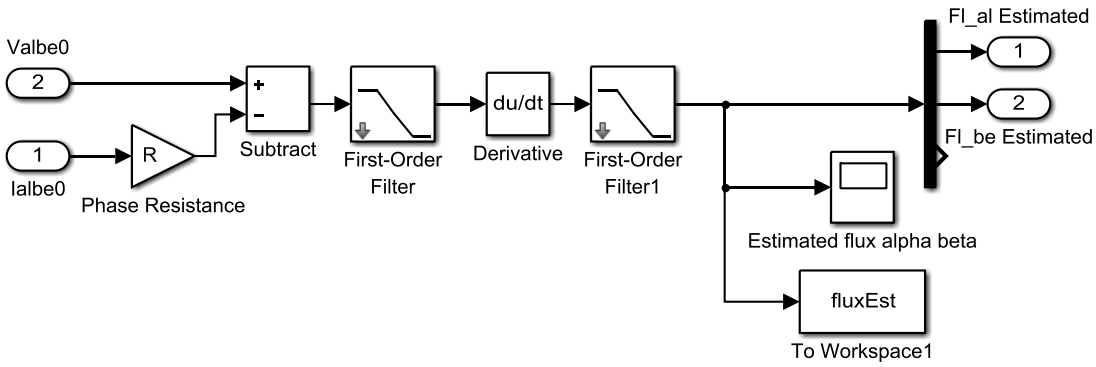

Figure 4.23 : Flux estimator model.

Position and speed is again extracted by using the angle-tracking observer. However, this model is now rearranged since alpha and beta flux estimations now correspond

to cosine and sine terms instead of the minus sine and cosine terms of extended back-EMF observer.

The simulation is done for the extended back-EMF observer first. The position and speed estimation results are obtained for each estimation method. Figure 4.24 shows the extended back-EMF estimation with zoomed-in view.

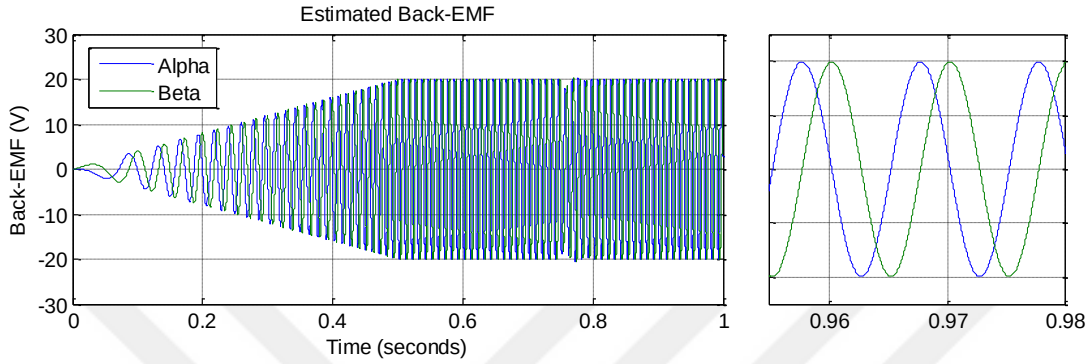

Figure 4.24 : Output of back-EMF observer with zoomed-in view.

Figure 4.25 shows the position estimation performance of extended back-EMF observer method.

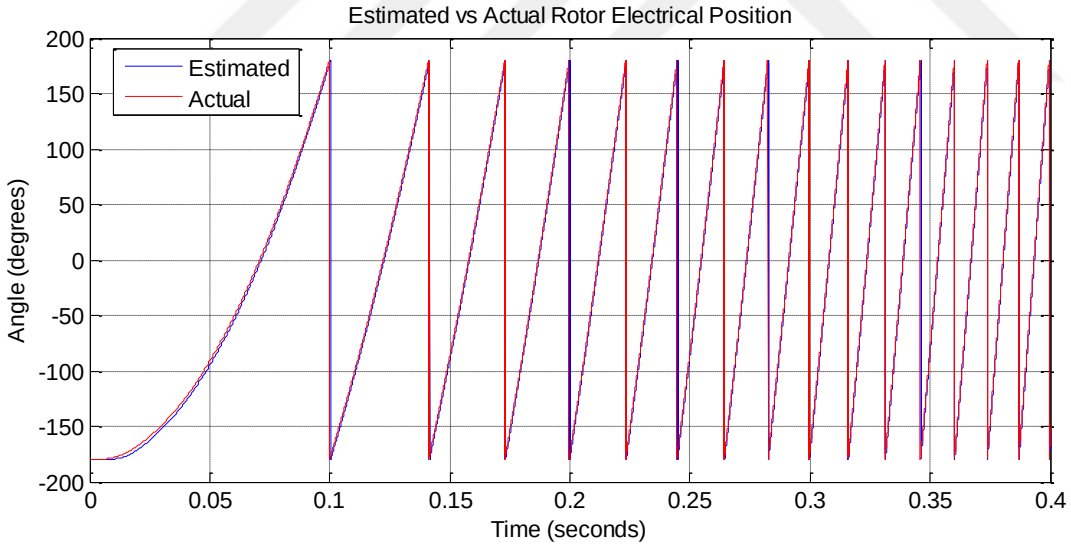

Figure 4.25 : Position estimation performance of extended back-EMF observer.

It can be said that position estimation is accurate and has a very high dynamic performance. Since the startup is done as open loop, position estimation error from standstill to 200 RPM has no effect on the performance of the control. Figure 4.26 shows the speed estimation performance.

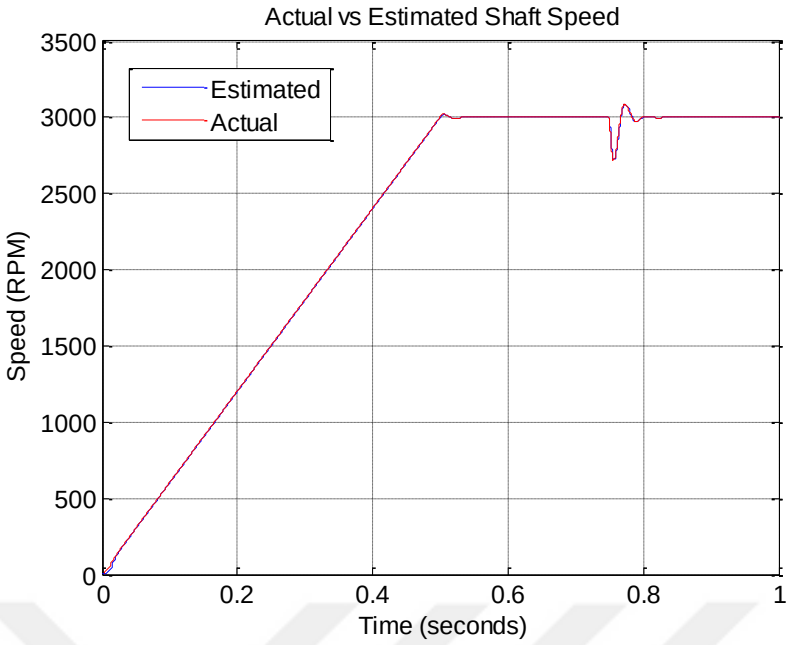

Figure 4.26 : Speed estimation performance of extended back-EMF observer.

Low pass filter used in the angle-tracking observer provides a smooth speed estimation output with no significant delay present. The simulation verifies transient and steady state operation of the extended back-EMF observer with angle-tracking observer.

Simulation is done for the position estimation based on flux estimation method. Figure 4.27 shows the output of flux estimator model. Alpha and beta values of estimated flux is shown with zoomed-in view.

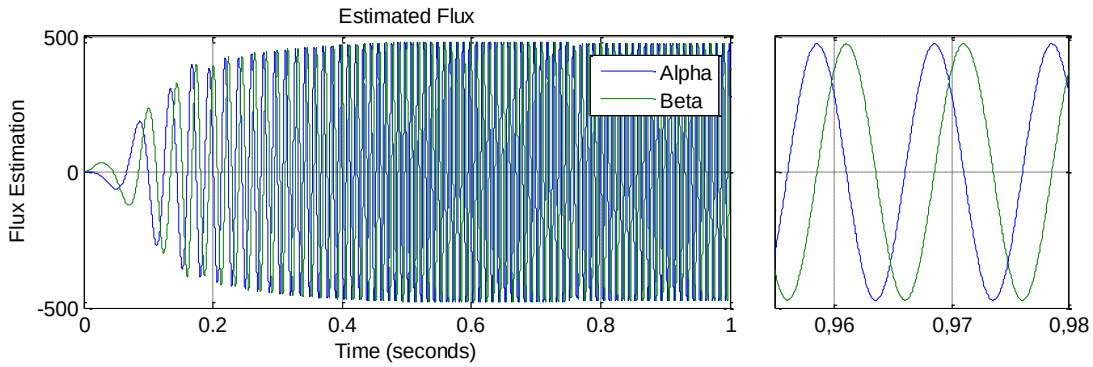

Figure 4.27 : Flux estimation with zoomed-in view.

It can be seen that amplitude of estimated flux is stabilized only after certain time of operation. This is caused by the time constants of low pass filters used in flux estimator model. Position estimation performance is given in Figure 4.28.

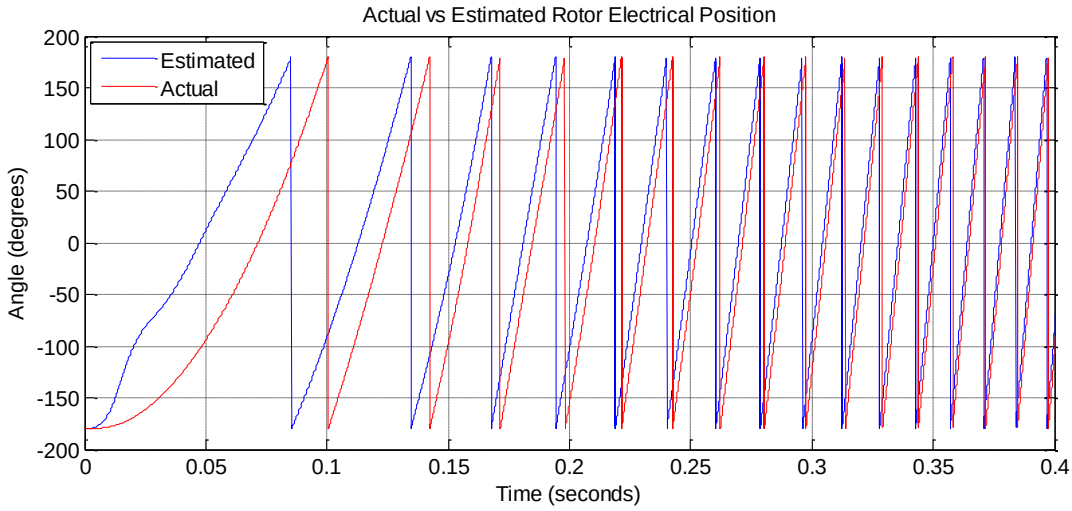

Figure 4.28 : Position estimation performance of flux estimator.

Effects of the initial start due to filter coefficients can be clearly seen in position estimation output. In open loop region, maximum position error is about 120 degrees. Around 0.4 seconds, position estimation became accurate and dynamic. Decreasing the time constants caused steady state position error to increase. Speed estimation performance is given in Figure 4.29.

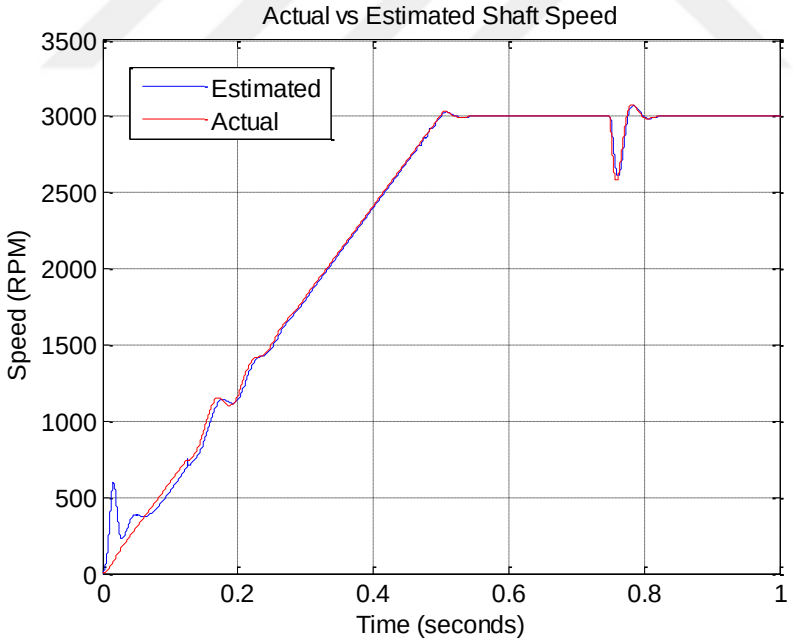

Figure 4.29 : Speed estimation performance of flux estimator.

Position error at initial startup also caused undesired increases in estimated speed. Due to non-smooth initial estimation, transition point between open loop startup and closed loop operation is increased to 700 rpm. With these simulations, it is observed that the extended back-EMF observer performed better than flux estimator.

4.4 Embedded Software Design

Design of the FOC embedded software is developed in IAR Embedded Workbench environment. The general structure of the software has multiple Finite State Machine (FSM) structures. Main state machine consists of the states “Init”, “Ready”, “Run” and “Fault” as shown in Figure 4.30 along with the state transitions. Microcontroller automatically goes through a Power-On Reset (POR) after it is powered up. After the reset microcontroller goes into initialize state. This state defines the functions necessary for initializing requisite microcontroller peripherals such as clock generation, general-purpose timers, PWM and ADC. State is automatically changed to ready after initializing is done. When microcontroller is in ready state, speed command is expected as a user input. If a non-zero speed reference is set, then the state transition from ready state to run state is executed.

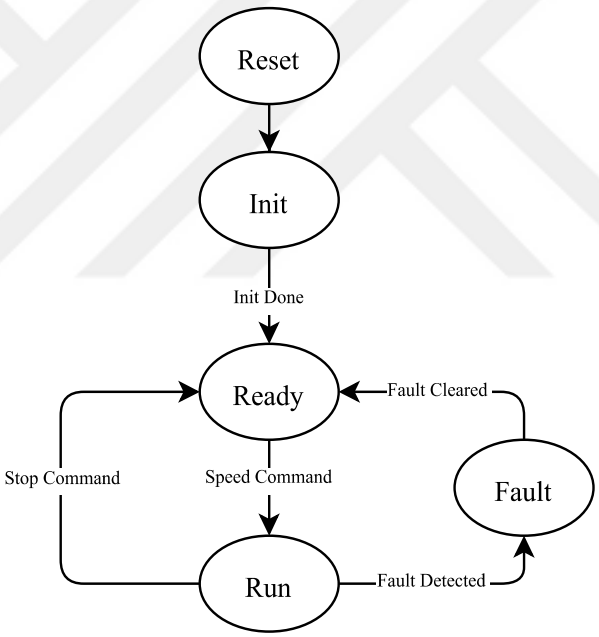

Figure 4.30 : Main state machine diagram.

4.4.1 Selection of switching and control loop frequencies

Switching frequency of the inverter is not directly calculated but selected based on certain parameters of the application and common rules. In order to select switching frequency for a FOC application, effects of the switching frequency and its relationship between control loops should be understood. Switching frequencies up to 30 kHz are generally used for motor control applications. There are advantages and disadvantages for both higher and lower frequencies. Current control loop

frequency is directly related to switching frequency. In fact, switching frequency defines the upper limit for control loop frequency. In digital implementation, this is achieved by calling the current control loop at every PWM interrupt. If a slower frequency is desired than control loop can be called at every second interrupt. Lower limit of the switching frequency can be defined by control loop frequency.

Selection of switching frequency starts with selection of the lower limit. This lower limit depends on several parameters. First of all, it should be equal or higher than the minimum control loop frequency. Minimum control loop frequency depends on two factors, which are related with the application specifications and motor parameters. In order to generate sinusoidal current shape correctly, control loop frequency must be at least 10 times higher than electrical output frequency. This means one period of the sine wave will have at least 10 independent points. Higher the amount of points, better the quality of the waveform in terms of harmonics. For this application, 4000 rpm is selected as maximum operation speed and at least 20 points for sine wave is selected. Electrical frequency of the sinusoidal output is calculated as given in equation 4.1.

$$f_{el} = \frac{N}{60} \cdot p \cong 134Hz \tag{4.1}$$

Then minimum control loop frequency can be calculated as given in equation 4.2.

$$f_{loop} \geq f_{el} \cdot 20 = 2680Hz \tag{4.2}$$

Another parameter that is closely related to control loop frequency is the electrical time constant of the motor. Control loop period must be at least 10 times faster than the time constant. This factor is important because loop stability issues and oscillations will occur if this rule is not followed correctly.

FOC has two inner control loops. Control loop frequency of each loop should also be determined. RL time constant of the motor in direct axis is calculated as given in equation 4.3

$$\tau_d = \frac{L_d}{R_S} = 0.001265s \tag{4.3}$$

RL time constant of the motor in quadrature axis is calculated as given in equation 4.4.

$$\tau_q = \frac{L_q}{R_S} = 0.001254s \tag{4.4}$$

Since time constant of the motor is very close in both axis' same control frequency can be utilized for both of the current controllers. Loop frequency must be at least 10 times faster than the time constant of q axis, which is faster than d axis. Equation 4.5 calculates the minimum loop frequency based on this time constant.

$$f_{loop} \geq \frac{1}{\tau_q} \cdot 10 = 7975Hz \tag{4.5}$$

Thus, minimum switching frequency in order to satisfy control loop requirements is calculated as 8 kHz. However, another parameter is taken into consideration for selecting minimum switching frequency. As the motor current increases to couple of amperes, high frequency vibrations that occur on the stator windings due to PWM become audible. Depending on the application, elimination of such noises is necessary most of the time. This defines a new lower limit and it is directly related to hearing ability of the people. Depending on the age, audible range is 20 Hz to 20 kHz for humans. However, from 16 kHz sound pressure levels detected by ears greatly decreases. That is why, in many motor control applications 16 kHz switching frequency is selected as a standard. In this application, this fact is also taken into consideration and thus minimum switching frequency is selected as 16 kHz.

Since the minimum required frequencies for switching and control loop is defined, actual frequencies should be selected. There is no definition for a practical upper limit for switching frequency. In fact, after the requirements on minimum switching frequency is satisfied, further increasing of the frequency will only result in increased switching losses or increased costs due to use of better performing semiconductors. Thus switching frequency for this application is selected as 16 kHz and dead time between high and low switch signals is set as 1.5 us.

Loop frequency can be selected as 8 kHz or 16 kHz. Higher loop frequency results in better dynamic performance and increased waveform quality.

There is an upper limit for control loop frequency and it depends on many factors. Since this control will be implemented digitally, all the process required for control loop should be executed in the selected loop period. There are no certain rules for calculating how long the control loop will take simply because it depends on the developer, type and the clock frequency of the microcontroller, compiler, optimization settings of the compiler and other necessary tasks that the application requires. Such as the safety routines for IEC60730 Class B software, that is very common in home appliances products.

In this application though, it is already known with prior practical experience that 16 kHz current control can be achieved with MKV46 series microcontrollers by using 144 MHz system clock (RAM clock) and 72 MHz fast peripheral clock settings. Thus, control loop frequency is also selected as 16 kHz.

Mechanical time constant of the motor is very large compared to electrical time constant. Therefore, it is necessary to use a slower frequency for speed control loop. In this application, 200 Hz speed control frequency is selected.

4.4.2 Design of control loops

Figure 4.31 shows the flowchart diagram of the speed control loop. Speed reference is transferred to speed controller with an acceleration-controlled manner. This is achieved by applying fixed ramp function to speed command. Every speed loop starts with this ramp calculation. Speed error between the ramp output and actual speed is then calculated and compensated with a PI controller. This PI controller outputs required motor current in amps. However, it should be noted that in normal operation only the quadrature axis current reference is generated this way. Direct axis current reference is kept zero for normal operations below nominal speed. For the field weakening operation above nominal speeds, a sophisticated field-weakening controller is necessary in order to generate direct axis current reference. Output of the PI controller is limited to maximum allowable current in the application. In this case, it is set to plus and minus 3.5 A as it is the motor maximum current.

Figure 4.32 shows the current control loop flowchart. This loop is repeated every 62.5 microseconds and it consists of the direct and quadrature axis current compensators along with the position and speed estimator. Every loop begins with the reading of the measured currents via ADC. These currents are then transformed

α-β and d-q axis currents respectively. Park transformation is done based on the previous output of the position estimator. Calculated currents and applied voltages in α-β axis are then used as input to back-EMF observer block. The observer outputs new estimations of position and rotor speed. New position estimation is then used for calculation of d-q axis currents and their errors. These errors are compensated with two independent PI control blocks, which outputs reference voltages in d-q axis. With the help of inverse Park Transformation and SVM, required duty cycle values for each PWM is calculated and then applied.

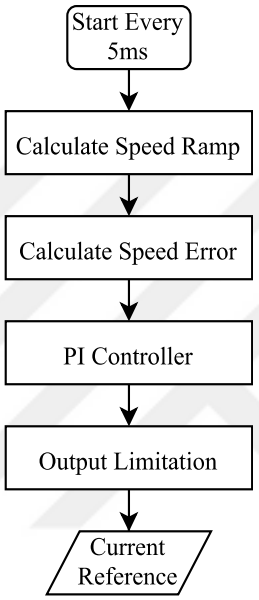

Figure 4.31 : Flowchart diagram of speed control loop.

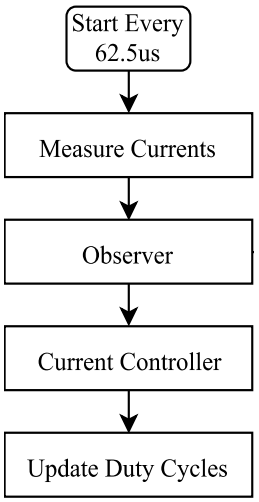

Figure 4.32 : Flowchart diagram of current control loop.

Block diagram of the speed and position estimator is given in Figure 4.33. Each loop starts with the calculation of estimated motor current in α-β axis. This is achieved by

implementing the motor model with the extended back-EMF term is excluded as given in Figure 4.9. Applied voltages, measured currents and previously estimated speed values are entered as inputs to motor model that calculates the estimated current. The error between estimated and measured current is then compensated with a PI controller that outputs excluded part of the motor model that consists of back-EMF term.

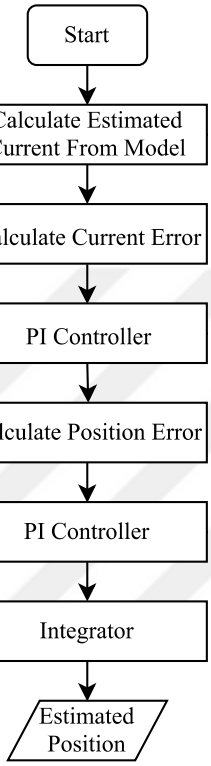

Figure 4.33 : Flowchart diagram of speed and position estimator.

Since the initial position of rotor is unknown and position estimation at very low speed has low performance due to low back-EMF generation, an open loop startup process is utilized. First, rotor is aligned to a known position. This is achieved by applying a vector that aligns the rotor to electrical zero degrees. Then an open loop speed ramp is applied to the speed controller. This is called open loop since the speed and position feedback necessary for the FOC is not obtained from the estimator but from the open loop ramp itself. When motor reached 200 rpm, induced back-EMF is enough for the observer to estimate rotor speed and position accurately. Thus, speed and position feedback is obtained from the estimator beyond 200 rpm.

5. EXPERIMENTAL RESULTS

Experimental verification of the driver system is done by the conducted experiments. The motor with its parameters given in Table 4.1 is driven with the designed drive system. In order to test dynamic behavior of the system, a test bench that is capable of loading the motor is set up. The test bench consists of a 400V rated PMSM coupled to the driven motor's shaft, which acts as a generator. Output of the generator is rectified using a three-phase rectifier. Obtained DC voltage is then fed into a variable resistor. Setup used for obtaining experimental results is given in Figure 5.1

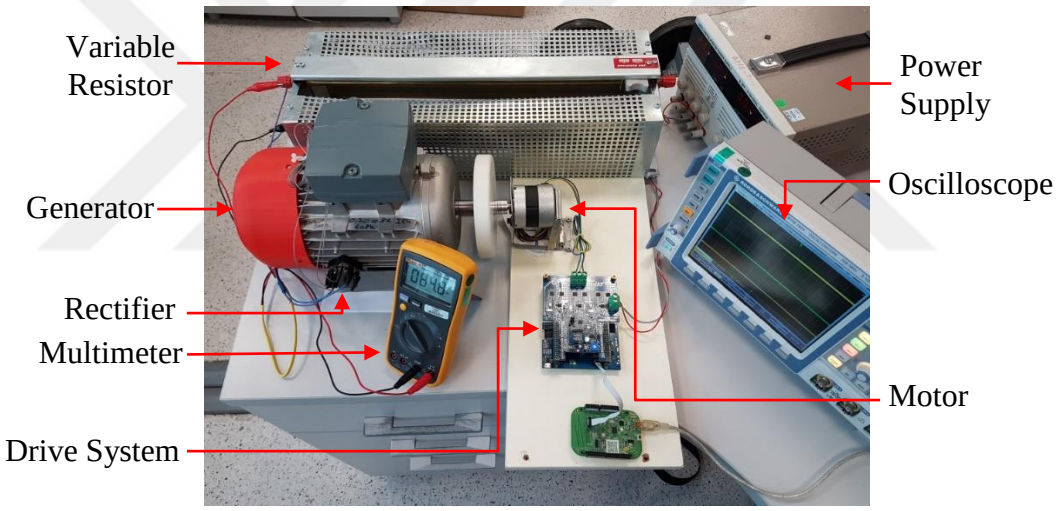

Figure 5.1 : Experimental test setup.

Online control and data acquisition of the drive system is done using the FreeMASTER Online Debug Tool. This tool is capable of sampling and modifying software variables along with the scope and recorder functionalities that provides time graphs of the signals. Performance of the extended back-EMF observer can be obtained from these graphs. The detailed waveforms of the position and speed estimation scheme in nominal speed are given in Figure 5.2. In this Figure, red and green waveforms correspond to the estimated back-EMF terms alpha and beta in order. Blue waveform shows the estimated position while orange waveform shows the estimated speed in rpms.

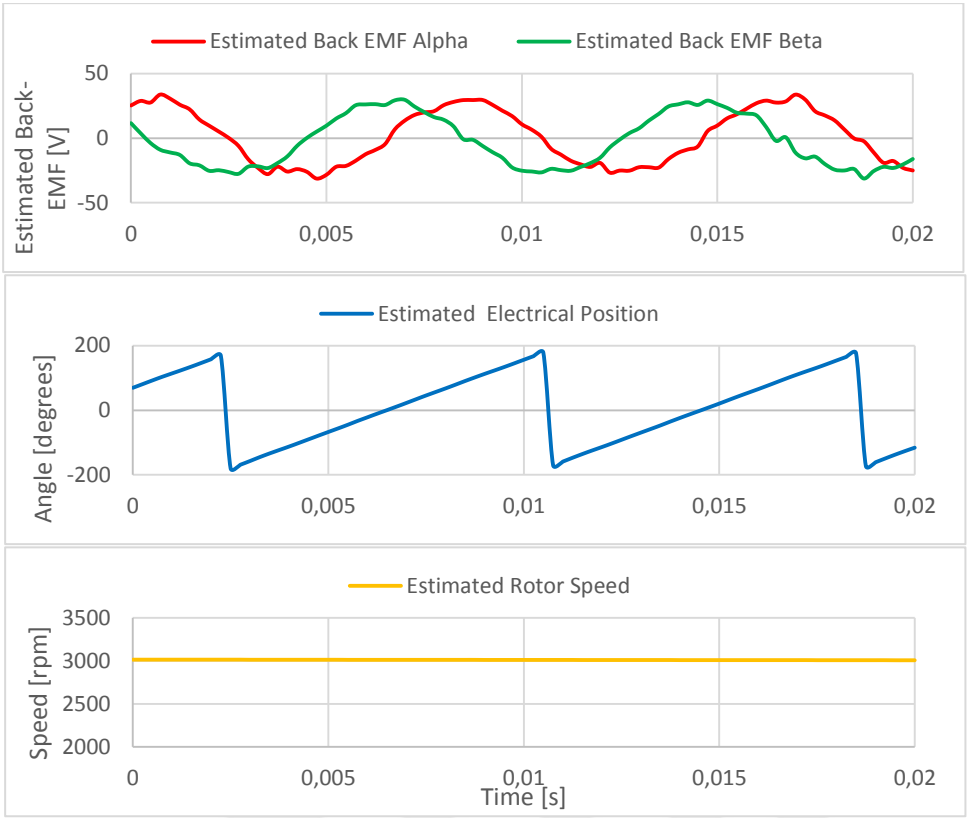

Figure 5.2 : Estimation outputs.

Performance of the drive system is evaluated by two different tests. No load performance of the system is tested first. Applying of nominal speed command with transient changes and speed reversal is tested. Figure 5.3 shows the speed ramp and actual shaft speed with red and green waveforms in order. Speed ramp is selected as 2000 rpm/sec. It can be seen that the drive system is capable of following the speed ramp accurately.

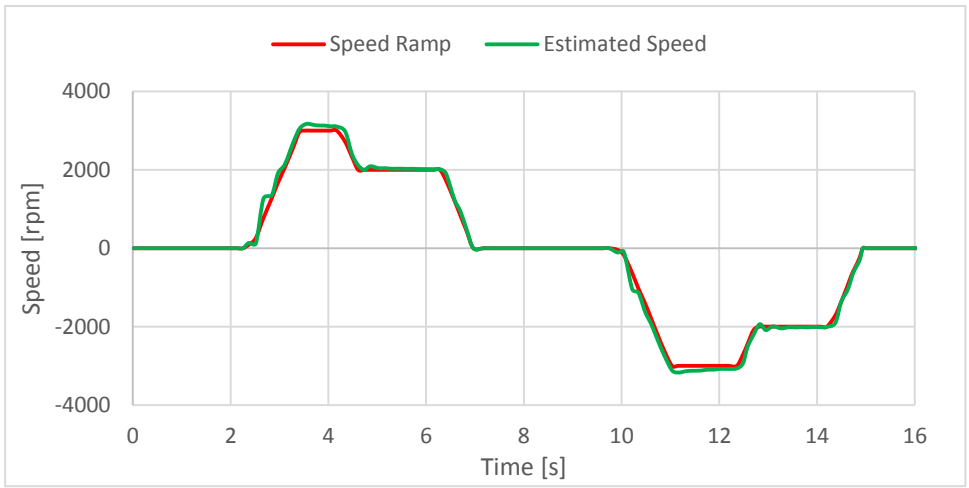

Figure 5.3 : Speed ramp and actual speed waveforms.

Figure 5.4 shows the applied voltages of alpha and beta at nominal speed in red and green waveforms in order.

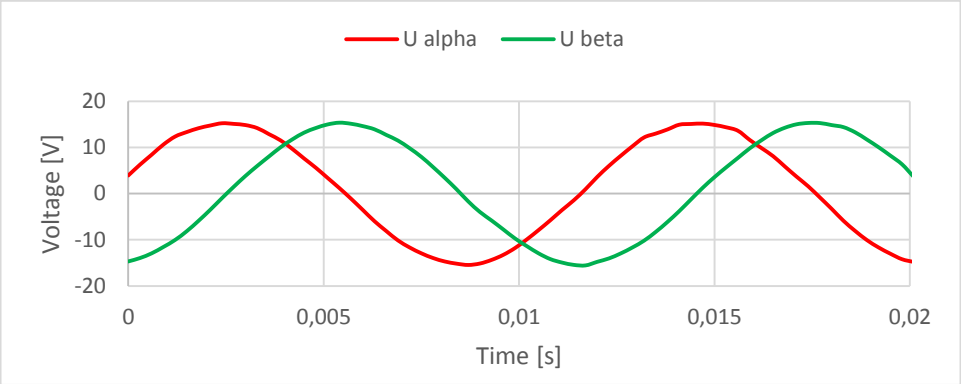

Figure 5.4 : Applied voltages of alpha and beta.

Output of the space vector modulation corresponding to reference alpha and beta voltage is given in Figure 5.5. In this Figure red, green and blue waveforms correspond to the duty cycle values of phase A, B and C in order.

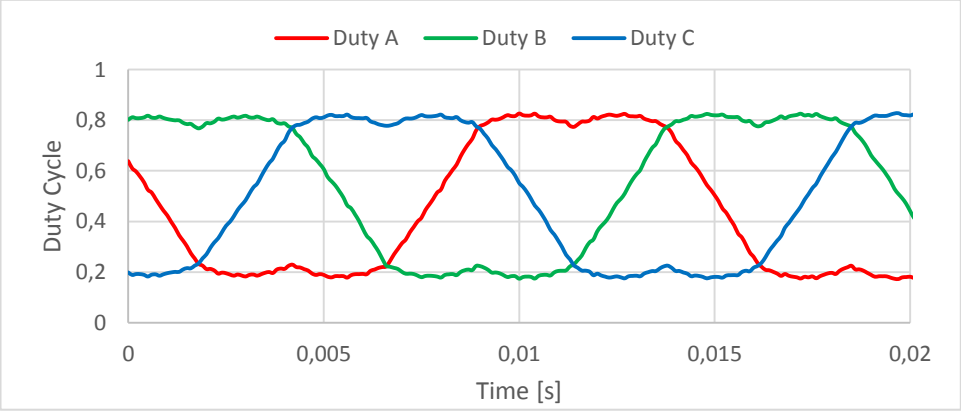

Figure 5.5 : Output of the SVM.

Waveforms of phase currents are shown in Figure 5.6.

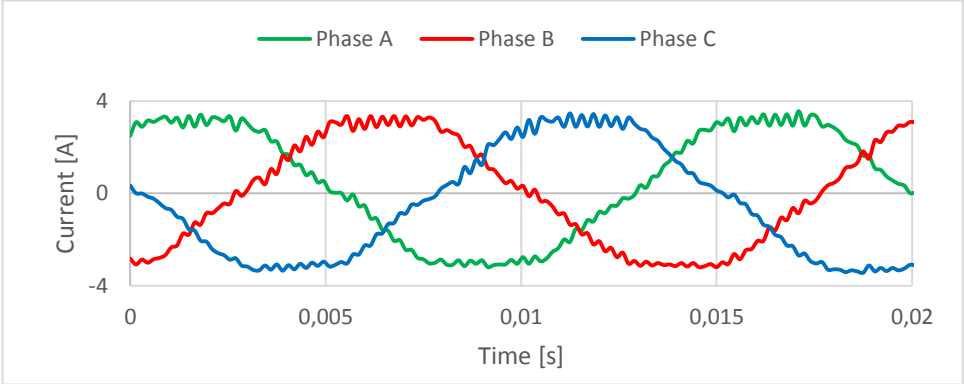

Figure 5.6 : Phase currents.

Figure 5.7 shows the calculated direct and quadrature axis currents. Red and green waveforms correspond to I_q and I_d in order. It can be seen that the direct axis current is kept at zero while quadrature axis current is increased to nominal load current. Figure 5.8 shows the oscilloscope capture of the one phase current at nominal load. Harmonics seen on the current waveform is due to motor having trapezoidal distributed windings.

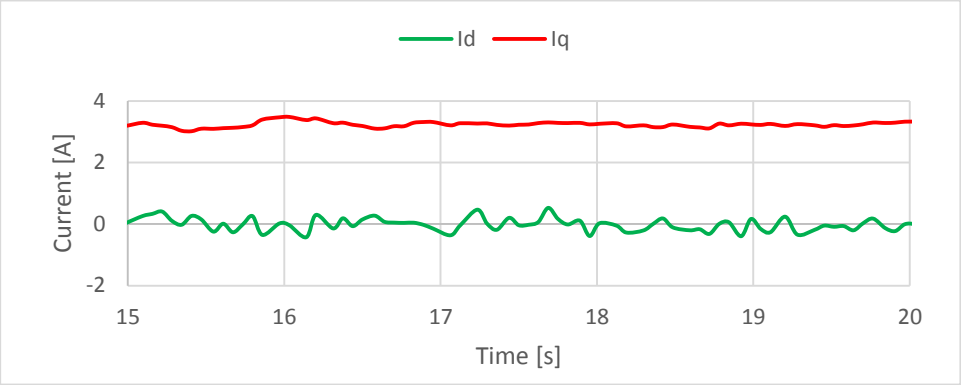

Figure 5.7 : Direct and quadrature axis currents.

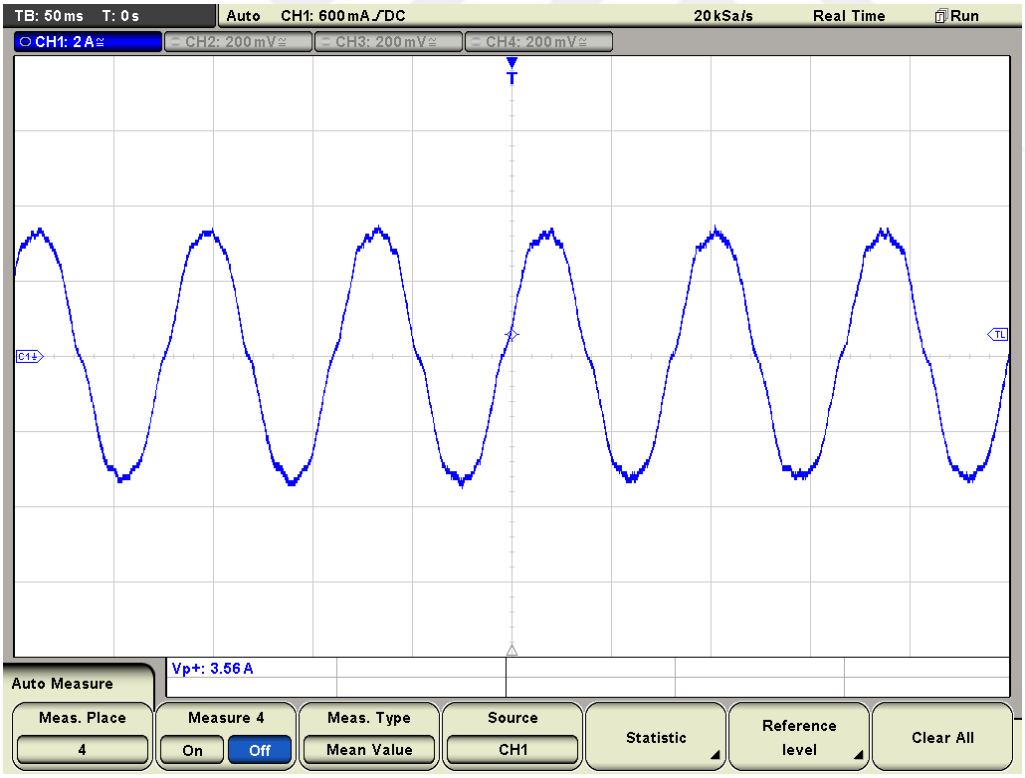

Figure 5.8 : One phase current at nominal load.

Figure 5.9 shows the induced back-EMF waveform of the motor when its shaft is rotated externally.

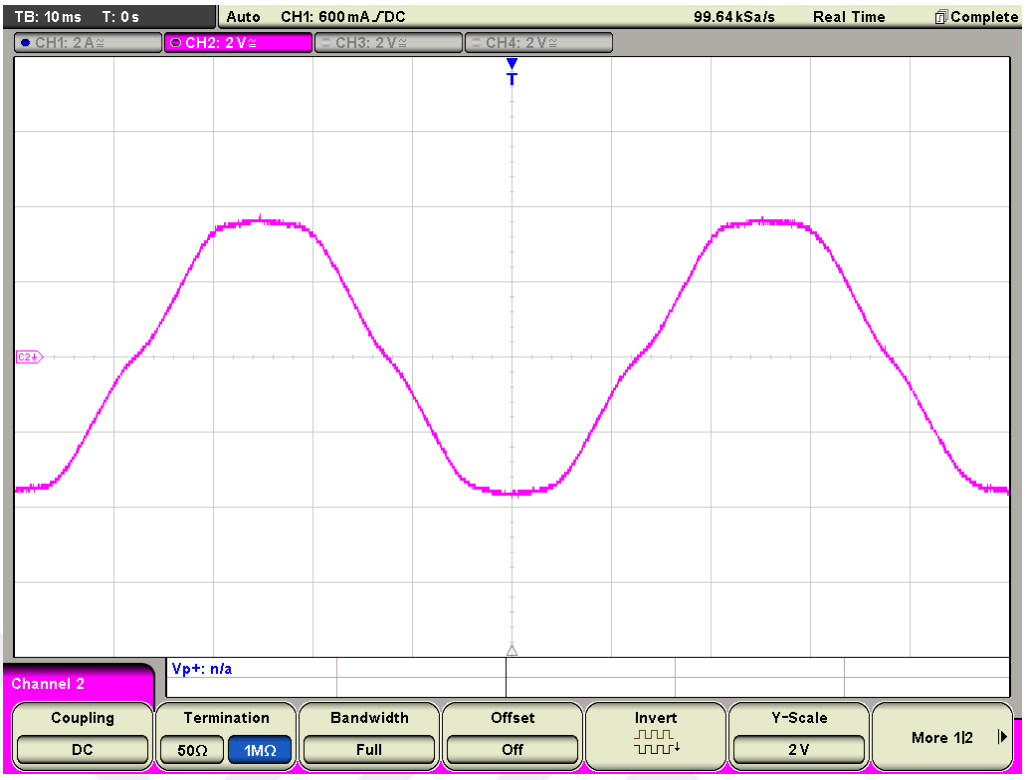

Figure 5.9 : Back-EMF waveform of the motor.

No load operation of the machine in field weakening region is also tested. 4000 rpm speed reference is set and achieved with the utilization of a direct axis current of -2 A. Quadrature and direct axis currents with the estimated speed is given in Figure 5.10 with red, green and cyan waveforms in order.

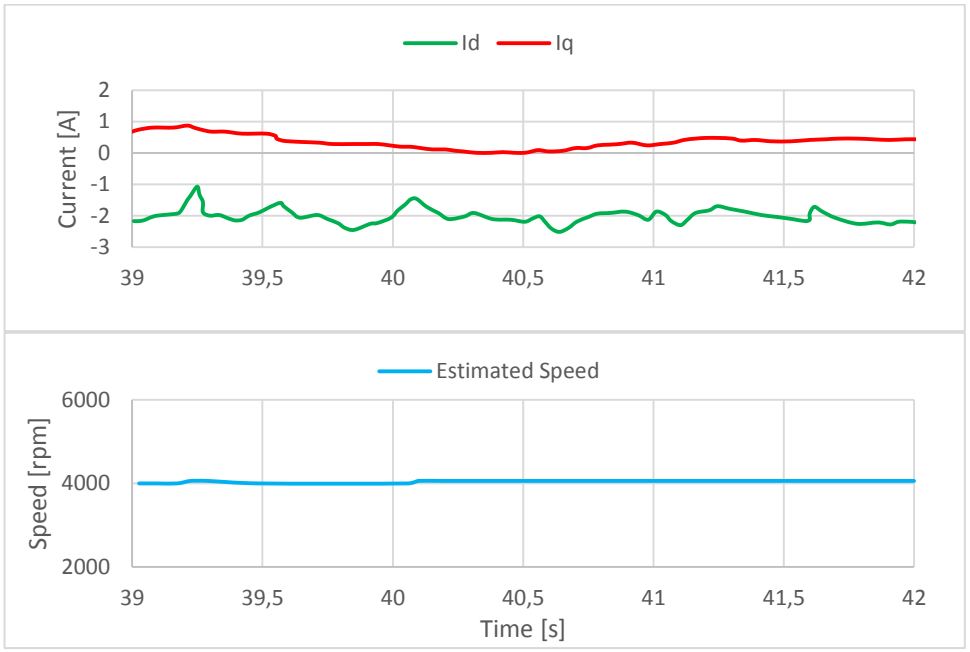

Figure 5.10 : Field weakening operation.

One phase current in no load field weakening operation at 4000 rpm is given in Figure 5.11.

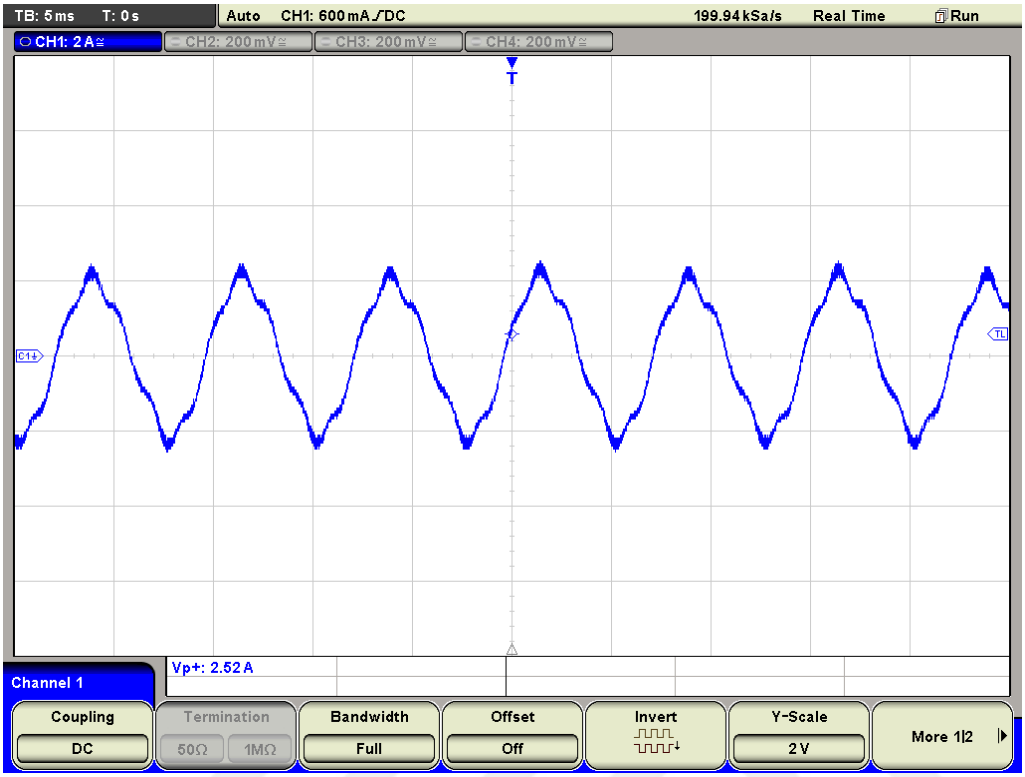

Figure 5.11 : Phase current waveform at field weakening region.

The second test for the validation of the drive system performance was the dynamic response of the system under transient changes on shaft load. This transient load change is achieved by switching the variable resistor to a fixed point. Figure 5.12 shows the system variables under transient changes. This graph starts with the machine loaded nominally, then when the time stamp shows 32s, connection to the load resistor is switched off. This causes the only load on the shaft to be inertia of the load generator. This sudden load change causes an overshoot of 10%. Speed overshoot is compensated within approximately 1 second. At time stamp of around 35.5s machine is again fully loaded. This transient loading cause machine shaft speed to decrease about 10%, which is then compensated in approximately 1 second.

It is observed that the system remains stable under transient changes in load. Figure 5.13 shows PWM output of a single phase. Dead time between two rising and falling edges can be seen as 1.5 us. Due to the gate drivers used on the inverter board (L6398 from STMicroelectronics) having inverted low side inputs, both signals have same polarity. Channel 2 is inverted on the oscilloscope.

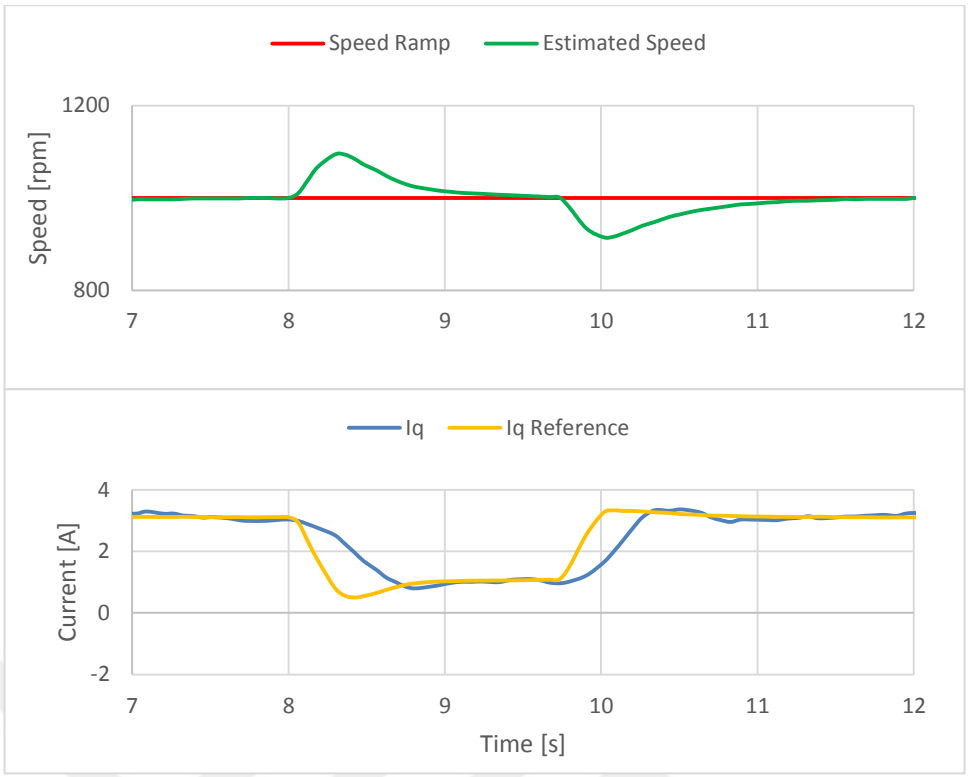

Figure 5.12 : Dynamic performance of the system under transient load changes.

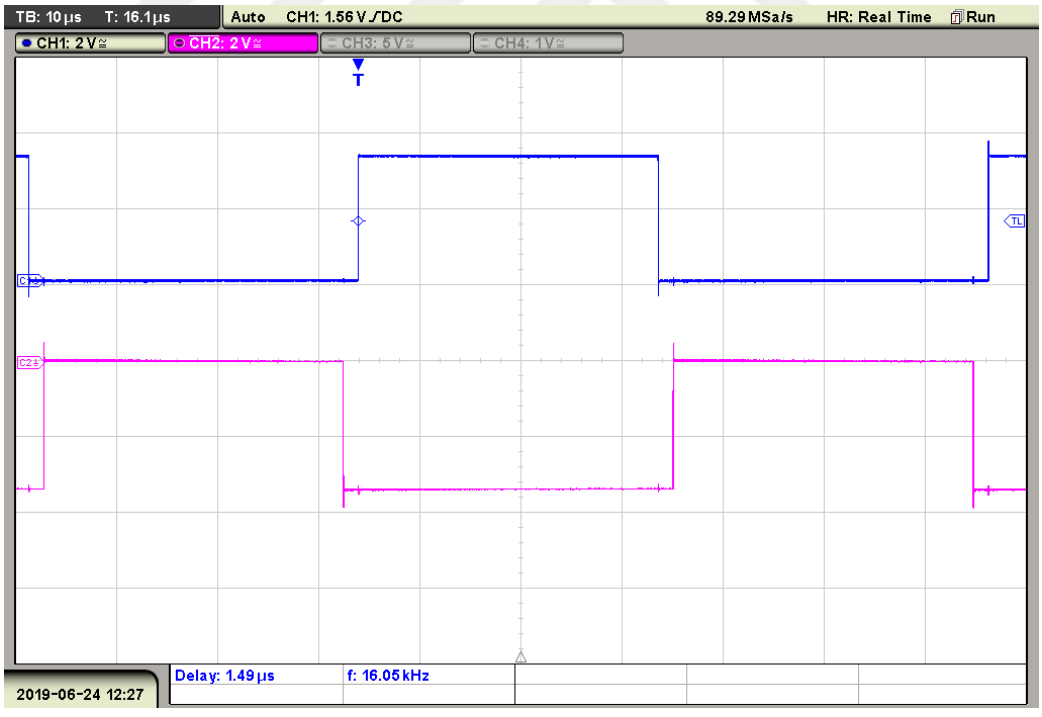

Figure 5.13 : PWM outputs of a single phase with inverted channel 2.

6. CONCLUSION AND FUTURE WORKS

In this thesis, a sensorless FOC drive system for PMSM is designed and implemented. The drive system consists of the three-phase inverter stage, control stage and embedded software. Scope of this thesis covers design of the control stage along with the embedded software. Inverter stage is obtained as a development board ready from market. X-NUCLEO-IHM08M1 development board is capable of driving three-phase motors up to 48V and 15A. Three-phase current shunts and differential amplifiers utilized for current sensing with an overcurrent comparator for fault detection.

Control stage of the drive system is designed as a module board that can be connected to the three-phase inverter board. Design of the controller board consists of selecting an appropriate microcontroller and necessary external peripherals, drawing of the schematics and PCB design. Altium tool is used for designing of the schematics and PCB. Component placement and board size selection is made according to three-phase inverter board. Two-layer construction is selected for PCB design. Matching of input and output signals along with the power supply buses is ensured between controller and three-phase inverter board. Designed controller board is then manufactured and assembled.

For the sensorless position estimation, two different approaches are investigated. Firstly, extended back-EMF observer is analyzed in detail. This observer is a Luenberger type state observer that utilizes the system model inside the controller. State estimation is based on processing measured and known state variables into the system model. If the system model is created with certain state deliberately excluded, then a compensator can be utilized in order to clear error between output of the Luenberger observer and measured value. Output of the compensator is then equal to the excluded state of the model. Implementation of the Luenberger type observer is done on machine mathematical model in two-phase stationary reference frame. Two current estimators with extended back-EMF terms removed from machine model are utilized. These current estimators use applied stator voltages and estimated electrical

speed. Error between actual currents and estimated currents are then corrected with the use of two PI controllers, which output the extended back-EMF term of the machine. Since this term includes sine and cosine terms of rotor electrical speed, an angle-tracking observer can extract rotor position information along with low pass filtered rotor electrical speed.

Rotor position estimation based on stator flux estimation method is also investigated. This method exploits the two-phase stationary reference frame model of the motor. Flux linkage expression consists of phase currents, inductance matrix and rotor position information as sine and cosine terms. Since the inductances are very small in value, it is assumed that the inductance matrix have no significant value in flux linkage. Thus, it is ignored and it is assumed that the flux linkages in α-β coordinate system give rotor electrical position as cosine and sine terms directly. These flux linkages can be estimated by back-EMF integration. Since pure integrators cannot be used practically due to ramp drift, DC offset and initial value problems, two low pass filters with a derivative operator in between are used instead. With sufficiently selected time constant for the filters, integration operation is achieved with ability to clear out offsets.

Verification of the sensorless position estimation schemes is done by MATLAB Simulink simulations. This is achieved by creating two FOC drive model simulations for extended back-EMF observer and flux estimator that estimates rotor position and speed. Three-phase currents are transformed into d-q axis currents using Clarke and Park transformations with position estimation. Error between desired and measured currents in d-q axis is then calculated and corrected with two PI controllers for each axis providing d-q axis reference voltage output. Reference output voltage is then transformed into three-phase stator voltage values using inverse Clarke and inverse Park transformations and applied to motor phases. Speed control is created in an acceleration-controlled manner. This is achieved by using a ramp generator that outputs a fixed acceleration ramp to desired speed reference controlled by ramp up and ramp down acceleration values in RPM/s unit. Output of the speed ramp is then used for speed error calculation, which is then corrected by a PI controller that outputs q axis reference current with output limitation.

Extended back-EMF observer is created based on a modified motor model in α-β coordinate system in which applied voltages, measured currents and estimated

electrical speed is entered as inputs, extended back-EMF term with sinus and cosine terms of rotor electrical position is obtained as outputs. Output of the extended back-EMF observer is then entered as input to angle-tracking observer that utilizes trigonometric identities to calculate position error, which is then corrected, by a PI controller and an integrator. PI controller clears the position error while integrator provides a smooth output. Placement of these two blocks is also in a convenient way that ensures both speed and position information is obtained using these blocks. Performance of the drive system is observed in no load and full load operation as well as transient changes in load. Position estimation is compared with actual position and it is found out that estimation is accurate and dynamic.

Stator flux estimator is implemented using machine mathematical model in two-phase stationary reference frame. Applied voltages, measured currents and phase resistances are used in order to calculate back-EMF of previous step. Calculated back-EMFs are then passed into integrator block, which is composed of two low pass filters and a derivative operator. Output of the integrator block provides rotor electrical position as cosine and sine terms. Angle-tracking observer is again used for speed and position extraction. This is achieved by modifying the inputs of angle-tracking observers since α and β terms now consist the cosine and sine terms respectively. It is found out that initial start is problematic due to offset at initial start. During the initial transient, speed and position estimation is not accurate. After the offset is cleared by low pass filters, speed and position estimation become accurate and dynamic enough to control the machine sensorless. It is observed that decreasing the time constants of the filters cause better speed estimation at initial start while it increases steady-state position estimation error. With the simulation results compared with extended back-EMF observer method, it is seen that the flux estimator method is not robust, accurate and dynamic enough to implement for experimental tests.

Embedded software is developed in IAR Embedded Workbench integrated development environment. Motor drive software is composed of multiple finite state machines. PWM frequency and current control loop frequency is selected as 16 kHz while speed control loop is 200 Hz. At each PWM period, phase currents and DC bus voltage is sampled via ADC. Three-phase currents are then transformed into two-phase rotating reference frame. Speed controller is implemented in d-q coordinate system to ensure proper utilization of quadrature axis current. Extended back-EMF

observer and angle-tracking observer are implemented as discrete systems. Open loop startup is implemented using an open loop speed ramp that also generates open loop position information.

System verification is done by conducting laboratory experiments. A 24 V, 62 W, 3000 rpm motor is driven with the drive system. A test setup capable of fully loading the motor is created using a generator that is coupled to the motor and a variable load resistor with rectification. No load and full load performance of the system is tested with experiments. It is observed that the system is capable of driving the motor in nominal speed range as well as field weakening operation from 200 rpm up to 4000 rpm. Motor is loaded fully and operated up to nominal speed. Dynamic performance of the system is tested with transient changes in loading. Transient and steady state response of the system is found stable and dynamic.

Additional improvements can be made on this study such as implementing the extended back-EMF observer in d-q reference frame. This is desirable since any filters implemented in α-β reference frame may introduce phase shift on state variables. Implementation of the observer in d-q reference frame is however more complex and prone to stability issues during tuning phase due to positive feedback nature. Comparing the observers developed in both of the reference frames could reveal transient and steady performance differences in them.

Since startup is managed using alignment and open loop startup functions, first rotational movement is not smooth. Although this causes no issues in many applications such as fans, pumps and washing machines, some applications such as electric vehicles and industrial drives disapprove any uncontrolled motions in startup. This issue can be eliminated by hybrid use of saliency based position estimation schemes with fundamental model based methods. Rotor position in standstill can be obtained using high frequency signal injection methods. This information on standstill position then provides the ability of starting the motor directly in closed loop mode.

Robustness of the system can also be improved by utilizing online parameter measurements or modeling parametric changes inside the controller. Fault detection algorithms that react in situations like blocked rotor, loss of a phase and hardware problems on inverter may also be developed in order to increase fault tolerance.

REFERENCES

[1] **Maheswaran, D., Rangaraj, V., Kailas, K. K. J. and Kumar, W. A.** (2012). Energy Efficiency In Electrical Systems, *IEEE International Conference on Power Electronics, Drives and Energy Systems (PEDES)*, 1-6.

[2] **Directive 2009/125/EC of the European Parliament and of the Council of 21 October 2009 establishing a framework for the setting of ecodesign requirements for energy-related products.** (2009). *OJ L 285*, 10–35.

[3] **NXP Semiconductors** (2016). Sensorless PMSM Field-Oriented Control on Kinetis KV and KE, *Application Note AN5237*

[4] **Renesas Electronics** (2018). Sensorless Vector Control for Permanent Magnet Synchronous Motor (Algorithm), *Application Note R01AN3786EJ0102*.

[5] **STMicroelectronics** (2007). Luenberger State Observer Rotor Position Estimation Simulink And Software Library, *Application Note AN2516.*

[6] **Kawamura, A. and Haft, R.** (1983). An Analysis of Induction Motor Field Oriented or Vector Control, *IEEE Power Electronics Specialists Conference*, 91-101.

[7] **Schieman, R. G., Wilkes, E. A., and Jordan, H. E.** (1974). Solid-state Control of Electric Drives, *Proceedings of the IEEE*, 62(12), 1643-1660.

[8] **Jordan**, **H. E.** (1965). Analysis of Induction Machines in Dynamic Systems, *IEEE Transactions on Power Apparatus and Systems*, 84(11), 1080-1088.

[9] **Novotny, D. W., and Wouterse, J. H.** (1976). Induction Machine Transfer Functions and Dynamic Response by Means of Complex Time Variables, *IEEE Transactions on Power Apparatus and Systems*, 95(4), 1325-1335.

[10] **Lipo, T. A., and Plunkett**, **A. B.** (1974). A Novel Approach to Induction Motor Transfer Functions, *IEEE Transactions on Power Apparatus and Systems*, 93(5), 1410-1418.

[11] **Krause, P. C., and Thomas**, **C. H.** (1965). Simulation of Symmetrical Induction Machinery, *IEEE Transactions on Power Apparatus and Systems*, 84(11), 1038-1053.

[12] **Blaschke, F.** (1972). Das Verfahren der Feldorientierung zur Regelung der Asynchronamaschine, *Siemens Forsch und Entwicklungs Bericht*, 1, 184.

[13] **Bose, B. K.** (1978). Introduction to AC Drives, Speed Control of AC Drives, *IEEE Collection*, 1-21.

[14] **Garcia, G. O., Stephan, R. M., and Watanabe, E. H.** (1991). Comparing the Indirect Field-oriented-control With a Scalar Method, *Proceedings IECON '91: International Conference on Industrial Electronics, Control and Instrumentation*, 1, 475-480.

[15] **Blaschke, F.** (1974). *U.S. Patent No. 3,805,135*. Retrieved from Google Patents.

[16] **Hasse, K.** (1969). *Zur Dynamik Drehzahlgeregelter Antriebe mit Stromrichtergespeisten Asynchron-Kurzchluslaufermachinen (On the Dynamics of Speed Control of Static AC Drives with Squirrel Cage Induction Machines).* (Ph.D. Dissertation), TH Darmstadt.

[17] **Hussain, S., and Bazaz, M. A.** (2015). Review of Vector Control Strategies for Three Phase Induction Motor Drive, *International Conference on Recent Developments in Control, Automation and Power Engineering (RDCAPE)*, 96-101.

[18] **Krishnan, R., and Doran, F. C.** (1987). Study of Parameter Sensitivity in High-Performance Inverter-Fed Induction Motor Drive Systems, *IEEE Transactions on Industry Applications*, 23(4), 623-635.

[19] **Krishnan, R., and Bharadwaj, A. S.** (1990). A Review Of Parameter Sensitivity and Adaptation in Indirect Vector Controlled Induction Motor Drive Systems, *21st Annual IEEE Conference on Power Electronics Specialists*, 560-566.

[20] **Garces, L. J.** (1980). Parameter Adaption for the Speed-Controlled Static AC Drive with a Squirrel-Cage Induction Motor, *IEEE Transactions on Industry Applications*, 16(2), 173-178.

[21] **Matsuo, T. and Lipo, T. A.** (1985). A Rotor Parameter Identification Scheme for Vector-Controlled Induction Motor Drives, *IEEE Transactions on Industry Applications*, 21(3), 624-632.

[22] **Koyama, M. Yano, M. Kamiyama, I., and Yano, S.** (1986). Microprocessor-Based Vector Control System for Induction Motor Drives with Rotor Time Constant Identification Function, *IEEE Transactions on Industry Applications*, 22(3), 453-459.

[23] **Lorenz, R. D.** (1990). A Simplified Approach to Continuous On-line Tuning of Field-Oriented Induction Machine Drives, *IEEE Transactions on Industry Applications*, 26(3), 420-424.

[24] **Sugimoto, H., and Tamai, S.** (1987). Secondary Resistance Identification of an Induction-Motor Applied Model Reference Adaptive System and Its Characteristics, *IEEE Transactions on Industry Applications*, 23(2), 296-303.

[25] **Liu, C. H., Hwu, C. C., and Feng, Y. F.** (1989). Modeling and Implementation of a Microprocessor-based CSI-Fed Induction Motor Drive Using Field-Oriented Control, *IEEE Transactions on Industry Applications*, 25(4), 588-597.

[26] **Heikkilä, S.** (2000). *U.S. Patent No. 6,094,364.* Retrieved from Google Patents.

[27] **Takahashi, I. and Noguchi, T.** (1986). A New Quick-Response and High-Efficiency Control Strategy of an Induction Motor, *IEEE Transactions on Industry Applications*, 22(5), 820-827.

[28] **Depenbrock, M.** (1988). Direct Self-Control (DSC) of Inverter-Fed Induction Machine, *IEEE Transactions on Power Electronics*, 3(4), 420-429.

[29] **Niu, F., Wang, B., Babel, A. S., Li, K., and Strangas, E. G. (**2016). Comparative Evaluation of Direct Torque Control Strategies for Permanent Magnet Synchronous Machines, *IEEE Transactions on Power Electronics*, 31(2), 1408-1424.

[30] **Habetler, T. G., Profumo, F., Pastorelli, M., and Tolbert, L. M.** (1991). Direct Torque Control of Induction Machines Using Space Vector Modulation, *Conference Record of the 1991 IEEE Industry Applications Society Annual Meeting*, 1, 428-436.

[31] **Zhang, Y. and Zhu, J.** (2011). A Novel Duty Cycle Control Strategy to Reduce Both Torque and Flux Ripples for DTC of Permanent Magnet Synchronous Motor Drives With Switching Frequency Reduction, *IEEE Transactions on Power Electronics*, 26(10), 3055-3067.

[32] **Pacas, M. and Weber, J.** (2005). Predictive Direct Torque Control for the PM Synchronous Machine, *IEEE Transactions on Industrial Electronics*, 52(5), 1350-1356.

[33] **Kang, J. K., and Sul, S. K.** (1999). New Direct Torque Control of Induction Motor for Minimum Torque Ripple and Constant Switching Frequency, *IEEE Transactions on Industry Applications*, 35(5), 1076-1082.

[34] **Ohtani, T., Takada, N., and Tanaka, K.** (1989). Vector Control of Induction Motor without Shaft Encoder, *Conference Record of the IEEE Industry Applications Society Annual Meeting*, 1, 500-507.

[35] **Schauder, C.** (1989). Adaptive Speed Identification for Vector Control of Induction Motors without Rotational Transducers, *Conference Record of the IEEE Industry Applications Society Annual Meeting*, 1, 493-499.

[36] **Holtz, J. and Quan, J.** (2002). Sensorless Vector Control of Induction Motors at Very Low Speed Using a Nonlinear Inverter Model and Parameter Identification, *IEEE Transactions on Industry Applications*, 38(4), 1087-1095.

[37] **Orlowska-Kowalska, T.** (1989). Application of Extended Luenberger Observer for Flux and Rotor Time-Constant Estimation in Induction Motor Drives, *IEEE Proceedings D - Control Theory and Applications*, 136(6), 324-330.

[38] **Elmas, C., and Zelaya-De La Parra, H.** (1993). Position Sensorless Operation of a Switched Reluctance Drive Based on Observer, *Fifth European Conference on Power Electronics and Applications*, 6, 82-87.

[39] **Kim, J. S., and Sul, S. K.** (1995). High Performance PMSM Drives without Rotational Position Sensors Using Reduced Order Observer, *IAS '95. Conference Record of the IEEE Industry Applications Conference Thirtieth IAS Annual Meeting*, 1, 75-82.

[40] **Senjyu, T., Shimabukuro, T., and Uezato, K.** (1995). Vector Control of Permanent Magnet Synchronous Motors Without Position and Speed Sensors, *Proceedings of PESC '95 - Power Electronics Specialist Conference*, 2, 759-765.

[41] **Soto, G. G., Mendes, E., and Razek, A.** (1999). Reduced-Order Observers for Rotor Flux, Rotor Resistance and Speed Estimation for Vector Controlled Induction Motor Drives Using the Extended Kalman Filter Technique, *IEE Proceedings - Electric Power Applications*, 146(3), 282-288.

[42] **Qiu, A., Wu, B., and Kojori, H.** (2004). Sensorless Control of Permanent Magnet Synchronous Motor Using Extended Kalman Filter, *Canadian Conference on Electrical and Computer Engineering 2004 (IEEE Cat. No.04CH37513)*, 3, 1557-1562.

[43] **Utkin, V. I.** (1993). Sliding Mode Control Design Principles and Applications to Electric Drives, *IEEE Transactions on Industrial Electronics*, 40(1), 23-36.

[44] **Furuhashi, T., Sangwongwanich, S., and Okuma, S.** (1992). A Position-and-Velocity Sensorless Control for Brushless DC Motors Using an Adaptive Sliding Mode Observer, *IEEE Transactions on Industrial Electronics*, 39(2), 89-95.

[45] **Peixo, Z. M. A., Freitas Sa, F. M., Seixas, P. F., Menezes, B. R., Cortizo, P. C., and Lacerda, W. S.** (1995). Application of Sliding Mode Observer for Induced E.M.F., Position and Speed Estimation of Permanent Magnet Motors, *Proceedings of 1995 International Conference on Power Electronics and Drive Systems. PEDS 95*, 2, 599-604.

[46] **Ertugrul, M., Kaynak, O., Sabanovic, A., and Ohnishi, K.** (1996). A Generalized Approach for Lyapunov Design of Sliding Mode Controllers for Motion Control Applications, *Proceedings of 4th IEEE International Workshop on Advanced Motion Control - AMC '96 - MIE*, 1, 407-412.

[47] **Schroedl, M.** (1988). Detection of the Rotor Position of a Permanent Magnet Synchronous Machine at Standstill, *Proc. ICEM Int. Conf. on Electrical Machines*, 195-197.

[48] **Schroedl, M., and Weinmeier, P.** (1994). Sensorless Control oOf Reluctance Machines at Arbitrary Operating Conditions Including Standstill, *IEEE Transactions on Power Electronics*, 9(2), 225-231.

[49] **Briz, F., Degner, M. W., Garcia, P., and Lorenz, R. D.** (2004). Comparison of Saliency-Based Sensorless Control Techniques for AC Machines, *IEEE Transactions on Industry Applications*, 40(4), 1107-1115.

[50] **Jansen, P. L., and Lorenz, R. D.** (1995). Transducerless Position and Velocity Estimation in Induction and Salient AC Machines, *IEEE Transactions on Industry Applications*, 31(2), 240-247.

[51] **Cilia, J., Asher, G. M., Bradley, K. J., and Sumner, M.** (1997). Sensorless Position Detection for Vector-Controlled Induction Motor Drives Using an Asymmetric Outer-Section Cage, *IEEE Transactions on Industry Applications*, 33(5), 1162-1169.

[52] **Teske, N., Asher, G. M., Sumner, M., and Bradley, K. J.** (2001). Encoderless Position Estimation for Symmetric Cage Induction Machines Under Loaded Conditions, *IEEE Transactions on Industry Applications*, 37(6), 1793-1800.

[53] **Ha, J. I., and Sul, S. K.** (1999). Sensorless Field-Orientation Control of an Induction Machine by High-Frequency Signal Injection, *IEEE Transactions on Industry Applications*, 35(1), 45-51.

[54] **Corley, M. J., and Lorenz, R. D.** (1998). Rotor Position and Velocity Estimation for a Salient-Pole Permanent Magnet Synchronous Machine at Standstill and High Speeds, *IEEE Transactions on Industry Applications*, 34(4), 784-789.

[55] **Briz, F., Degner, M. W., Garcia, P., and Guerrero, J. M.** (2005). Rotor Position Estimation of AC Machines Using the Zero-Sequence Carrier-Signal Voltage, *IEEE Transactions on Industry Applications*, 41(6), 1637-1646.

[56] **Xu, P. L., and Zhu, Z. Q.** (2016). Novel Carrier Signal Injection Method Using Zero-Sequence Voltage for Sensorless Control of PMSM Drives, *IEEE Transactions on Industrial Electronics*, 63(4), 2053-2061.

[57] **Zhang, B., and Doppelbauer, M.** (2014). Numerical Iron Loss Calculation of a New Axial Flux Machine With Segmented-Armature-Torus Topology, *7th IET International Conference on Power Electronics, Machines and Drives (PEMD 2014)*, 1-6.

[58] **Duesterhoeft, W. C., Schulz, M. W., and Clarke, E.** (1951). Determination of Instantaneous Currents and Voltages by Means of Alpha, Beta, and Zero Components, *Transactions of the American Institute of Electrical Engineers*, 70(2), 1248-1255.

[59] **Park, R. H.** (1929). Two Reaction Theory of Synchronous Machines, *AIEE Transactions*, 48, 716-730.

[60] **Tu, W., Xiao, G., Suo, C., and Yang, K.** (2017). A Design of Sensorless Permanent Magnet Synchronous Motor Drive Based on V/F Control, *20th International Conference on Electrical Machines and Systems (ICEMS)*, 1-5.

[61] **Tazerart, F., Mokrani, Z., Rekioua, D., and Rekioua, T.** (2015). Direct Torque Control Implementation With Losses Minimization of Induction Motor for Electric Vehicle Applications With High Operating Life of The Battery, *International Journal of Hydrogen Energy*, 40(39), 13827-13838.

[62] **Aguirre, M., Calleja, C., Lopez-de-Heredia, A., Poza, J., Aranburu, A., and Nieva, T.** (2011). FOC and DTC Comparison in PMSM for Railway Traction Application, *Proceedings of the 14th European Conference on Power Electronics and Applications*, 1-10.

[63] **Renesas Electronics Corporation** (2009). SH2/2A Sensorless Vector Control of Three-Phase Permaneng Magnet Synchronous Motors, *Application Note REU05B0103-0100*

[64] **Lara, J., and Chandra, A.** (2018). Performance Investigation of Two Novel HSFSI Demodulation Algorithms for Encoderless FOC of PMSMs Intended for EV Propulsion, *IEEE Transactions on Industrial Electronics*, 65(2), 1074-1083.

[65] **Risfendra, Y. K., Lin, Y., and Huang, L.** (2016). FPGA-Based Sensorless Controller for PMSM Drives Using Sliding Mode Observer And Phase Locked Loop, *2016 International Conference on Applied System Innovation (ICASI)*, Okinawa, 2016, pp. 1-4.

[66] **STMicroelectronics** (2017). Low-Voltage BLDC Motor Driver Epansion Board Based on STL220N6F7 for STM32 Nucleo, *Data brief DocID028748 Rev 3*.

[67] **NXP Semiconductors** (2016). 168 MHz ARM Cortex-M4 Core Based Microcontroller with FPU. *KV4x Data Sheet KV4XP100M168*.

APPENDICES

APPENDIX A: PCB layouts.

APPENDIX A

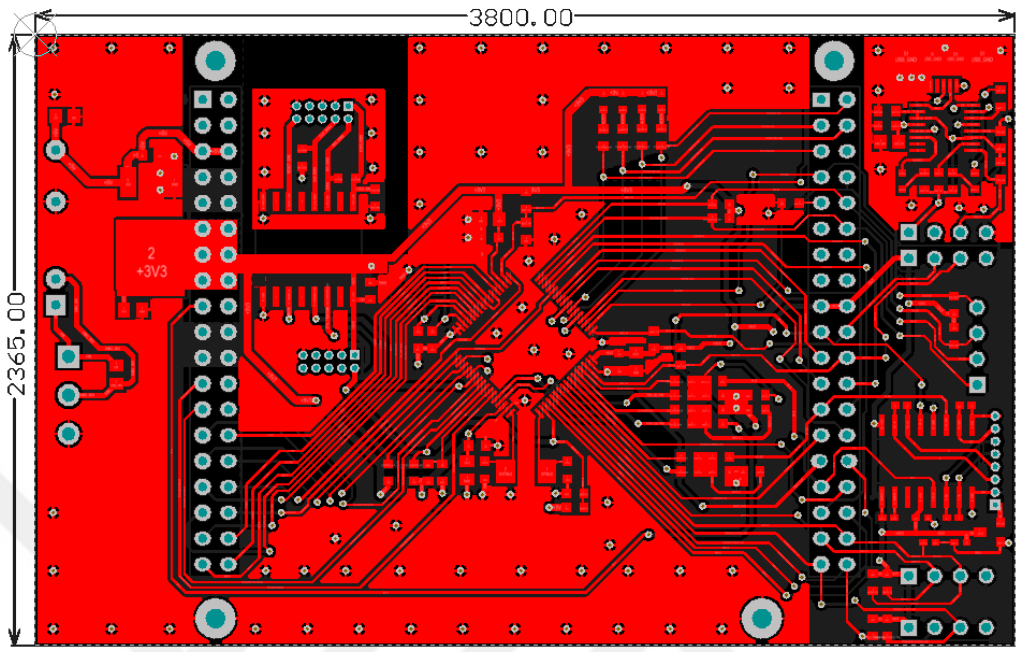

(a)

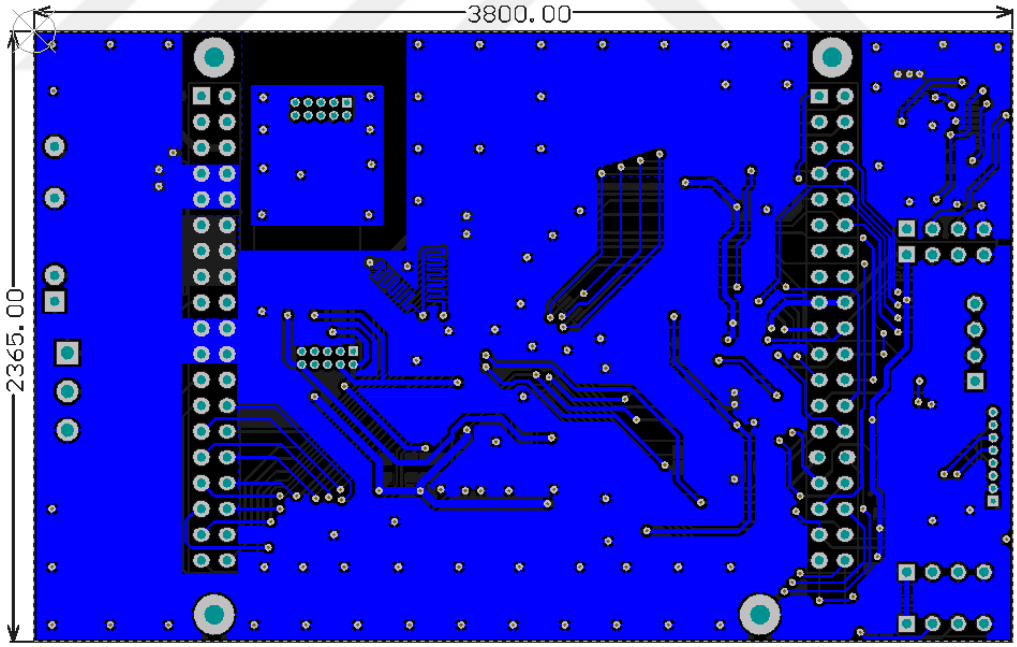

(b)

Figure A.1 : PCB layouts: (a)Top side. (b)Bottom side.

CURRICULUM VITAE

Name Surname	**:** Burak GÖRDÜK
Place and Date of Birth	**:** İzmir, 1994
E-Mail	**:** gorduk@itu.edu.tr

EDUCATION **:**

- **B.Sc.** **:** 2016, Istanbul Technical University, Faculty of Electrical and Electronics, Department of Electrical Engineering

PROFESSIONAL EXPERIENCE AND REWARDS:

- Best Graduation Project Award, The Chamber of Electrical Engineers (EMO) 2016 June.
- Electronic Design Engineer at Pavo Tasarım since 2016 July.